USF UNIVERSITY OF SOUTH FLORIDA
Civil & Environmental Engineering

DESIGN AND CONSTRUCTION OF PRECAST PILES WITH STAINLESS REINFORCING STEEL

BDK84 977-07

DRAFT FINAL REPORT

Principal Investigators:
Gray Mullins, Ph.D., P.E.
Rajan Sen, Ph.D., P.E.
Alberto Sagüés, Ph.D., P.E.

Researchers:
Danny Winters, Cara Morton, Joseph Fernandez, Kevin Johnson, Vincent DePianta, Jeff Vomacka, and Elizabeth Mitchell

January 2014

Disclaimer

The opinions, findings, and conclusions expressed in this publication are those of the authors and not necessarily those of the State of Florida Department of Transportation.

SI* (MODERN METRIC) CONVERSION FACTORS

APPROXIMATE CONVERSIONS TO SI UNITS

SYMBOL	WHEN YOU KNOW	MULTIPLY BY	TO FIND	SYMBOL
LENGTH				
in	inches	25.4	millimeters	mm
ft	feet	0.305	meters	m
yd	yards	0.914	meters	m
mi	miles	1.61	kilometers	km

SYMBOL	WHEN YOU KNOW	MULTIPLY BY	TO FIND	SYMBOL
AREA				
in^2	squareinches	645.2	square millimeters	mm^2
ft^2	squarefeet	0.093	square meters	m^2
yd^2	square yard	0.836	square meters	m^2
ac	acres	0.405	hectares	ha
mi^2	square miles	2.59	square kilometers	km^2

SYMBOL	WHEN YOU KNOW	MULTIPLY BY	TO FIND	SYMBOL
VOLUME				
fl oz	fluid ounces	29.57	milliliters	mL
gal	gallons	3.785	liters	L
ft^3	cubic feet	0.028	cubic meters	m^3
yd^3	cubic yards	0.765	cubic meters	m^3
NOTE: volumes greater than 1000 L shall be shown in m^3				

SYMBOL	WHEN YOU KNOW	MULTIPLY BY	TO FIND	SYMBOL
MASS				
oz	ounces	28.35	grams	g
lb	pounds	0.454	kilograms	kg
T	short tons (2000 lb)	0.907	megagrams (or "metric ton")	Mg (or "t")

SYMBOL	WHEN YOU KNOW	MULTIPLY BY	TO FIND	SYMBOL
TEMPERATURE (exact degrees)				
°F	Fahrenheit	5 (F-32)/9 or (F-32)/1.8	Celsius	°C

SYMBOL	WHEN YOU KNOW	MULTIPLY BY	TO FIND	SYMBOL
ILLUMINATION				
fc	foot-candles	10.76	lux	lx
fl	foot-Lamberts	3.426	candela/m^2	cd/m^2

SYMBOL	WHEN YOU KNOW	MULTIPLY BY	TO FIND	SYMBOL
FORCE and PRESSURE or STRESS				
lbf	poundforce	4.45	newtons	N
lbf/in^2	poundforce per square inch	6.89	kilopascals	kPa

APPROXIMATE CONVERSIONS TO SI UNITS

SYMBOL	WHEN YOU KNOW	MULTIPLY BY	TO FIND	SYMBOL
LENGTH				
mm	millimeters	0.039	inches	in
m	meters	3.28	feet	ft
m	meters	1.09	yards	yd
km	kilometers	0.621	miles	mi

SYMBOL	WHEN YOU KNOW	MULTIPLY BY	TO FIND	SYMBOL
AREA				
mm^2	square millimeters	0.0016	square inches	in^2
m^2	square meters	10.764	square feet	ft^2
m^2	square meters	1.195	square yards	yd^2
ha	hectares	2.47	acres	ac
km^2	square kilometers	0.386	square miles	mi^2

SYMBOL	WHEN YOU KNOW	MULTIPLY BY	TO FIND	SYMBOL
VOLUME				
mL	milliliters	0.034	fluid ounces	fl oz
L	liters	0.264	gallons	gal
m^3	cubic meters	35.314	cubic feet	ft^3
m^3	cubic meters	1.307	cubic yards	yd^3

SYMBOL	WHEN YOU KNOW	MULTIPLY BY	TO FIND	SYMBOL
MASS				
g	grams	0.035	ounces	oz
kg	kilograms	2.202	pounds	lb
Mg (or "t")	megagrams (or "metric ton")	1.103	short tons (2000 lb)	T

SYMBOL	WHEN YOU KNOW	MULTIPLY BY	TO FIND	SYMBOL
TEMPERATURE (exact degrees)				
^oC	Celsius	1.8C+32	Fahrenheit	^oF

SYMBOL	WHEN YOU KNOW	MULTIPLY BY	TO FIND	SYMBOL
ILLUMINATION				
lx	lux	0.0929	foot-candles	fc
cd/m^2	$candela/m^2$	0.2919	foot-Lamberts	fl

SYMBOL	WHEN YOU KNOW	MULTIPLY BY	TO FIND	SYMBOL
FORCE and PRESSURE or STRESS				
N	newtons	0.225	poundforce	lbf
kPa	kilopascals	0.145	poundforce per square inch	lbf/in^2

*SI is the symbol for the International System of Units. Appropriate rounding should be made to comply with Section 4 of ASTM E380.

1. Report No. *FHWA Report #, if applicable*	2. Government Accession No.	3. Recipient's Catalog No.
4. Title and Subtitle *Design and Construction of Precast Piles with Stainless Reinforcing Steel*		5. Report Date *January 2014* 6. Performing Organization Code
7. Author(s) *G. Mullins and R. Sen*		8. Performing Organization Report No.
9. Performing Organization Name and Address *University of South Florida* *Department of Civil and Environmental Engineering* *4202 E. Fowler Avenue, ENB 118s* *Tampa, FL 33620*		10. Work Unit No. (TRAIS) 11. Contract or Grant No. *BDK-84-977-07*
12. Sponsoring Agency Name and Address Florida Department of Transportation 605 Suwannee Street, MS 30 Tallahassee, FL 32399		13. Type of Report and Period Covered *Final Report* 14. Sponsoring Agency Code
15. Supplementary Notes *FDOT Project Manager:* *Larry Jones,MSCE., P.E.*		
16. Abstract The service life of prestressed concrete piles is, in part, dictated by the time required to corrode the steel once chloride ions are at the surface of the steel. Stainless steel materials, although limited in availability in strand form, have a higher tolerance to chloride ions and hence may provide a means to extend the service life. This study scrutinized the corrosion and structural performance of three candidate stainless steel materials with the goal of identifying a possible solution that uses stainless steel for prestressed concrete piles.		
17. Key Word *Prestress Piles, Stainless Steel,*	18. Distribution Statement No restrictions.	

19. Security Classif. (of this report) Unclassified.	20. Security Classif. (of this page) Unclassified.	21. No. of Pages 126	22. Price $210,000

Form DOT F 1700.7 (8-72) Reproduction of completed page authorized

Acknowledgments

The authors would like to acknowledge the Florida Department of Transportation for funding this project with specific thanks to the review team for their insightful contributions. Additionally, the support from Henderson Prestress in Tarpon Springs is likewise appreciated.

Executive Summary

In Florida, approximately two thirds of the 5500 bridges reside in marine environments making corrosion damage one of the main sources of service life reduction. Most of this damage pertains to substructural elements (e.g. piles or drilled shafts, footings, and columns). Therein, the service life of these elements is, in part, dictated by the time required to corrode the steel once chloride ions are at the surface of the steel.

Stainless steel materials have a higher tolerance to chloride ions and therefore can be expected to extend the service life of marine structures. For prestressed piles, however, the high strength requirements for prestressing strands make many stainless steel grades unsuitable and in most cases are not available in strand form. Further, if the strength of the stainless steel is increased through cold working or similar, concerns exist dealing with the increased potential for stress corrosion cracking (SCC). This study scrutinized the corrosion and structural performance of three candidate stainless steel materials with the goal of identifying a possible solution that uses stainless steel for prestressed concrete piles suitable for Florida marine environments.

The three candidate stainless materials selected for evaluations were an austenitic Grade 316 stainless steel, a low nickel but high manganese XM-29, and a duplex 2205. The primary components of this study included: (1) screening for potential SCC development in single wire specimens, (2) documenting the tensile strength and relaxation properties of 7-wire strands, and (3) transfer length determination from the fabrication and testing of full scale prestressed piles. It should be noted that the candidate materials were largely selected on the basis of their availability in strand form.

Corrosion testing was conducted at various temperatures in MgCl2 solutions and also in a simulated concrete pore water solution at 60 deg C, followed by an anodic polarization regime as an alternative test acceleration method. Although none showed startlingly poor performance, the results suggest that duplex high-strength stainless UNS# S32205 performed overall better than the other two alloys.

Relaxation testing was conducted on all the candidate stainless steel materials as well as commonly used low-lax Grade 270 carbon steel strand. The low magnetic permeabililty of the stainless steels meant that induction furnaces could not be used to relax the material and therefore each material was not relaxed in the as-received state. As a result, tests showed high relaxation values that exceeded normally accepted levels. A cyclic loading methodology was adopted to mechanically relax the stainless strands bring the relaxation to a usable level.

Finally, full scale piles were cast with each of the candidate stainless steel strand materials along with a low-lax Grade 270 carbon steel control pile. The use of stainless steel strand showed no adverse effects on transfer length compared to traditional low-lax Grade 270 carbon steel.

Intentionally Left Blank

Table of Contents

List of Tables

List of Figures

Intentionally Left Blank

Chapter 1: Introduction

Over 87,000 or fifteen percent of U.S. bridges are structurally deficient on the basis of corrosion damage. The estimated annual cost for corrosion repair and maintenance of just the substructural bridge components (not including those to be replaced) is $2 billion, nationwide for the next several years (FHWA, 2002; Koch, 2009). When considering all corrosion repairs to U.S. bridges (and related replacements), these costs soar to $8.3 billion (annually). In Florida, approximately two thirds of the 5500 bridges reside in marine environments making corrosion damage one of the main sources of service life reduction (Sagüés, 2001). Most of this damage pertains to substructural elements (e.g. piles or shafts, footings, and columns, Figure 1.1).

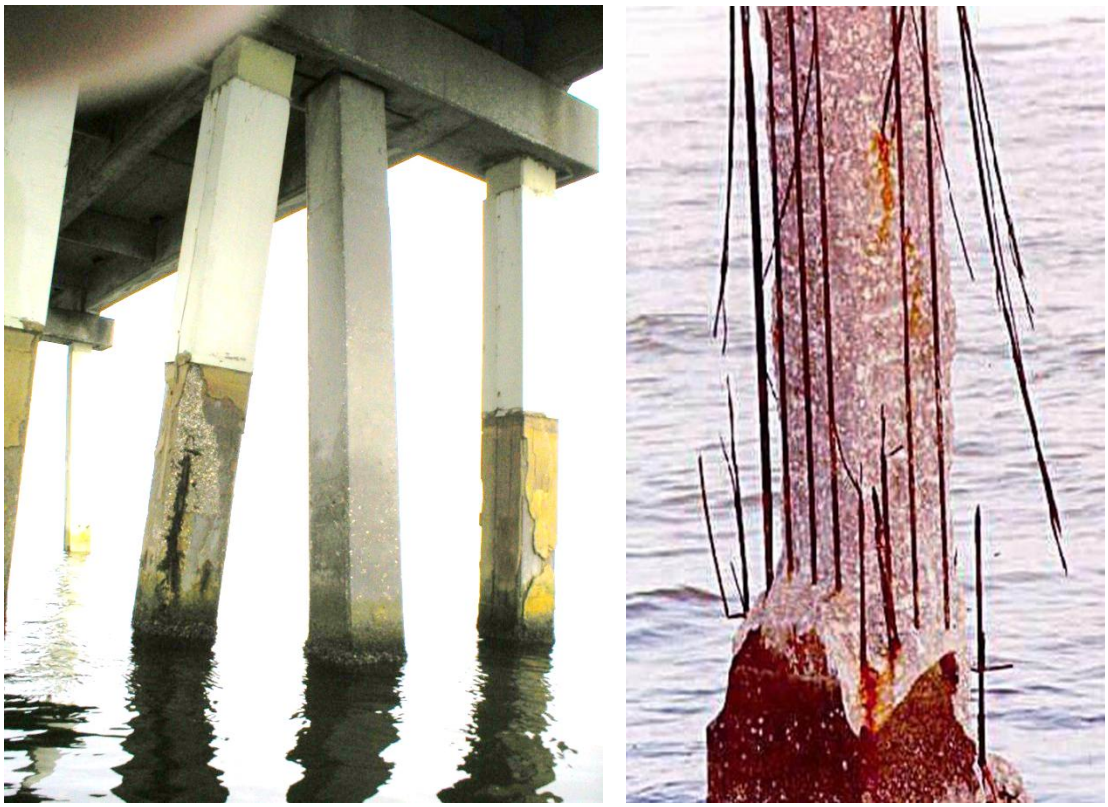

Figure 1.1 Pile damage caused by corrosion.

Over the past decades, there has been increasing interest in the use of alternative corrosion-resistant materials (Hartt, 2009) to reduce maintenance costs as future bridge designs are tasked with finding effective ways to extend the service life of Florida highway bridges beyond that previously accepted. Materials considered include fiber reinforced polymers, galvanized steel, MMFX steel and stainless steel. Of these, stainless steel provides compelling evidence of long term durability in aggressive environments. Figure 1.2 is a photograph of a concrete pier constructed nearly 70 years ago in Yucatan, Mexico using stainless steel rebars. Exposure conditions in the Yucatan are similar to those in Florida yet the structure shows little signs of corrosion damage. In contrast, another pier built using carbon steel in the foreground (circa1969) has almost completely

deteriorated. Despite the higher initial cost of using stainless steel, life cycle costs have clearly good potential for being less costly, especially when designing for a long service life.

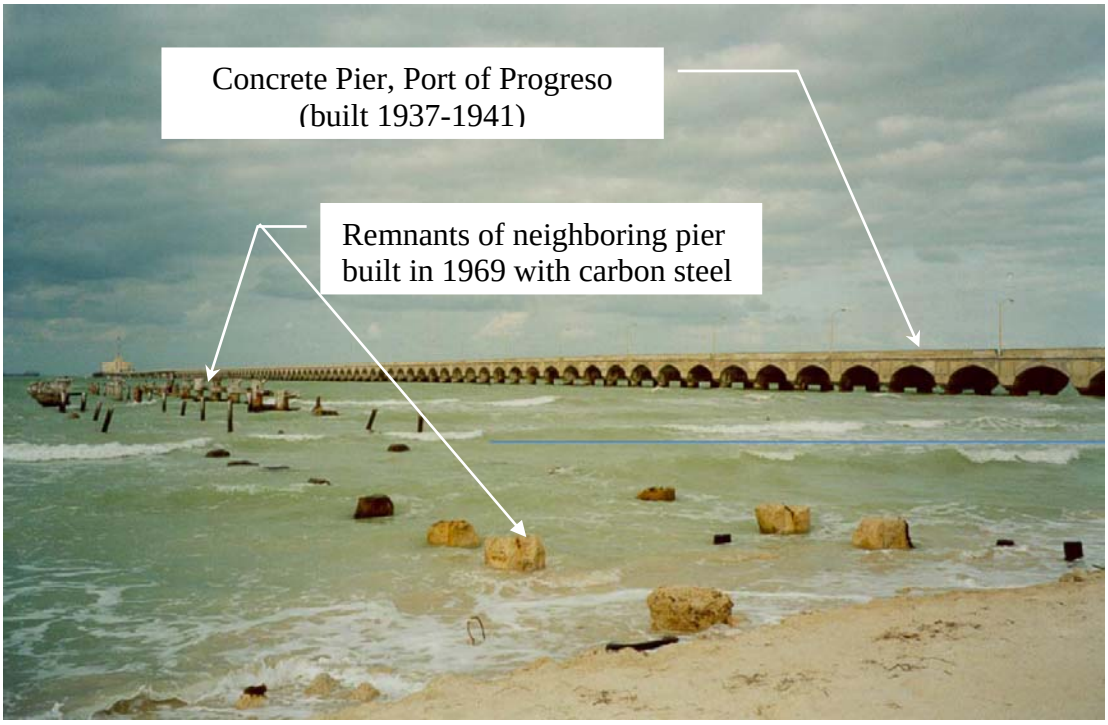

Figure 1.2 Progreso pier in Yucatan, Mexico (right) built using 220 tons of 30 mm 304 stainless steel reinforcing bars in porous concrete with w/c ratio of 0.55 – 0.6. Late 60's pier (left) built with carbon steel reinforcing bars is almost completed destroyed by corrosion (Arminox, 1999; Castro, 2002).

1.1 Background

Two aspects of design are necessarily coupled when selecting appropriate foundation elements for marine environments: corrosion resistance and structural capacity. With the latter being perhaps the more manageable, much of the recent attention has been focused on efforts to increase corrosion resistance. This has been largely successful via high performance concrete and increased reinforcement cover requirements. However, with bridge designs facing longer service lives of 75 – 100 years, these measures alone may not always be able to effectively provide the increased service life needs. In particular, even high performance concrete with low bulk permeability will have a certain incidence of cracks and other local deficiencies (Lau, 2008). Corrosion of plain steel in those places could be severe and aggravated by adverse galvanic coupling with the rest of the structure (Kranc, 1998; Raupach, 1996). Alternatively, corrosion resistant reinforcing steel, although more expensive, may provide the needed additional durability at locally deficient regions, while simultaneously placing a lower overall cost burden on concrete performance and cover thickness. Thus, the use of stainless steel may merit strong consideration as being more cost effective over the life of the structure.

To date, there is overwhelming evidence that stainless steel reinforcement can drastically improve corrosion resistance and the associated service life of reinforced concrete structures. However, in the form of prestressing reinforcement, stainless steel has far fewer case studies. Conventional prestressed concrete piles have the obvious advantage of increasing drivability while decreasing the total required steel when compared to reinforced concrete piles (of years past). *For clarity the authors will use the terms strands and bars when referring to prestressed and reinforced concrete, respectively*. Available stainless steel strands (in Grades 220 and 240 ksi) do not have the same strength as conventional low-lax or stress-relieved prestressing strands (270 ksi). Further, they may be prone to stress-induced corrosion complications depending on the material structure. Although reinforced concrete piles with stainless steel bars are likely to be a successful option, there is motivation to address the use of stainless steel prestressing strands to reduce the overall reinforcement costs. Balancing the corrosion resistance with the strength requirements continues to be the primary objective and formed the basis of this study.

Corrosion Resistance

In concrete, corrosion occurs on the embedded steel upon breakdown of the passive film normally present on the steel surface due to the high pH of the concrete pore water. Expansive corrosion products then build up that cause cracking and spalling of the concrete cover and consequent need for repair and rehabilitation. Passivity breakdown of steel in concrete in Florida bridges is overwhelmingly the result of chloride ion penetration from the salt in the environment. If the environmental chloride content is relatively small and the concrete cover is thick, dense and sound, concrete can provide effective long-term protection of embedded steel against corrosion (Sagüés, 2001). However, by increasing the corrosion resistance of the steel an even longer life span can be expected.

In sound concrete four primary factors control the corrosion-dependent service life of reinforced or prestressed concrete marine structures: (1) the diffusion rate of chloride ions into the concrete, (2) the thickness of the concrete cover, (3) the chloride concentration at the concrete surface (and water salinity), and (4) the chloride concentration threshold at the surface of the steel required to initiate corrosion. The first two can be controlled by concrete quality and geometry, while the latter is dictated by the reinforcing material properties. The water salinity and the resulting splash zone surface chloride concentration are site dependent but are essentially capped by the solubility limit. For completeness, each of these factors are briefly discussed although the primary focus of the corrosion aspects of the study were the chloride concentration threshold of stainless reinforcing steel and stress effects on corrosion resistance.

Diffusion. The diffusion rate of chloride ions into the concrete is strongly affected by the concrete quality mainly controlled by cement content and its constituents, w/c ratio, fly ash or slag content, age, and construction techniques. Post construction effects such as moisture content and temperature also affect diffusion but are not considered in the mix design. In good quality concrete using fly ash, the apparent diffusion rate coefficient can be as low as 2×10^{-9} cm^2/s whereas poorer concrete (no fly ash) has shown values as high as 5×10^{-7} cm^2/s (Sagüés, 2001).

Cover. While the time to initiate corrosion is inversely related to the diffusion rate, in sound concrete it is directly proportional to the square of the cover thickness, which has the

strongest effect on controlling corrosion of all the above parameters. Chloride concentration at the surface tends to be quite high in marine environments, in regions just above the high water elevation and in the splash zone. In those regions, cumulative effects of wet / dry cycles ultimately saturate the pore water to the solubility limit, leading to chloride ion levels typically in the order of 20 kg/m^3 of concrete. Higher salinity environments achieve this level more rapidly.

Chloride Concentration. The chloride concentration threshold for corrosion initiation of carbon steel in concrete is much smaller (e.g. 1 kg/m^3) than the marine service surface concentration. Consequently, that threshold is rapidly reached and corrosion started unless the concrete cover is thick and the concrete very dense; hence the emphasis on those parameters to achieve long service life if regular strand or bar is used.

Chloride Threshold. The chloride concentration threshold is the key parameter that can be favorably altered through the use of stainless steel reinforcing strands or bars. If the threshold is increased to approach a significant fraction of the value of the chloride surface concentration, the relative benefit in extending the time to corrosion initiation increases substantially (Sagüés, 1996). Such is the case of stainless steel, for which one study conservatively sets the threshold level to be 7 – 10 times higher than that of carbon steel (McDonald, 1995). Other estimates place the stainless steel chloride concentration threshold 16 times higher than carbon steel for Grade 304 and even higher for Grade 316 (Sorensen, 1990). More recent work by Hurley (2006) finds also improvements of one order of magnitude or greater on the threshold of various stainless steels over that of carbon steel. Thus, stainless steels can be expected to have thresholds in the order of 10 kg/m^3 (about ½ of the typical high end of surface concentration values) or higher. All else being similar, corrosion free service life multipliers ranging from several fold to a nominally unlimited benefit could conceptually be achieved in sound concrete over the performance of conventional carbon steel.

In concrete locations with cracks and other local deficiencies the transport of chloride to the steel surface may be essentially unimpeded (Sagüés 2001; Lau 2008), and the surrounding impermeability or thickness of the concrete cover may be of little avail locally. Some incidence of through-cover cracks is unavoidable, and tropical corrosion protection at those locations may be required in the future even in structures built with the best concrete practice if carbon steel is used. FDOT is carefully monitoring such locations in its existing structures, and indeed signs of early corrosion at cracks were uncovered at the Howard Frankland bridge after only 15 years of service despite the otherwise high quality of the concrete used there (Lau 2008). It is noted that the corrosion there occurred in epoxy-coated rebar, highlighting the failure of simple metal coating systems when an intrinsically corrosion resistant material is not used. The use of stainless steel represents one of the few options to deal with the particularly adverse conditions of cracked concrete with a high chance of success, as the corrosion initiation event may be prevented (or statistically made very rare) by the choice of an adequate alloy grade. Moreover, the rate of corrosion propagation in the case of initiation would be also expected to be substantially lower than that with carbon steel. Additionally, stainless steels with surface free of mill scale lower the extent of adverse galvanic coupling of a corroding spot with the rest of the system. That benefit derives from the much lower rate of oxygen reduction that can be supported on a stainless steel surface compared with that of carbon steel (Cui 2008).

The above considerations show than for sound concrete, given a specific service life design goal (e.g. 100 years) the use of stainless steel could permit the use of significantly relaxed concrete cover specifications, or less demanding concrete permeability requirements, than those required for carbon steel construction. For example, cover requirements could be reduced by 1 inch or more in certain applications and the use of microsilica or other expensive admixtures could be lessened. Those changes would represent not only a reduction of cost in materials, but in some instances may result in lower incidence of cracks from mechanical or shrinkage factors with consequent less demand in special concrete curing and finishing requirements. Moreover, the risk noted above of corrosion at local deficiencies would be synergistically decreased.

This project investigated the availability and use of stainless steel prestressing strand for bridge piles. This included: an all-encompassing review of stainless steel products and applications pertaining to bridge substructures, structural considerations of various reinforced and prestressed schemes, identifying the corrosion resistance enhancements / limitations of stainless reinforcement, full scale prototype pile fabrication, life cycle evaluation, and recommendations for a long-term performance monitoring program of stainless steel reinforced piles.

1.2 Report Organization

The overall organization of this report is outlined below wherein five ensuing chapters provide the following: a background of prestress and stainless steel concepts, the evaluation of corrosion resistance of various grades of stainless steel strand material, the testing and evaluation of the relaxation properties of available stainless steel strand material, full scale fabrication of piles cast with available strands materials, and the study findings.

Chapter 2 provides a background of prestressed pile considerations coupled with the technical challenges associated with using available stainless steel strand material for prestressing applications. A comprehensive corrosion evaluation of three candidate stainless steel grades is presented in Chapter 3. Results from comparative tests conducted on these materials are presented. Chapter 4 contains the material testing of the candidate stainless steel strand materials including ultimate strength and relaxation tests. Chapter 5 describes the preparations for and fabrication of four full-scale piles cast with each of three candidate stainless steel materials as well as a carbon steel control pile. The results therein provide an indication of the transfer length and the suitability of these materials for prestressing applications. Finally, Chapter 6 presents the conclusions and recommendations for the use of stainless steel prestressing strand.

Intentionally Left Blank

Chapter 2: Background

This chapter provides an overview on material and design requirements for using stainless steel in prestressed piling application.

2.1 Objectives

The goal of the study was to (1) identify stainless steels that were suitable for prestressing piles in a marine environment, (2) to determine material properties required for their design and, (3) fabricate and instrument full-sized stainless steel prestressed piles for further evaluation and testing by the Department.

2.2 Types of Stainless Steel

Stainless steel derives its corrosion resistance from the presence of a nanometer-scale thin passive surface film primarily of chromium oxide. Chromium is thus the key element, which needs to be present above a minimum concentration to be effective. Steel with more than 10% chromium (by weight) is classified as stainless steel (AISI, 2009), but a minimum level of 12% chromium is normally considered necessary to impart sufficient corrosion resistance in many applications.

Numerous grades of stainless steel are available (Table 2.1). Alloys containing only iron and chromium make up the martensitic (typically ~12% Cr) and ferritic (typ. >17% Cr) grades which are less expensive but have limited ductility and relatively moderate corrosion resistance. Ferritic and martensitic stainless steels are ferromagnetic. The inclusion of nickel in appropriate proportions creates an austenitic (face centered cubic) microstructure which is inherently more ductile, and with added corrosion resistance. The austenitic steels are usually non-magnetic unless cold worked when the resulting martensite introduces a certain amount of ferromagnetic response. Duplex steels have a mixed austenitic-ferritic microstructure, while precipitation hardened grades rely on other alloying additions to obtain exceptional high strength. Not included are a series of specialty high strength, low stress corrosion, very low magnetic susceptibility stainless steels denoted by ASTM XM-28, 29, or 32. These are austenitic grades developed for electromagnetic equipment, mine sweepers, or other military applications, and for certain medical imaging facilities.

Key compositional modifications in addition to chromium to improve corrosion resistance are the addition of molybdenum and of nitrogen to improve the pitting corrosion resistance, as well as the reduction in the carbon content to prevent intergranular corrosion. A highly corrosion resistant and readily available stainless steel with those additions and with some of the most desirable characteristics for reinforcing steel is the austenitic grade Type 316 LN (Table 2.2). However, commonly used austenitic stainless steel, with nickel content ~10% are particularly sensitive to stress corrosion cracking (SCC) in chloride environments. Austenitic stainless steels also have a

higher thermal coefficient of expansion, 17 x 10^{-6} cm/cm/C (Skovsgaard, 1997) when compared to carbon steel, 11-12 x 10^{-6} cm/cm/C, and concrete, 6 x 10^{-6} cm/cm/C (Mindess, 2003). Duplex steels (e.g. 2205 or 2207) can be more expensive than austenitic but combine good mechanical properties with increased resistance to localized corrosion (pitting or crevice corrosion *if enough Mo is in the alloy)* and stress corrosion cracking.

Table 2.1 Stainless steel designations and crystalline structure (Wikipedia, 2009).

Crystalline Structure	**SAE Stainless Steel Designation (bold most common)**
Austenitic	101, 102, 201, 202, 205, 301, **302**, 302B, 303, 303Se, **304**, **304L**, 304Cu, 304N, 305, 308,309, 309S, 310, 310S, 314, **316**, **316L**, 316F, 316N, 317, 317L, 321, 329, 330, 347, 348, 384, 904L
Ferritic	405, 409, 429, 430, 430F, 430FSe, 434, 436, 442, 446
Duplex	**2205**, 2207
Martensitic	403, 410, 414, 416, 416Se, 420, 420F, 422, 431, 440A, 440B, 440C
Precipitation Hardened	601-604, 610-613, 614-619, **630**, 630-635, 650-653, 660-665

Far fewer designations are used for civil engineering applications. Table 2.2 shows a representative sample of those grades used for reinforcing steel bars (Tullman, 2009b). Iron (Fe) provides the remaining percentage for each of the grade compositions shown.

Stainless steel clad carbon steel rebar has been introduced in recent years as a much less expensive alternative to solid stainless steel (Cui 2006, Hurley 2006). Such products have excellent potential for practical implementation as strength and thermal property compatibility issues would be reduced as long as adequate provision for handling bar terminations is made. However, large scale availability of the product with appropriate quality control needs yet to be demonstrated.

Table 2.2 Compositions of various stainless steel grades used for rebar (%wt).

Grade	**UNS No.**	**Cr**	**Ni**	**Mo**	**C (max.)**	**N**	**Type**
304	S30400	19	9.5		0.08		austenitic
304L	S30403	19	10		0.03		austenitic
316	S31600	17	12	2.5	0.08		austenitic
316L	S31603	17	12	2.5	0.03		austenitic
316LN	S31653	17	12	2.5	0.03	0.13	austenitic
2205	S31803	22	5	3.0	0.03	0.14	duplex

Commonly used 7-wire strand (that may be suitable for prestressing) are scarce. Therein, the relatively few grades of stainless which are readily commercially available are typically restricted to types 316 and 302. Some duplex products are available as a high

strength wire although uncommon; likewise with almost countless composition combinations specialty strands can be obtained that provide higher strength and better corrosion resistance, but at significant added cost before a large enough market develops. Tables 2.3 and 2.4 provide strength and composition information, respectively, for readily available stainless steel strands (Wire World, 2009).

Table 2.3 Strength of various stainless steel strands.

Size	Wires	Grade	Min Break Strength (lbs)	Weight per 1000 feet
1/2"	1x7	302	33700	535 lbs
1/2"	1x7	316	30200	535 lbs

Table 2.4 Compositions of various stainless steel strand (% by wt).

Alloy	C (max)	MN (max)	Cr	Ni	P	S	Si	Mo
302	0.15	2	17.00/19.00	8.00/10.50	0.045	0.03	1	
316	0.08	2	16.00/18.00	10.00/14.00	0.045	0.03	1	1.00/3.00

Two austenitic stainless steels, Grade 316 and XM-29 and one duplex stainless steel, Grade 2205 were evaluated in this project following consultations with industry based on their corrosion resistance, suitability, cost and availability.

2.2.1 Previous Research

Case Studies

Stainless steel reinforcement in concrete has been largely applied to reinforced applications; some dating back to the 1930's. Prestressed concrete being a younger technology has been less used, accordingly.

Reinforced Concrete. Numerous applications of stainless reinforcing steel have documented the merits of stainless rebar (Table 2.5). These cases cite the use of austenitic stainless steel (Grades 302, 304 or 316), solid or stainless-clad bars, and more recently duplex grade 2205 (22% Cr / 5% Ni). In most cases, stainless steel was used to minimize the effects of de-icing salts in decks. Initial construction costs have been reported to be 6 to 16% higher than carbon steel alternatives depending on the degree of stainless steel replacement (McDonald, 1995).

Table 2.5 Stainless steel case studies w/rebar (Tullman, 2009a; Wikipedia, 2009).

Application	Description	Comment
Marine Pier, Progreso, Yucatan	2.1 km pier constructed 1937-41 using type 304 stainless rebar. No major repairs or significant maintenance over lifetime of this structure	Neighboring pier constructed in the 1960's using carbon steel 200m west of the structure severely deteriorated
I-696 Bridge Decks, Detroit, MI, 1985	Used 33 tons of Type 304 rebars	Exposed to de-icing salts. Cores taken after 9 years showed bars to be in excellent condition
I-295 Bridge Deck, Trenton, NJ, 1985	Used carbon steel rebars with external cladding of Type 304	Condition of clad rebars was excellent despite exposure to de-icing salt
Highway 407, Toronto, 1996	Bridge used 11 tons of Type 316LN stainless steel bars	
Brush Creek Highway Bridge, OR (1998)	More than 75 tons of type 316LN stainless rebar used	
Ramp, Garden State Parkway, NJ, 1998	165 tons of 2205 duplex stainless steel rebar used	
Smith River Bridge, OR, 1998	125 tons of type 316LN rebars used	
Ocean Parkway Belt Bridge, Brooklyn, NY, Nominated for Nova Award 2008	Stainless steel reinforcing bars duplex 2205. 200 tons of steel used	Life cycle cost indicated 1% increase in total cost associated with an estimated doubling of service life
Stonecutters Bridge, Hongkong, 2008	Duplex 2205 Code Plus Two hot-rolled plate (S32205) to clad the top 120 meters of the towers with a stainless-steel skin. Stainless pipe was selected for cable sheeting. In addition, an S30400 stainless-steel reinforcing bar for concrete piers and main-tower splash zones.	Design for 120 year life
Driscoll Bridge, NJ	Construction of a new eight lane bridge including 28 piers, some over 100 feet tall, and a bridge deck spanning the Raritan River. 1300 tons of stainless rebar (Type 2205 and 316LN) specified.	
Woodrow Wilson Bridge linking Virginia and MD (2007)	1000 tons of stainless steel rebar (Type 2205 and 316LN) specified	

Prestressed Concrete.

There have been relatively few studies on the use of stainless steel for prestressing concrete. In a recently completed doctoral dissertation, Moser (2011) reported that there have been some investigations in recent years, mostly in Europe and limited to austenitic stainless steels.

In earlier studies in the United States, Jenkins 1987; FGE 2009, austenitic stainless steel, Grade XM-29 (aka Nitronic 33) was used because of its magnetic transparency and corrosion resistance that was critically important for the U.S. Navy's operations. Both applications focused on using stainless steel for prestressed piling in a marine environment.

Study by Jenkins

Jenkins 1987 conducted ten series of tests that included those on full-scale carbon and stainless steel prestressed piles driven in the port of Tacoma, WA. Few details are available on the piles; assessment was based on non-destructive electro-chemical measurement followed by forensic examination of regions identified as problematic.

The ultimate strength of the 7-wire strand used is relatively low (136 ksi) compared to what is attainable nowadays (240 ksi). A total of ten series of tests were conducted though no relaxation or stress corrosion testing was carried out. Laboratory scale durability testing indicated that the Nitronic 33 was more durable than carbon steel.

The durability of the full-scale carbon and Nitronic 33 prestressed piles driven in Port Tacoma was monitored for 17 months. The performance of the two materials was found to be statistically identical. Forensic examination revealed that corrosion had occurred only in the carbon steel wire tie that was used to bind the stainless steel prestressing strands. There was no corrosion damage in the Nitronic 33 stainless steel prestressing strands. Stainless steel tie wire was used for this study (Chapter 5) in response to this possibility.

Pearl Harbor Project

The Navy Submarine Drive-in Magnetic Silencing Facility in Pearl Harbor, Hawaii (Figure 2.1) used stainless prestressing strands. As implied by the project name, the main motivation for using stainless steel strands was to eliminate all magnetic materials. To that end, even local concrete aggregate were not used as it is igneous making the nearest "convenient" source of non-magnetic aggregate Guam. The cost of the piles is unknown, but based on the extenuating circumstances involving both imported aggregate and stainless steel reinforcement with low magnetic permeability, estimates are near $500/ft. The selected strand material was ASTM XM-29, also called Nitronic 33, which is capable of maintaining low magnetic permeability even after extensive cold working. This strand was manufactured in Sanderson, FL by Insteel, Inc.

The octagonal piles were 24 in. in diameter and 26 – ½ in Grade 240 Nitronic 33 stainless steel strands were used. Pile lengths range from 72 to 195 ft with ultimate capacities between 400 and 800 kips. Due to long lengths in some areas, some piles have been outfitted with 8 – 80 mm corrugated plastic dowel tubes for splicing (FGE, September, 2009).

Figure 2.1 Navy Magnetic Silencing Facility shown during construction in Pearl Harbor using 24” octagonal piles prestressed with 26 - ½”, 240 ksi austenitic stainless steel strands (Courtesy Foundation & Geotechnical Engineering, Plant City, FL).

Georgia DOT

Recently, the Georgia Department of Transportation funded a study to explore the feasibility of using stainless steels in prestressed applications, Moser 2011, Moser et al. 2013. In that study, six different stainless steels were evaluated: two austenitic (Grade 304, 316); three duplex (Grade 2101, 2205, 2304) and one precipitation-hardened martensitic grade (Grade 17-7).

The study investigated mechanical behavior, stress corrosion and production of stainless steel prestressing strands. Mechanical properties and stress corrosion characteristics were established from tests using 0.16 in. (4 mm) dia cold drawn wires. Based on results of 200 hr relaxation tests at 70% of the ultimate tensile strength, the 1000 hr relaxation loss was predicted to be between 6% and 8% of the initial stress.

All steels showed excellent chloride resistance but poorer carbonate resistance. Grade 2205 was found to be not susceptible to stress corrosion but to hydrogen embrittlement. The latter is only possible in the event of excessive cathodic protection.

Duplex grades 2205 and 2304 were identified as optimal for prestressing application based on both strength and corrosion resistance.

2.3 Material Properties for Design

The design of prestressed elements requires information on the mechanical properties of the prestressing material and also of the prestressed concrete element. Mechanical properties are relevant for setting limits for the stressing operation, for calculating prestress losses, evaluating ductility and estimating ultimate capacity. Properties of the concrete element are required for determining transfer length and development length.

2.3.1 Stress-Strain

Moser et al. 2013 determined the engineering stress-strain curves for the six materials tested. These are reproduced in Figure 2.2. These plots were obtained by testing a single 0.16 in. diameter wire (comparable to the diameter of a single wire in a 0.5 in. prestressing strand). They reported that for carbon steel, the material properties of the strand can be derived from those of wire tests by taking a 1.5 per cent reduction.

Inspection of Figure 2.2 indicates that stainless steel has a non-linear stress strain variation even at relatively low stresses. Its modulus and ultimate stress are lower.

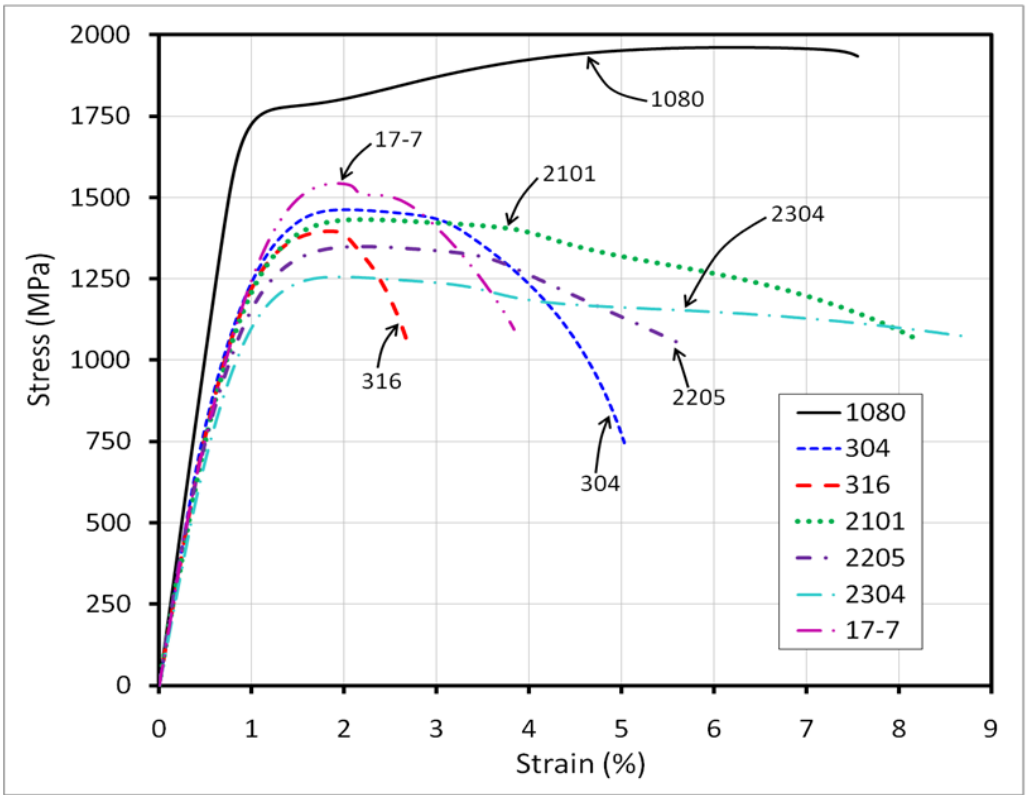

Figure 2.2 Stress-strain behavior of high strength stainless steel compared to carbon steel based on 4 mm wire (Moser et al. 2013).

2.3.2 Relaxation

Relaxation is the loss of stress in a material under constant stress and held at a constant strain. The prestressing industry uses low-relaxation carbon steel. This is produced using thermo-mechanical heat treatment but it requires the steel to be ferromagnetic.

Moser et al. (2013) determined the relaxation loss for six different stainless steel 0.16 in. diameter wires at a 70% ultimate stress level and compared them with that of carbon steel. Those results are reproduced in Figure 2.3. They show that the stress relaxation for stainless steels is 3 to 4 times higher than carbon steel. This was because the carbon steel tested was low-relaxation steel that had undergone thermo-mechanical heat treatment unlike the stainless steel where it is only possible for duplex stainless steels that are sensitive to magnetism. For austenitic stainless steels, pre-forming methods have to be used in which the load is applied and released a number of times to offset relaxation losses. This procedure was used in this study in the experimental tests reported in Chapter 4 that were repeated in the field fabrication reported in Chapter 5.

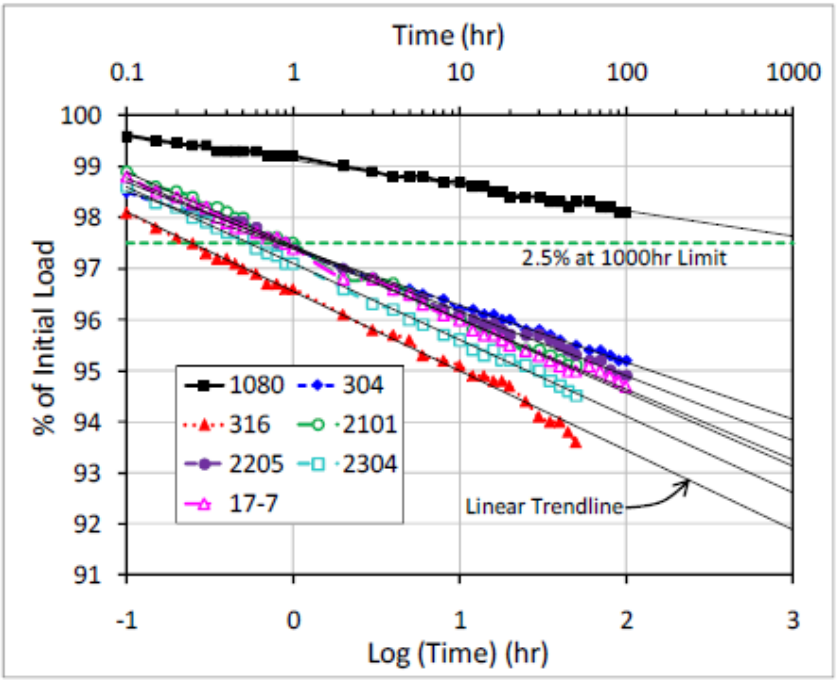

Figure 2.3 Stress relaxation at an initial stress of 70% of ultimate (Moser et al. 2013).

2.3.3 Transfer Length

Transfer length is the distance over which the prestressing force in pretensioned members is fully transferred to the concrete by bond. This parameter is important because stresses at release are generally checked at the transfer length location.

The transfer length depends on many factors, e.g. size and tendon type (wire or strand); surface condition (smooth or deformed); method of transfer (sudden or gradual); concrete

strength and confinement (Naaman 2012). As a result, measured transfer lengths show a large scatter ranging from 50 to 160 times the diameter of the tendon.

The AASHTO code (2010) specifies that the transfer length can be taken as 60 times the diameter (Section 5.11.4.1). Thus, for the ½in strands used in this project the design transfer length is ½ x 60 = 30in. This distance was used in deciding the layout and extent of the strain gauge placement to experimentally determine the transfer length of the stainless steel prestressing strands described in Chapter 5.

2.3.4 Development Length

Development length differs from transfer length as it is the length required to fully develop the strand ultimate capacity. This generally refers to the length a strand must be embedded in concrete so that it can develop its full tensile capacity for the purposes of moment capacity. Since stainless steel has a lower ultimate tensile strength compared to carbon steel the required development will be commensurately smaller. This is not being investigated in this study.

2.4 Corrosion Resistance of Stainless Steels

Despite the additional cost of stainless steel, it is commonly perceived that the life span of steel reinforced or steel structures can be increased virtually indefinitely through the use of stainless steel. The higher initial cost is simply amortized over the life of the structure to justify the additional cost. Unfortunately, this is not always true. In high temperature scenarios, and or container/structures in caustic materials stainless steels have been shown to be vulnerable to the same forms of degradation. However, in more mild ambient temperature conditions catastrophic failures can also occur.

In the literature, stainless steel types including SS316 were found to be susceptible to low temperature stress corrosion cracking (SCC). SCC occurs when the combined effects of stress and corrosion result in greater loss of strength than when stress and corrosion act separately. SCC is the conjoint action of stress and a corrosive environment which leads to the formation of a crack which would not have developed by the action of the stress or environment alone.

Two case studies dealing with stress corrosion cracking involving indoor swimming pool ceilings are summarized: one occurred in Uster, Switzerland (1985) and the other in Steenwijk, Netherlands (2001). In both incidences, the load bearing components were in tension with significant chloride deposits. The average temperature was kept at approximately 30C (86F) which was significantly lower than the high temperatures >50C (122F) at which stress corrosion cracking is more widely known to occur. The relative humidity fluctuated above and below the chlorides' deliquescence point which allowed the chlorides to concentrate repeatedly (Iversen, 2009). Another factor that contributed was the inaccessibility of the connectors to be cleaned or examined. In the Switzerland collapse, a brittle failure occurred at 94 of the 207 connectors examined. Switzerland

(Swiss Society of Engineers and Architects) and Germany (Federal Republic of Germany) further researched the types of stainless steels susceptible to low temperature stress corrosion cracking. Many other grades of stainless steel (including SS316) were found to be inadequate in such harsh environments. They and other authors have asserted that only stainless steels with high molybdenum (7%) are sufficient for the aggressive environment found in the indoor swimming pool atmosphere (Iversen, 2009 and Faller, 2003).

Figure 2.4 Suspended ceiling collapse of Uster swimming pool caused by transcrystalline stress corrosion cracking (Faller, 2003).

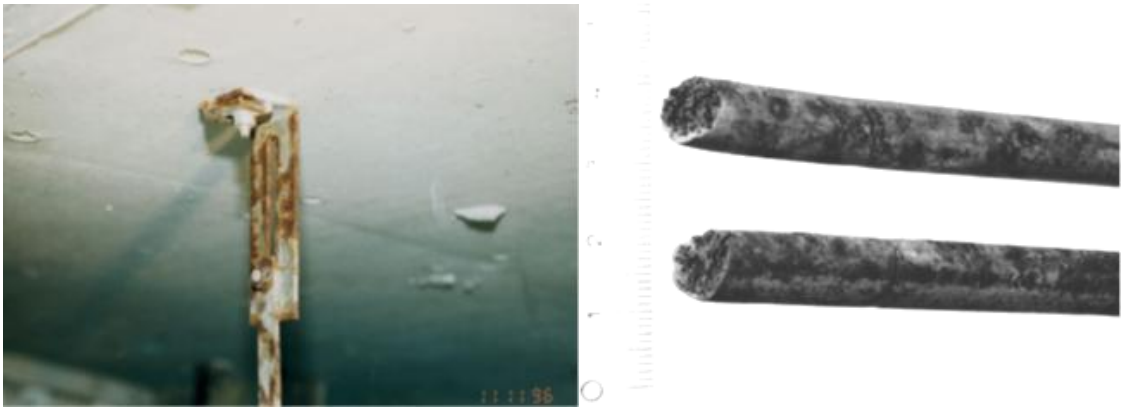

Figure 2.5 Corrosion damage to stainless ceiling connections, left; corrosion cracks and brittle failure of 304 ceiling rods, right (Iversen, 2009).

Wu and Nürnberger (2009) studied SCC in high-strength stainless steels for use in prestressed concrete structures. Their work focused on the 300 series austenitic stainless steel alloys cold-worked to high-strength. Partial testing of a duplex stainless steel was also included, but no manganese substitute stainless steel alloy was considered. The austenitic alloys (UNS #S30400, S31600, S31653, and S31753) were tested at three pH regimes (4.5, 8.5, and 12.1) at temperatures from 30C to 80C. During those tests, SCC occurred in all of the steel alloys at 80C at all pH conditions. At 60C, only UNS# S30400 and S31600 experienced SCC within 20,000 hours and in the case of UNS# S31600, this was only at pH 4.5. Increased susceptibility to SCC occurred when either the pH was decreased, or the temperature was increased. UNS# S31753 performed better than the other alloys. The authors also evaluated prestressed piles fabricated using strands made of UNS# S31600, S31653, and S31753 alloys. The testing time in concrete with chloride solution added onto the piles, to simulate de-icing cycles, was 2.5 years with no signs of corrosion after that time. The findings supported the satisfactory use of UNS# S31753 stainless steel alloy as prestressed strand material for concrete construction.

Later work by Sanchez (2007) used the work of Nürnberger as a starting point and expanded upon those initial tests. Sanchez focused on the Arrhenius relationship between crack growth rate and inverse temperature as it relates to the onset of SCC in high-strength steels in a bicarbonate solution. At 25C, the crack growth rate was found to be 1.85E-09 m/s for cold drawn steel and 1.74E-09 m/s for modified parent pearlitic steel.

Moser (2011) used not only the work of Nürnberger, but many others as a basis for his work. Moser analyzed UNS # S30400, S31600, S31653, S32101, S32105, S32304 and S32205 and compared them using Slow Strain Rate Testing (SSRT) in varying concentrations of Cl^- to determine the best candidate high-strength stainless steel among those evaluated. The testing included both alkaline and carbonated solutions with Cl^- molar concentrations ranging from 0.25 to 1.0. The results showed pitting in the alloys with less Cr (S30400 and S32105) at lower Cl^- concentrations while S32205 showed the best corrosion resistance even in carbonated solution at 1.0M of Cl^-. Corrosion detected was in the form of pitting corrosion, with more pitting at either higher Cl^- concentrations or lower pH (Carbonated solution versus alkaline solution).

Although much is known about stainless steels and their performance in various environments, there are very few case studies where stainless steel was used as prestressing steel. Therein, the effects of high pH pore fluid environment of concrete and the limitations in ultimate strength must be addressed. The primary focus of this study was to identify both the physical and electrochemical effects of using stainless steel in precast piles with the ultimate goal of increasing the service life to 75 – 100 years.

Intentionally Left Blank

Chapter 3: Corrosion Testing

3.1 Supplied Material Specifications

The three alloys tested for corrosion resistance were 316, S24000, and S32205 (common names 316L, XM29 and 2205, respectively). The materials tested were sourced from three different manufacturing companies. The 316, 7-wire strand was supplied by National Strand Products Company in Houston, TX, the XM-29, 7-wire strand was supplied by the Insteel Wire Products Company[(a)] in Sanderson, FL, and the 2205 single wire was supplied by Carpenter Steel (Carpenter Technology Corporation)[(b)] in Houston, TX. 2205 material was later received in strand form from Sumiden in Tennessee for the relaxation and transfer length testing discussed in Chapters 4 and 5, respectively.

The diameters of each alloy wire were as follows: 4.36 mm (0.171 inches) for 316, 4.47 mm (0.178 inches) for XM-29, and 4.56 mm (0.179 inches) for 2205. Their yield strengths as reported by the manufacturers were: 1.24 GPa (180 ksi), 1.59 GPa (230 ksi), and 1.59 GPa (230 ksi) for the 316, XM-29 and 2205, respectively. These values are discussed in more detail in *Chapter 4 Mechanical Properties Testing*.

The two main experimental methodologies used were designated as Phases 1 and 2 and are described in the following text. The polarization alternative testing was done as a separate evaluation from both phases and is also described below.

3.2 Phase 1 - Multiple Temperatures, $MgCl_2$ solutions

In Phase 1, the supplied material was cut into segments 114 mm (4.5 inches) in length, unwound from a 7-wire strand to use only one of the wires from the strand (only for 316 and XM-29 as 2205 was supplied in a single wire form), and inserted into a three-point bending frame. As shown in Figure 3.1, an ~ 2 cm long portion of the wire length on the tension side (in the bending frame) was coated with Magnesium Chloride ($MgCl_2$) crystals that absorbed moisture from the test cell's airspace creating a mixture that was to remain saturated throughout the experiment. A wick was attached (using PTFE tape) to the wire to ensure the solution stayed against the wire throughout the experiment. The three-point bending frame was placed in a small enclosure 12.5 cm long by 5.5 cm wide by 5.5 cm tall (Figure 3.2) containing its own heating element and control thermocouple. The wire was then stressed by use of the three-point bending frame, and heated by a heating element underneath the frame.

The amount of stress applied to each specimen by the applied turns was calculated to be 1.15 GPa (167 ksi), 1.43 GPa (207 ksi) and 1.38 GPa (200 ksi) for the wires of alloy 316, XM-29 and 2205, respectively. This corresponded to 93%, 90%, and 87% of the yield strength of each alloy, respectively (Davis, 1994 and AK Steel, 2007).

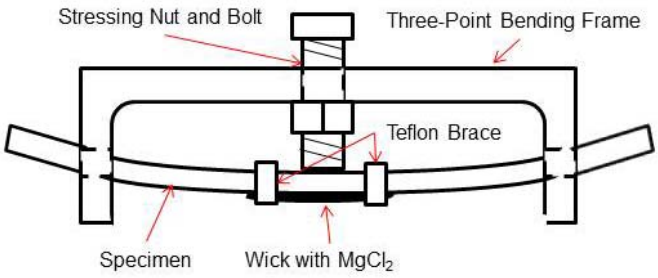

Figure 3.1 Diagram of Bending Frame

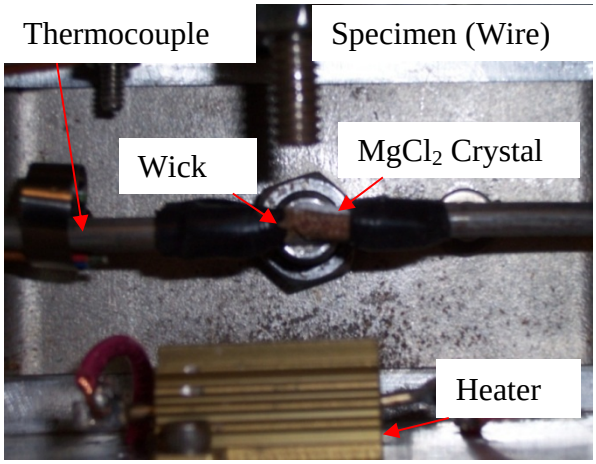

Figure 3.2 Small Enclosure (Bending Frame, Thermocouple, and Heater).

The small enclosure was in turn placed in the air space of a larger enclosure (Figure 3.3) that had deionized (DI) water placed at the bottom which was heated (by a heater underneath the large enclosure) to a temperature (T_1) corresponding to the water temperature needed for the Relative Humidity (RH) to be around 25% in the small enclosure. That RH level promoted the formation of a saturated $MgCl_2$ solution in the wick.

The temperature of the water in the large enclosure was controlled at its power supply. The large enclosure was sealed to minimize the loss of water and ensure the air space above the water was at the appropriate RH. The temperature of the wire (T_2) was measured by a thermocouple attached to the wire inside the small enclosure. This thermocouple output also controlled the heating element in the small enclosure through a process controller connected into the power loop of the heater. This setup caused the airspace in the small enclosure to be at a different RH (RH_2) than the rest of the large enclosure (RH_1).

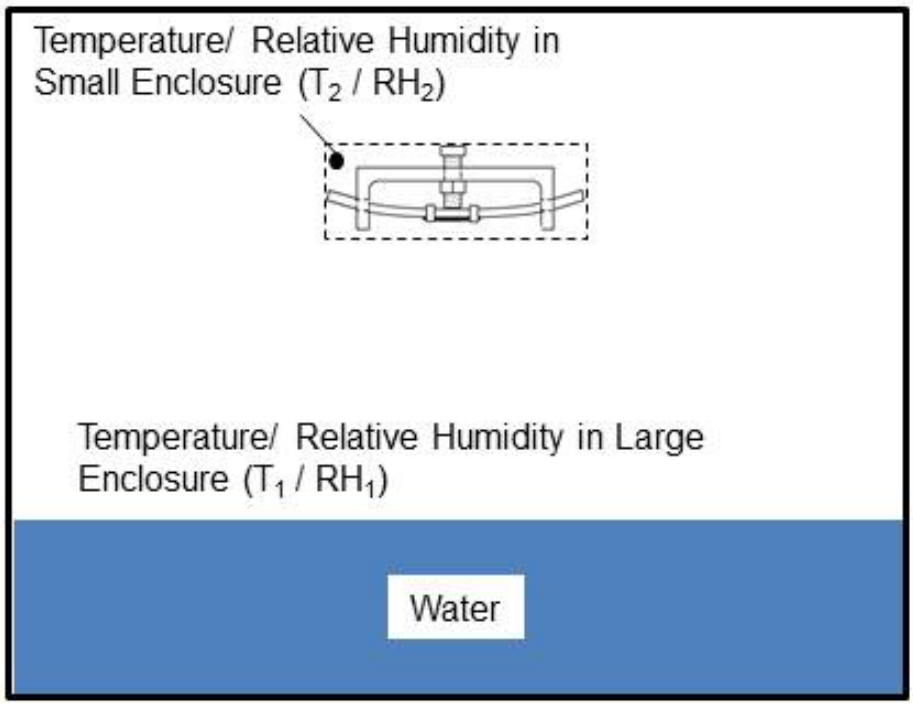

Figure 3.3 Diagram with Test Setup Process Parameters.

3.3 Phase 2 - 60C, Simulated Concrete Pore Solution with Cl^-

For phase 2, the alloys provided were cut down to 178 mm (7 inches), unwound in the case of 316 and XM-29 7-wire strands (Only the center wire was used for this phase). After cutting, the specimens were briefly (~< 1min) exposed to a 1M nitric acid solution to clean off any low alloy steel particles that may have been embedded on the surface from the cutting process, degreased using ethanol, and rinsed with DI water. Six specimens of each of the three alloys were tested in phase 2 (for a total of 18 specimens with specimens #1 through #6 being UNS# 31603, #7 through #12 being XM-29 and #13 through #18 being 2205).

Once cleaned, each specimen was placed in a bending jig, and bent into a "U" bend. Stainless steel plates then placed onto the specimens to hold to them in the "U" bend (Figure 3.4a).

Measurements of the amount of spring-back each specimen displayed after bending were taken prior to being placed into the test chamber. These measurements provided an additional way by which to determine if SCC occurred in the specimens and not just pitting corrosion. If the specimen after testing did not spring-back as much as before the test, then this reduction in spring-back would be a sign that the material had experienced cracking

The potentials of each of the 18 specimens were recorded using an activated titanium reference (ATR) electrode. The electrode was periodically calibrated against a saturated calomel electrode (SCE) but was permanently placed in the solution and wire connections to each of the specimens (through the air-tight fittings in the test chamber wall) were made to a connector box with contacts for each specimen. A significant drop in the potential of a specimen was used to indicate that corrosion was occurring in that specimen. As this method of detection did not discriminate between types of corrosion, a secondary method of differentiating whether or not it was SCC was necessary.

For phase 2, specimens of each type of stainless steel were placed in a large container (12 inches inside diameter and 15 ½ inches tall) in a solution that contained 15% by weight Cl^- ($NaCl$ added to the solution in a sufficient quantity to reach that level of Cl^-), NaOH, KOH, $Ca(OH)_2$, and pure water to simulate concrete pore water (Cui 2006; Baumeister 1958; Weast 1973-74). The simulated pore water solution (SPS) was created following the base solution composition shown in Table 3.1.

Table 3.1 Solution Composition for 15 wt% Cl and SPS Solution.

Chemical Composition (g/L) and pH Values of Model Solutions							
	$Ca(OH)_2$[(A)]	NaOH	KOH[(B)]	Na_2CO_3	$NaHCO_3$	pH[(C)]	pH[(D)]
SCS	2.0	-	-	-	-	12.6	12.0
SPS	2.0	8.33	23.3	-	-	13.6	13.0
CPA	-	-	-	4.21	2.66	9.7	8.6

(A) Most of the $Ca(OH)_2$ was not dissolved.
(B) Reagent-grade KOH had a purity of only 85.3%.
(C) Before addtopms pf Cl.
(D) With 15% Cl.

Therefore, 8.33g of NaOH, 23.3g of KOH, and 2g of $Ca(OH)_2$ were added per liter of solution desired (per Table 3.1). NaCl was added to obtain a final 15% by weight Cl^- content. The solution had pH between 13 and 13.5. As the SPS solution when exposed to atmospheric conditions tends to drop in pH especially at higher temperatures (due to carbonation), the testing chamber was covered with a rubber sealed lid to minimize the interaction with atmospheric CO_2 and possible decrease in pH as a result. Periodic pH measurements confirmed that it remained above 13 throughout the test.

A process controller maintained the temperature of the solution within the container typically within 5C of the target value (60C). Two calibrated thermocouples were placed at two different points in the solution to ensure uniform temperature measurements of the solution. All wires for potential and temperature measurements went through air-tight fittings in the wall of the enclosure to maintain the air-tight seal. The entire setup was externally insulated to assist in maintaining temperature uniformity inside the test cell and is shown in Figures 3.4b and 3.5.

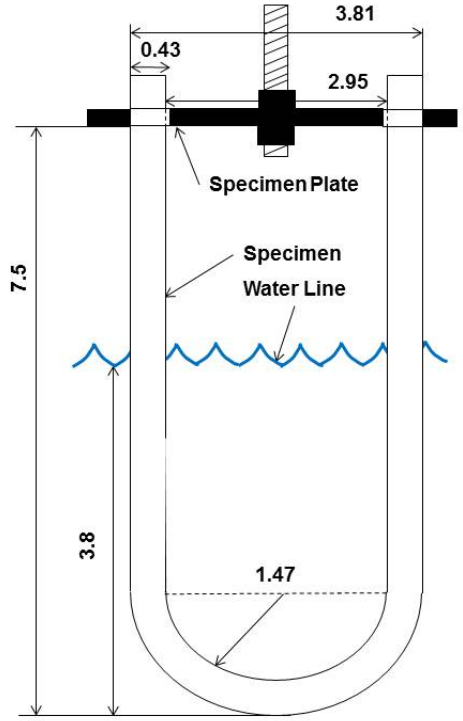

Figure 3.4a U-Bend Specimen Configuration (units in centimeters).

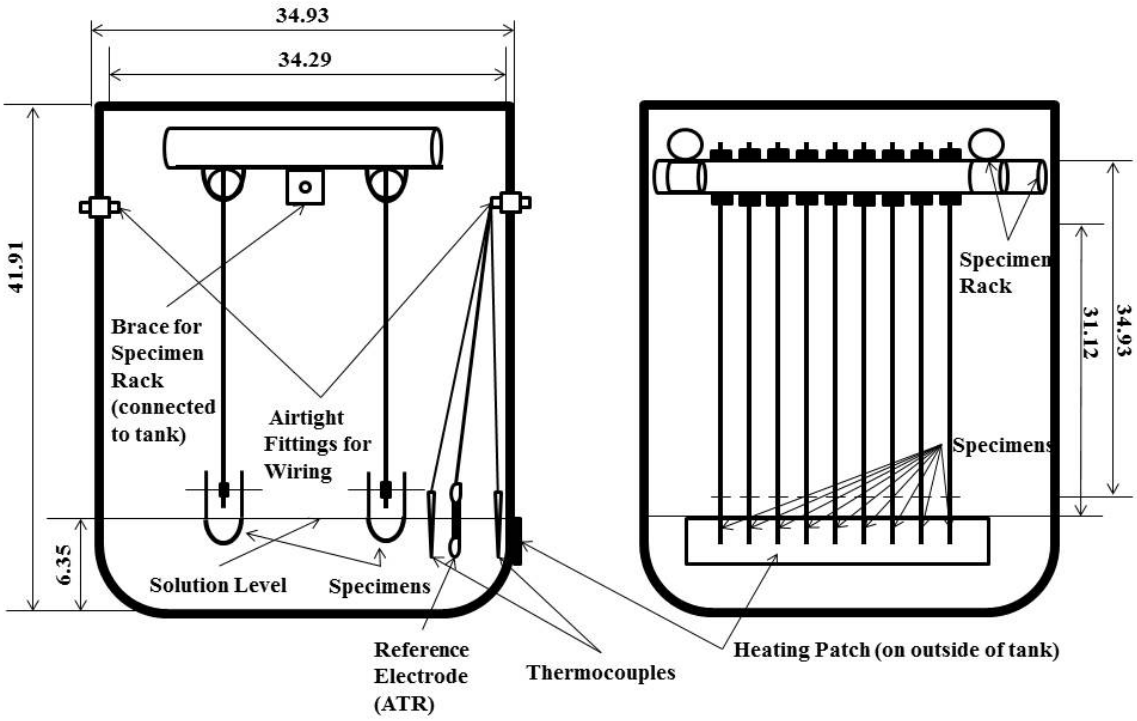

Figure 3.4b Diagram of Phase 2 Setup (units in centimeters).

Figure 3.5 Picture of Phase 2 Setup.

3.4 Anodic Polarization of Selected Specimens

After 2160 hours of testing in phase 2, anodic polarization was imposed on selected specimens using a multiple potentiostatic device. The objective of the increased polarization was to act as a test accelerator to induce SCC directly or by promoting pitting that then would increase local stress intensity and initiate cracking. Three specimens of each type of alloy were polarized to a potential that was 100 mV higher than the average Open Circuit Potential (OCP) recorded shortly beforehand for each individual specimen. After 1900 hours of polarization, the polarization was increased an additional 100 mV. After 2000 hours at the higher potential, the polarization was increased again by 100 mV. Finally, after 1300 hours at the new higher potential, the polarization was increased yet again (to 400 mV higher than the initial OCP), and the specimens were exposed for an additional 2200 hours.

3.5 Corrosion Test Results

3.5.1 Phase 1

Figure 3.6 summarizes the results of the tests done on all three alloys. An SCC cracking event was declared if cracks were observed on the surface of the specimen by magnified visual inspection at the time of experiment conclusion. If no cracks were visually apparent in the specimens while still placed in the stressing frame, the specimen was removed, bent further to a hairpin shape with an inner radius of ~ 7 mm and examined again. If cracks were visible in that condition a "cracked" or SCC event was declared as well. A "not-cracked" event was declared otherwise.

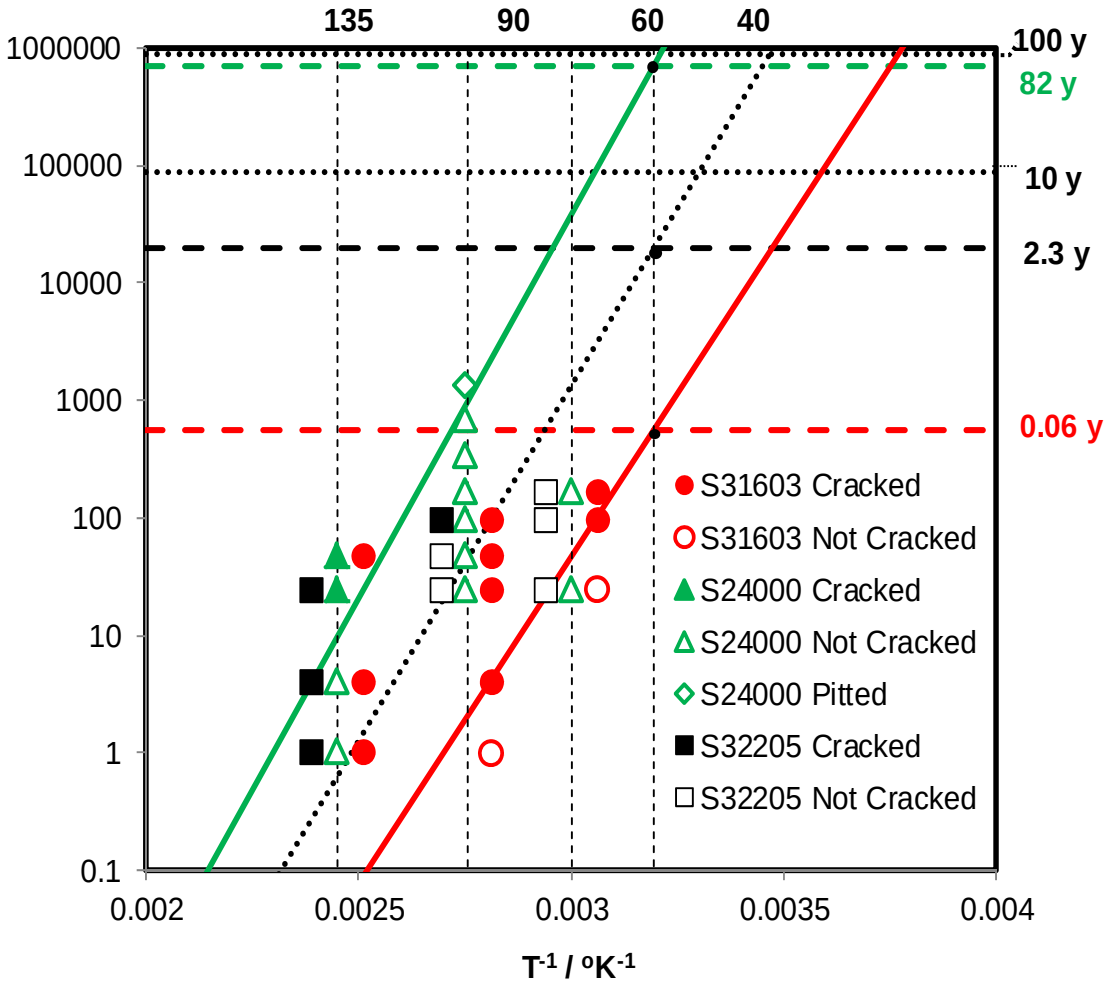

Figure 3.6 Graph of exposure time (Log Scale) indicating test outcome as function of inverse absolute temperature.

SCC occurred in all three alloys tested. Only alloy 316 experienced cracks at 60C (140F). Some data was offset left and right for display clarity. Sloping lines indicate

Arrhenius abstraction of the results using estimated activation energies (Q). Estimating Q was performed by using a time for cracking assigned as the halfway point between the earliest *cracked* observation and the latest *not-crack* condition. The data obtained allows estimation of an apparent activation energy for 316 and XM-29, Q ~ 72 kJ/mol (left green line) and ~ 81 kJ/mol (right red line), respectively. The quantity of data for alloy 2205 was not sufficient to establish a cracked / not-cracked transition so one was established only at 90C (194F). The middle dotted line was traced using the working assumption that Q for that material was comparable to that of 316 and XM-29. Nominal time to SCC at 40C was obtained for each material by extrapolation. The 10 year and 100 year markers are shown for contrast. Extrapolation of those trends would suggest that at 40C (an estimated service temperature extreme for prestressed piles) cracking time would be in the order of one week for 316, a few years for 2205, and 80 plus years for the XM-29. In this test, XM-29 performed the best followed by 2205 and lastly 316.

One indicator that SCC has occurred rather than another form of corrosion or mechanical failure is the branching of cracks that lead to failure. Branching cracks that are transgranular are a clear sign that the failure mechanism was SCC rather than failure due to pitting corrosion causing the loss of cross section. Figures 3.7a, 3.7b, and 3.7c show the surface cracks (circled for clarity) on a specimen of 316 tested at 60C for 168 hours, a specimen of XM-29 tested at 90C for 1344 hours, and a specimen of 2205 tested at 135C for 1 hour. Figures 3.8a, 3.8b, and 3.8c show the metallographic cross-sections of those specimens with branching cracks that cut across the grain boundaries (the grains are stretched into thin strips due to the cold working process, with the drawing direction vertical for Figures 3.8a, 3.8b, and 3.8c and as shown clearly in Figure 3.8c).

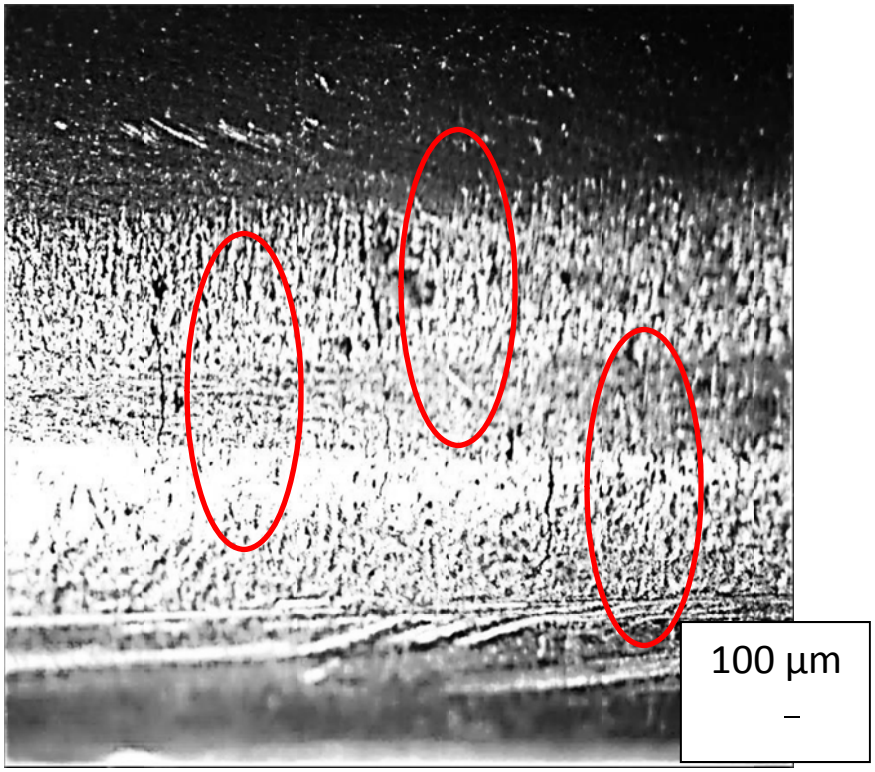

Figure 3.7a Picture of SCC at Surface of Cracked 316Specimen - Phase 1.

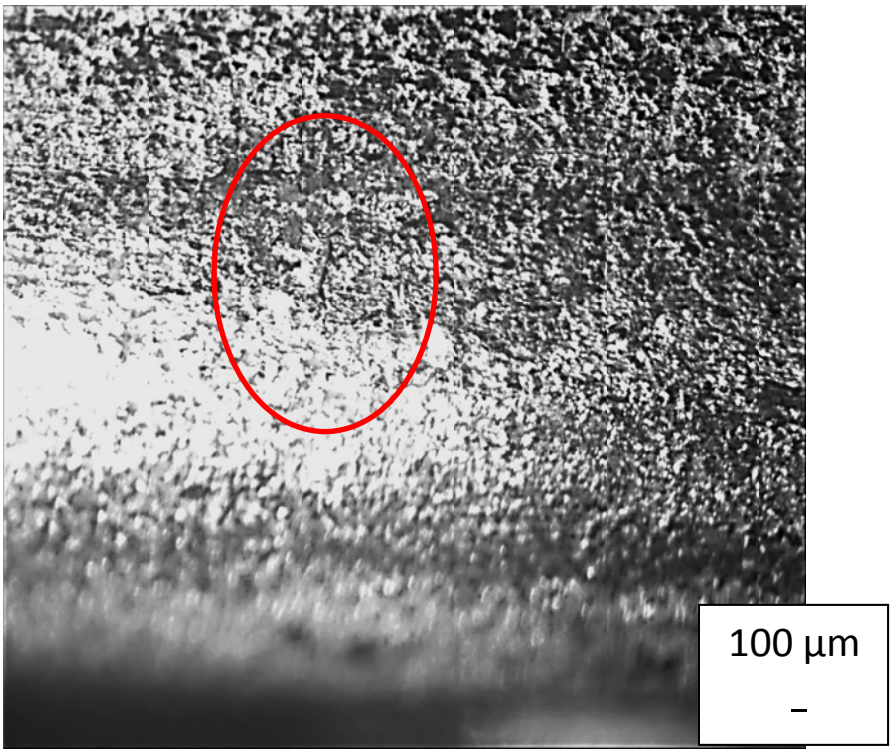

Figure 3.7b Picture of SCC at Surface of Cracked UNS # S24000 Specimen - Phase 1.

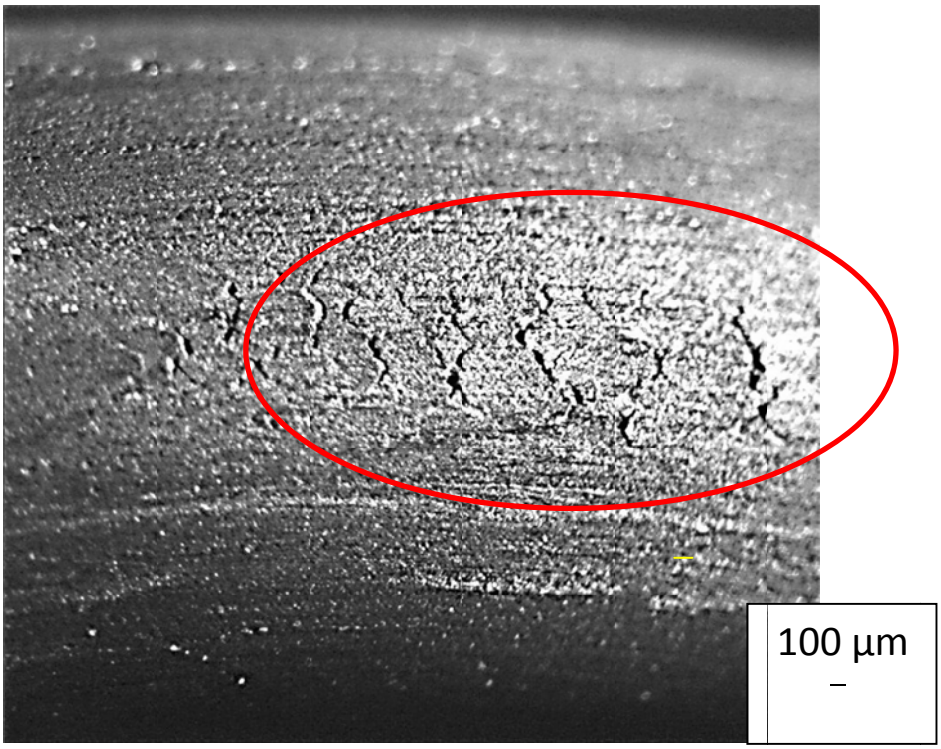

Figure 3.7c Picture of SCC at Surface of Cracked UNS # S32205 Specimen - Phase 1.

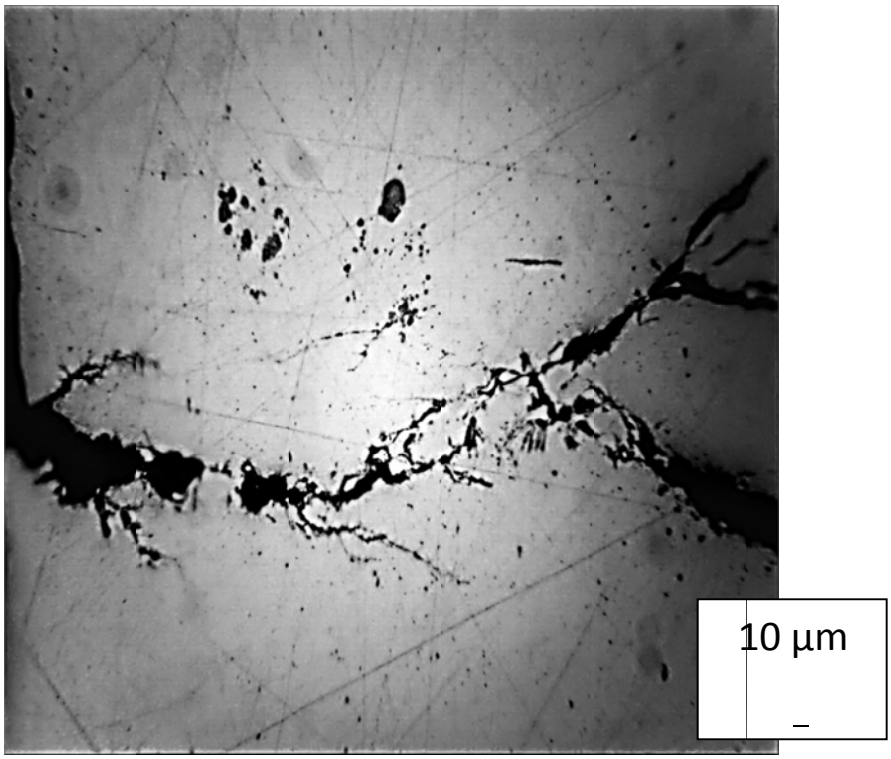

Figure 3.8a Metallographic Cross-Section of Cracked 316 Specimen - Phase 1.

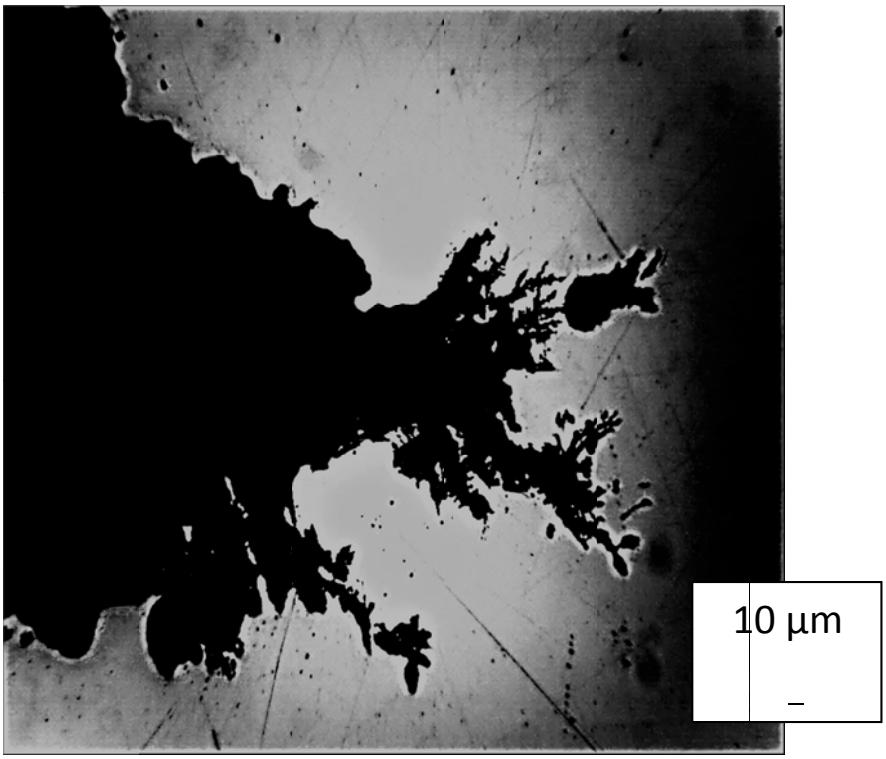

Figure 3.8b Metallographic Cross-Section of Cracked XM-29 Specimen - Phase1.

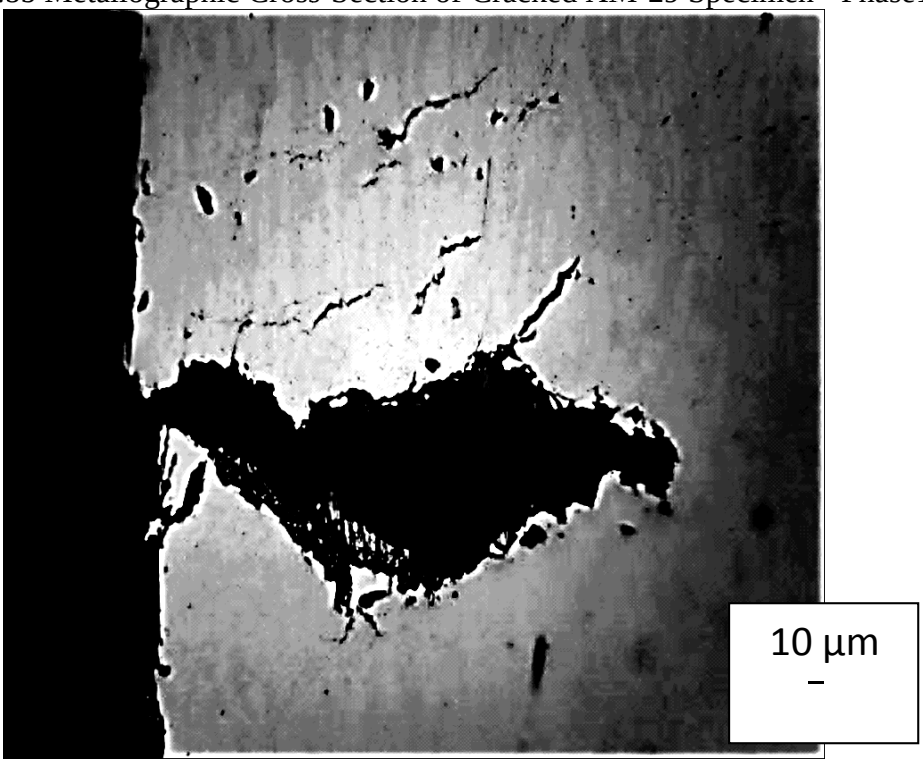

Figure 3.8c Metallographic Cross-Section of Cracked 2205 Specimen (The austenitic phase are shown as the light regions while the ferritic phase as the dark regions) - Phase 1

3.5.2 Phase 2 - Initial Stage

Figure 3.9 displays the potential range (highest and lowest valued) as function of time measured in the multiple specimens of each alloy evaluated for the initial 2160 h test period. This display form was used for clarity given the large number of specimens involved. None of the specimens of any alloy (18 specimens total) showed signs of corrosion after 2160 hours. None of the potentials dropped to below -300 mV versus SCE, and most potentials stayed under -100 mV versus SCE. All alloys performed equally well in this stage of the test.

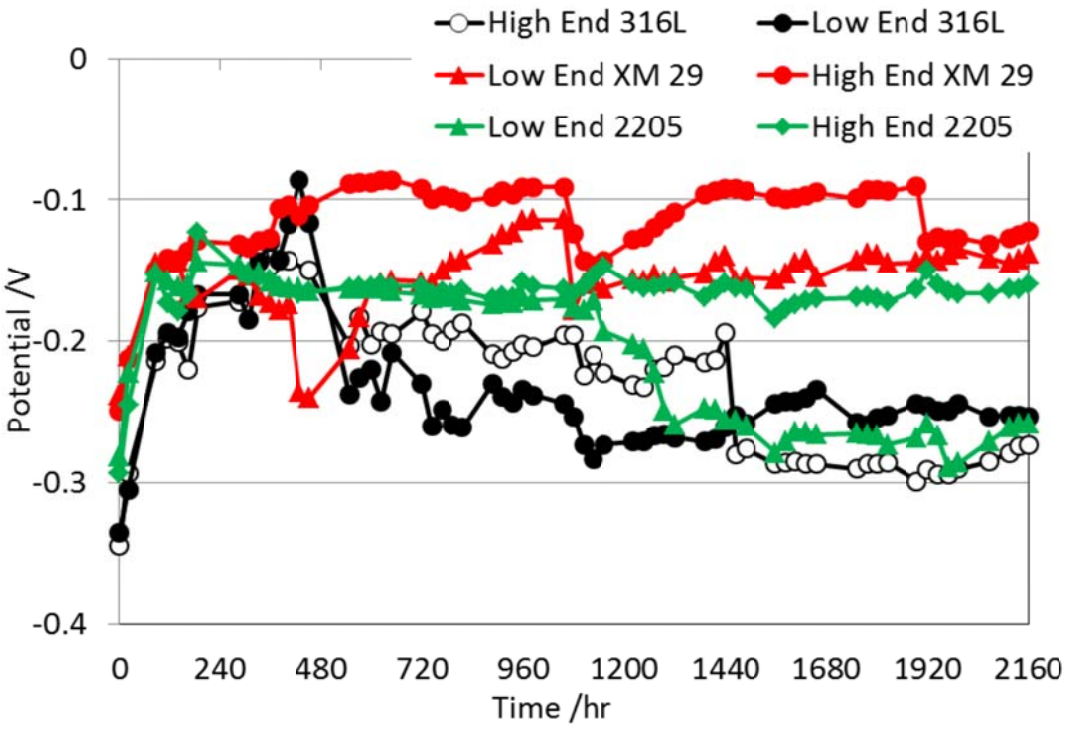

Figure 3.9 Potential (SCE scale) versus Time during Phase 2 tests at 60^{o}C (140 ^{o}F) for 316, XM-29, and 2205. Initial 2160 hour stage. Specimens #1 through #18.

3.5.3 Phase 2 - Subsequent Anodic Polarization of Selected Specimens

Table 2 summarizes the data obtained during the polarization stage of the tests. Nine of the 18 specimens from phase 2 were polarized, and only 2 of those 9 (both 2205 alloy specimens) did not experience pitting or SCC during the polarization time period. Two of the XM-29 specimens (specimens #10 and #11) failed at +100 mV over the initial OCP (IOCP), while the third XM-29 specimen failed at +200 mV over IOCP. All three specimens of 316 failed at +300 mV over IOCP, with specimen #6 left in for ~2.5 weeks

following the initial sign of corrosion. After those ~2.5 weeks, specimen #6 showed clear signs of SCC, while its initial corrosion indication by a spike in the current demand showed only signs of pitting at that time. The pitting evolving into SCC as shown by this specimen confirmed as expected that pitting promoted SCC and that propensity for pitting should be then considered as a derating factor in assessing the susceptibility to SCC of a particular alloy. Only specimen #16 (2205) failed, and that failure started as pitting and was allowed to continue (for ~3.5 weeks) to the stage of SCC at +400 mV over IOCP.

In summary, one 2205 specimen failed only at the highest polarization of +400 mV over IOCP while all three 316 specimens failed at +300 mV over IOCP. All three XM-29 specimens failed at or below +200 mV over IOCP polarization, showing that this alloy had the poorest performance in this test. Therefore, 2205 was considered to have performed better in this test when compared to XM-29 and 316.

A clear indicator of fully developed SCC as opposed to just precursory pitting in these specimens was loss of spring-back. Significant percentage of spring-back loss (~ 30% and above) was deemed to indicate that the specimen has experienced SCC. If there were visual signs of pitting, but the percentage of spring-back loss was below 30%, only pitting corrosion was deemed to have occurred. It is noted that due to minor measurement uncertainty, some specimens showed negative loss of spring-back (increase resistance), but the effect was small when compared to the differences of spring-back in failed specimens.

Table 3.2 Results of Polarization of Select Specimens of Phase 2 and Percent Difference from Final Bent and Relaxed Values.

Specimen # / Alloy UNS#	Final Condition	Percent Difference from Initial Value to Final Spring-back (%)
#2 / S31603	Pitting	-0.79%
#4 / S31603	Pitting	-1.43%
#6 / S31603	SCC	30.32%
#8 / S24000	Pitting	5.87%
#10 / S24000	SCC	48.89%
#11 / S24000	SCC	50.63%
#16 / S32205	SCC[(A)]	18.69%
#17 / S32205	No Pitting /SCC	-16.26%
#18 / S32205	No Pitting /SCC	-1.87%

[(A)] Note: specimen experienced severe deformation from "U"-bend shape.

Intentionally Left Blank

Chapter 4: Mechanical Properties of Strands

The design of prestressed structural elements and specifically piles is dependent on the mechanical properties of the strands, concrete strength and level of effective prestress. With regards to strands, these properties are relevant for setting limits for the stressing operation, calculating prestress losses, evaluating ductility, and estimating ultimate capacity. Although equally important, the properties of the concrete are used to determine transfer length and development length. While a principal focus of this study, transfer length testing is discussed later and forms the basis of Chapter 5; this chapter focuses on the mechanical testing of the strands for yield strength, ultimate capacity, and relaxation.

4.1 Tensile Properties

Tensile testing was a major focal point during this segment of the project. Therein, the exact strength of new strand materials needed to be accurately determined prior to proposing alternate pile reinforcement schemes / designs. To this end, the lower strength of stainless steel (relative to low-lax carbon steel) affects the level of effective prestress or the number of required strands to provide an acceptable level of prestress.

Tensile testing has always been prone to complications associated with the connect details to the specimen. For many applications dog-bone shapes or reduced sections are used to dictate the zone of failure and to minimize or even eliminate stress concentrations. For strands, however, reduced sections are not possible. ASTM A-370-09a, (Standard Test Methods and Definitions for Mechanical Testing of Steel Products), allows for multiple material test gripping mediums to be utilized. Two readily available methods to transform conventional grips for strand applications are the use of aluminum foil wrapping or epoxy coating. Standard testing methods require at least 6in of material to be inserted into the grips, allowing for full transfer of the load to the strand.

In an effort to test strands in standard grips, metal foil was wrapped around the ends of a 24in long strand sample (Figure 4.1) which increased overall diameter making placement in the grips problematic and resulted in a non-uniform grip pressure. Grip slippage became apparent moments after the start of the test. Visual examination revealed the effects of the grip slippage on the strand and its overall dimensions. The teeth on the grips caused small indentations in the material surface, and this paired with slippage resulted in grooving and gross deformation of the test material (Figure 4.2). The deformations in turn caused stress concentrations and premature failure.

Figure 4.1 Placement of foil covered strand in testing jaws.

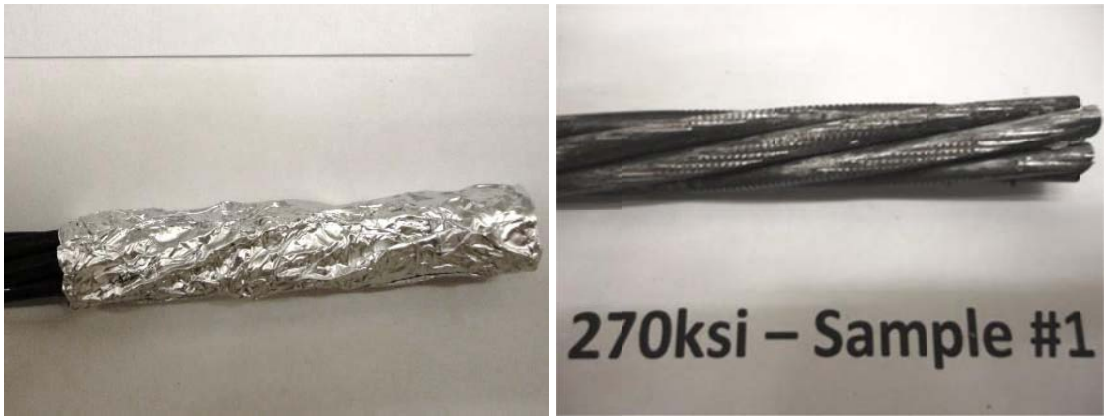

Figure 4.2 Foil wrapped strand end (left); deformations on strand (right).

A second trial specimen was prepared using a two-part epoxy. The ends of the test strand were dipped (Figure 4.3) in *Tyfo® SW-1* epoxy to create a satisfactory medium between the gripping jaws and test specimen. Dripping and running of the epoxy, while liquid, resulted in an irregular cross section. Light sanding was required for a proper fit in the testing jaws. Ultimately, testing of the epoxy coated strand was discontinued due to the availability of the FDOT State Materials Office (SMO) for testing with alternate approved methodologies.

Figure 4.3 Tyfo SW-1 epoxy (top left); mixing two-part epoxy (top rt); strand dipped in epoxy (bot left); epoxy coated strand end (bot rt).

The SMO facility (Figure 4.4) provided the best possible equipment and personnel to aid in the testing where four strand samples (1-XM29, 2-316, and 1-Low-lax carbon steel) were prepped and tested over a two day period (one day for sample preparation and one day for testing). Standard test methods recommend having 3 samples from each material type; however, limited initial material quantities and SMO equipment required a 50in strand for each tensile test making multiple tests impractical at that time.


Figure 4.4 FDOT materials testing lab (left); protective enclosure (right).

A custom built 800 kip Instron Universal Testing System, UTS, (Figure 4.4 and 4.5) was used for all tensile tests. The UTS was equipped with heavy, v-wedge grips (Figure 4.5) and ½in half round inserts. These attachments allow for maximum gripping force and negligible deformation of the strands. Testing required 8 inches of each strand end to be inside the grip/insert assembly. The 8in development length along with the tapered nature of the grips alleviated potential problems with stress concentrations and premature grip failure.

Figure 4.5 Universal Testing System (top left); testing jaws (top rt); tapered ½in half-round insert (bot left); strand in jaws (bot rt).

FDOT technicians initially planned on epoxy coating the ends of the samples to provide a gripping medium, however, after examining the stainless steel strands, FDOT engineers suggested using the more common silicon carbide grit (Figure 4.6) in conjunction with the ½in half round inserts. The combination provided a gripping surface that satisfied the

load requirements while eliminating jaw failure. The silicon carbide had a CAMI grit designation of #80, offering a medium grit that provided an abrasive interface between the strand and the jaws which did not appreciably deform the test specimens. Elmer's glue is commonly used to bond the grit to the sample long enough to be held in place by the jaws.

Figure 4.6 #80 grit silicon carbide powder.

Preparation of test strands:

1) Clean and degrease strands with alcohol.
2) Mix Elmer's glue – water at 1:1.
3) Apply glue mixture to both ends of strand (8" of end coverage required).
4) Liberally apply Silicon Carbide on wet glue.
5) Allow to fully dry 24 hours prior to testing.

Stranding of the XM-29 was prone to unraveling once cut to length (also noted during field testing discussed in Chapter 5). The resulting misaligned wires could result in uneven clamping force in the jaws resulting in stress concentrations and premature failure. The wires were therefore realigned and fastened with a heavy gage tie wire wrap (Figure 4.7). The smooth, almost defect free surface of the 316 strand made adhesion difficult. Therein, the silicon carbide-glue mixture, when dried, was too easily removed from the 316 strand by applying light abrasion (Figure 4.8). Therefore the strands were re-cleaned and a solvent cement was used instead of the Elmer's mixture. This resulted in a more robust bond between strand and grit. Additionally, curvature of the as-shipped stainless steel specimens further exacerbated inadvertent grit removal upon placement into the UTS jaws so care was exercised to minimize damage to the grit fortified surface. For all samples, the modified glue cement worked well.

Figure 4.7 Unraveled XM-29 strand (left) tie wire-restrained XM-29 with silicon grit.

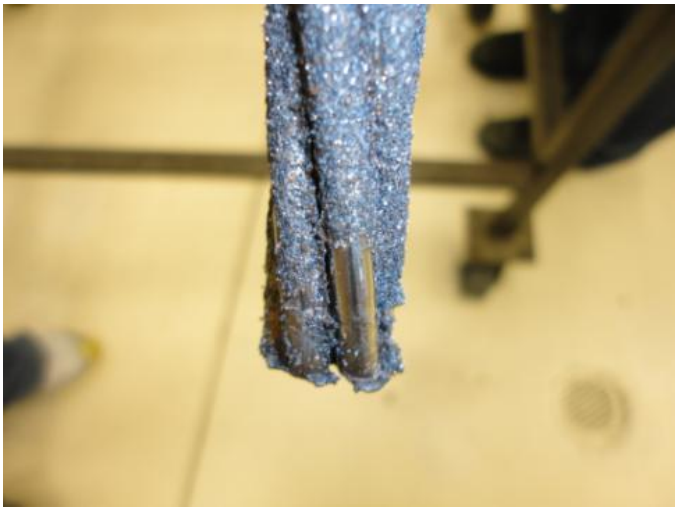

Figure 4.8 Silicone carbide grit easily rubbed off 316 sample.

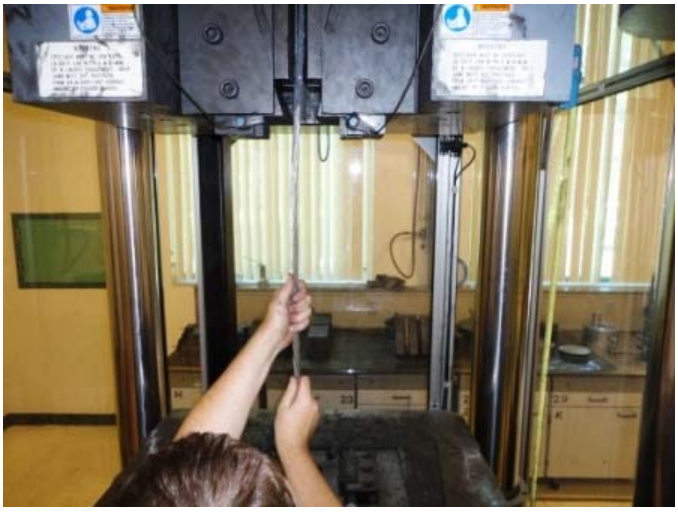

Figure 4.9 Sample carefully placed in jaws to prevent inadvertent grit removal.

The 50in sample length allowed for adequate grip length (8in per end) and room for the placement of a 24in extensometer while providing 5in clear distance between the jaws and extensometer. After placement and initial gripping, a preload of 3000 pounds was applied, helping to align the wires and seat the ends in the grips. Displacement measurements were taken with the 24in Tinius Olsen Type-R-400 extensometer (Figure 4.10). This device calculated strain up to the yield point, was then removed and further readings were collected by displacement of the UTS crosshead. Strands were loaded to failure, defined as the point where "necking" and ultimately, rupture occur. This observed failure mode was indicative of a pure tensile break in the center most portions of the sample confirming no adverse effects from gripping forces (Figure 4.11). The silicon carbide combined with the ½in half-round inserts proved to be effective, leaving no visual signs of material deformation at the grip locations.

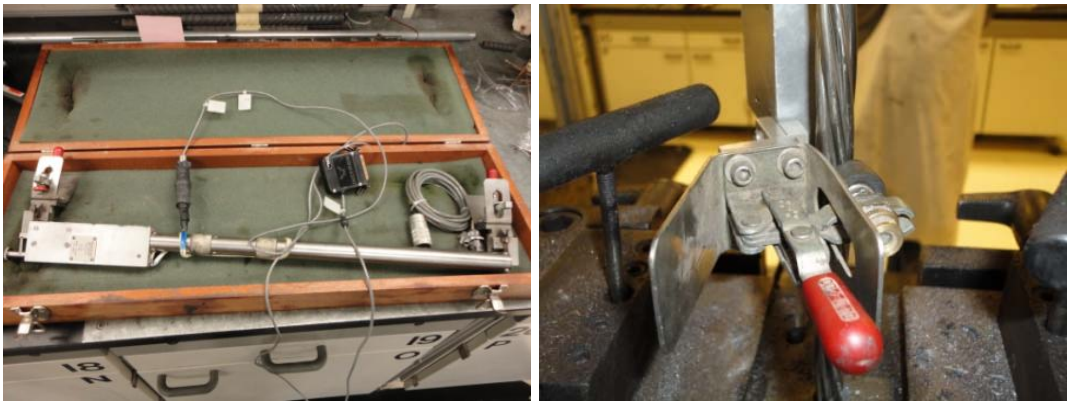

Figure 4.10 24in extensometer (left); close-up of extensometer strand clamp (right)

Plots of the observed stress versus strain relationship (Figure 4.12) show discontinuities around the yield points which can be attributed to the extensometer removal and subsequent collection of displacement by the UTS. The after-break data is included in Figures 4.12 and 4.13 to differentiate from the literature results shown in Figure 4.13. In general, test results from 7-wire strands (SMO) were in close agreement with single wire results cited by Moser, et al. (2011) for low-lax carbon steel. For the 316 which was also tested in both manners, the 7-wire strand showed more elongation and slightly lesser ultimate strength which could easily be a by-product of different suppliers and inconsistent standards for that material. The results of the SMO tensile tests are also shown in Table 4.1. Values of ultimate strength and modulus of the low-lax carbon steel are in close agreement with anticipated ranges. The modulus for both stainless steel grades showed markedly lower values compared to low-lax strand material.

Figure 4.11 Testing after extensometer removal (left); after failure (right).

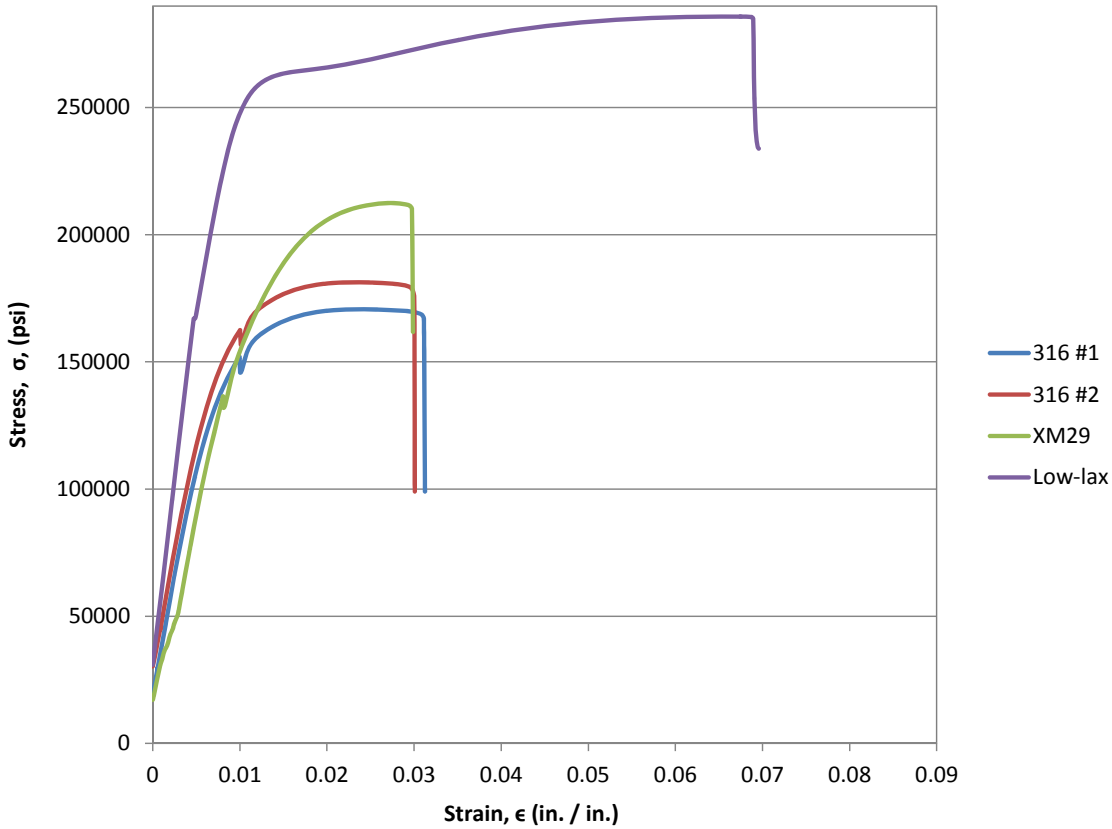

Figure 4.12 Stress-strain results from SMO tensile testing.

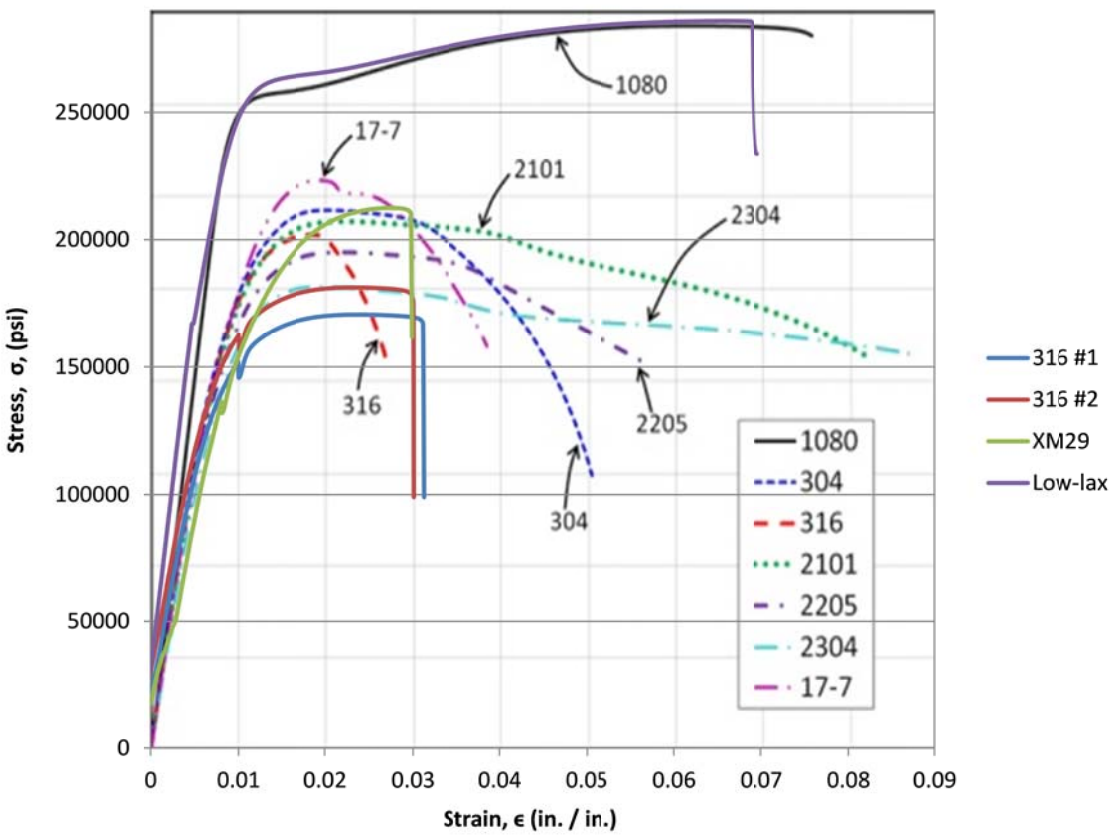

Figure 4.13 Stress-strain results from SMO compared with Moser, et al. (2013).

Table 4.1 Material properties of strands.

Material	Yield Strength (ksi)	Tensile Strength (ksi)	Young's Modulus (ksi)
Low-lax carbon steel	240	288	29,300
XM29	173	241	17,400
316	156	191	17,800

4.2 Relaxation Testing

Results from the mechanical properties testing showed the 316 strand to have the lowest tensile strength which limits the allowable prestressing per strand and results in requiring more strands per pile to obtain the same prestress in a pile. This required the design of the proposed 14in square prototype piles to use a 12 strand configuration and not the typical 8 strand configuration. Table 4.2 shows the proposed prestress load and percent ultimate load for each strand.

Table 4.2 Proposed strand loading for 12 strand pile configuration.

Material	Area (in^2)	Tensile Strength (ksi)	Proposed Stress (ksi)	Percent Ultimate (%)
Low-lax carbon steel	0.156	288	134.6	46.7
XM29	0.153	241	137.3	57.0
316	0.147	191	142.9	74.8
Duplex 2205	0.161	240*	130.4	54.4

*Tensile strength for the Duplex 2205 was provided by the manufacturer.

ASTM A416 (Standard Specification for Steel Strand, Uncoated Seven-Wire for Prestessed Concrete) allows a 3.5% relaxation at $0.80f_u$ and 2.5% relaxation at $0.70f_u$ at 1000 hours for low-relaxation stands. Relaxation limits are set to assure a minimum prestressed level throughout the life of the pile. Therefore, the low-lax carbon steel, XM29 and Duplex 2205 should be limited to 2.5% relaxation and the 316 limited to 3.0% (interpolated value) relaxation to meet ASTM recommendations. However, for design of prestressed piles the actual loss is more important than the percentage.

4.2.1 Specimen

The relaxation testing of four strand samples (XM29, 316, Duplex 2205, and low lax low-lax carbon steel) were prepped and tested at the University of South Florida Structural Testing Lab. A minimum of two tests were performed on each sample to ensure repeatability of the tests.

4.2.2 Test Setup

Relaxation tests conducted in the structures lab followed ASTM E328 (Standard Test Methods for Stress Relaxation for Materials and Structures) where each specimen was loaded in tension to a target stress and decreases in stress over time were monitored under constant strain. The temperature was also recorded throughout the test.

The test setups used steel two header blocks bolted to a strengthened floor with a separation of eight feet. Load was applied to the test specimens using a hollow-core hydraulic jack with a load cell between the header block and hydraulic jack. This resulted in a specimen length of approximately 10ft for each test. A displacement transducer was attached to the hydraulic jack to ensure constant strain during testing. Both load and displacement were monitored using a Campbell Scientific CR1000 data collection system. The data was collected at a 1Hz sampling rate during loading and switched to 5 minutes between samples during the relaxation period. Figures 4.14 to 4.17 show the relaxation test setup.

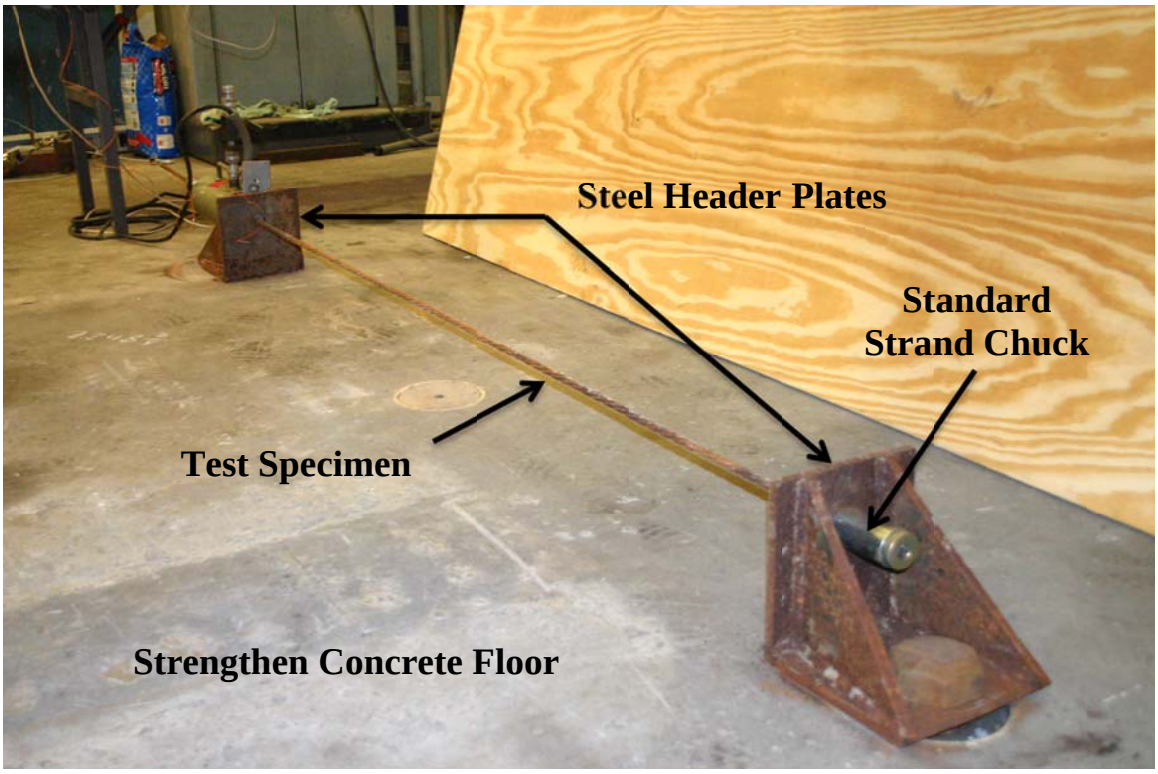

Figure 4.14 Relaxation test setup (dead-end side).

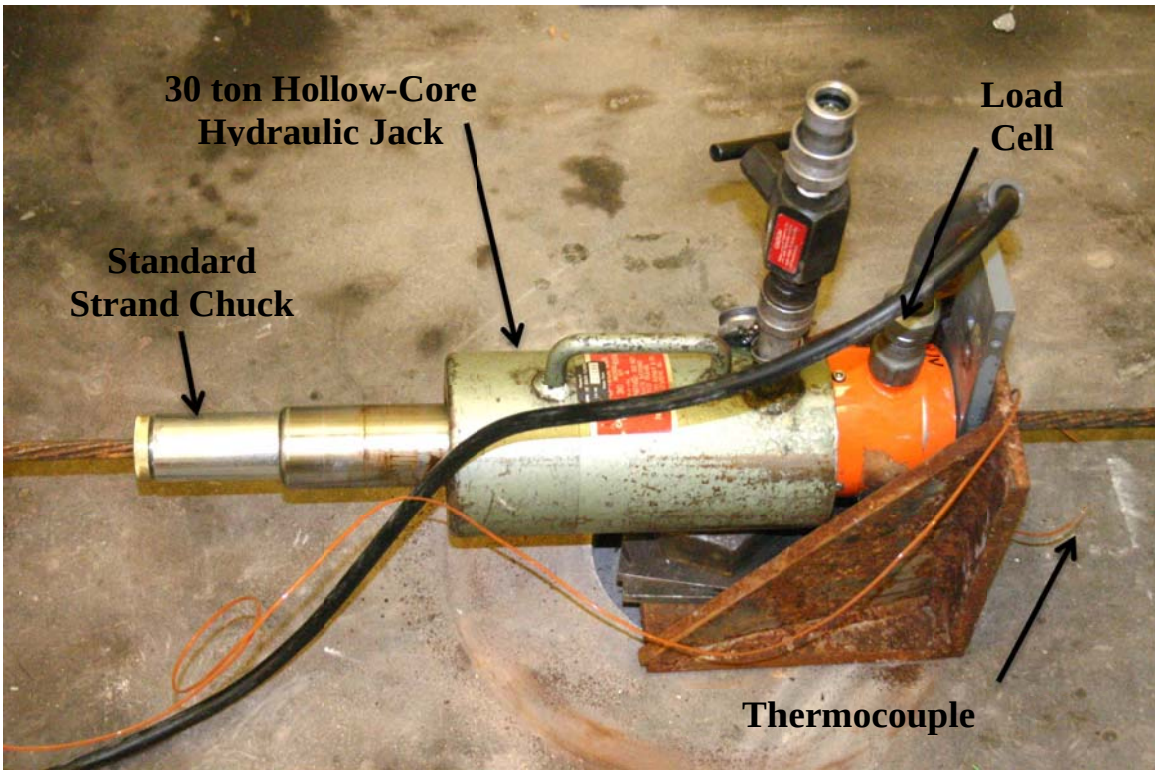

Figure 4.15 Relaxation test setup (live-end side).

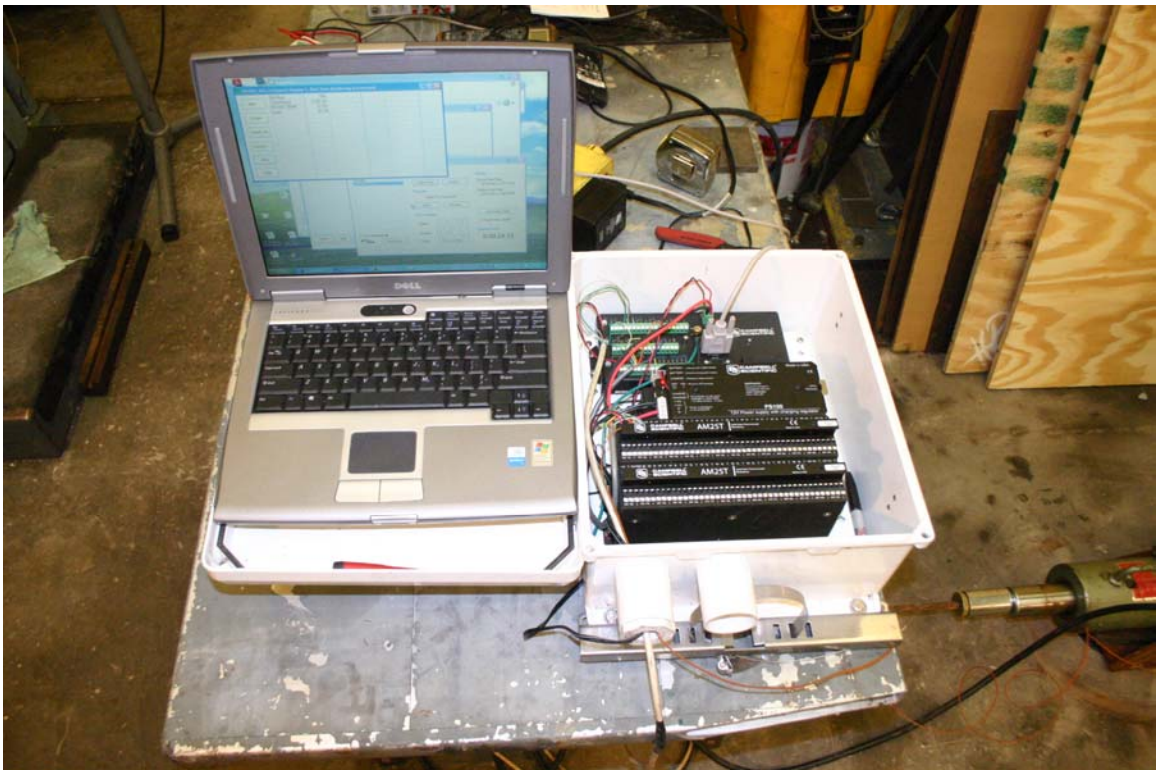

Figure 4.16 Relaxation test data collection system.

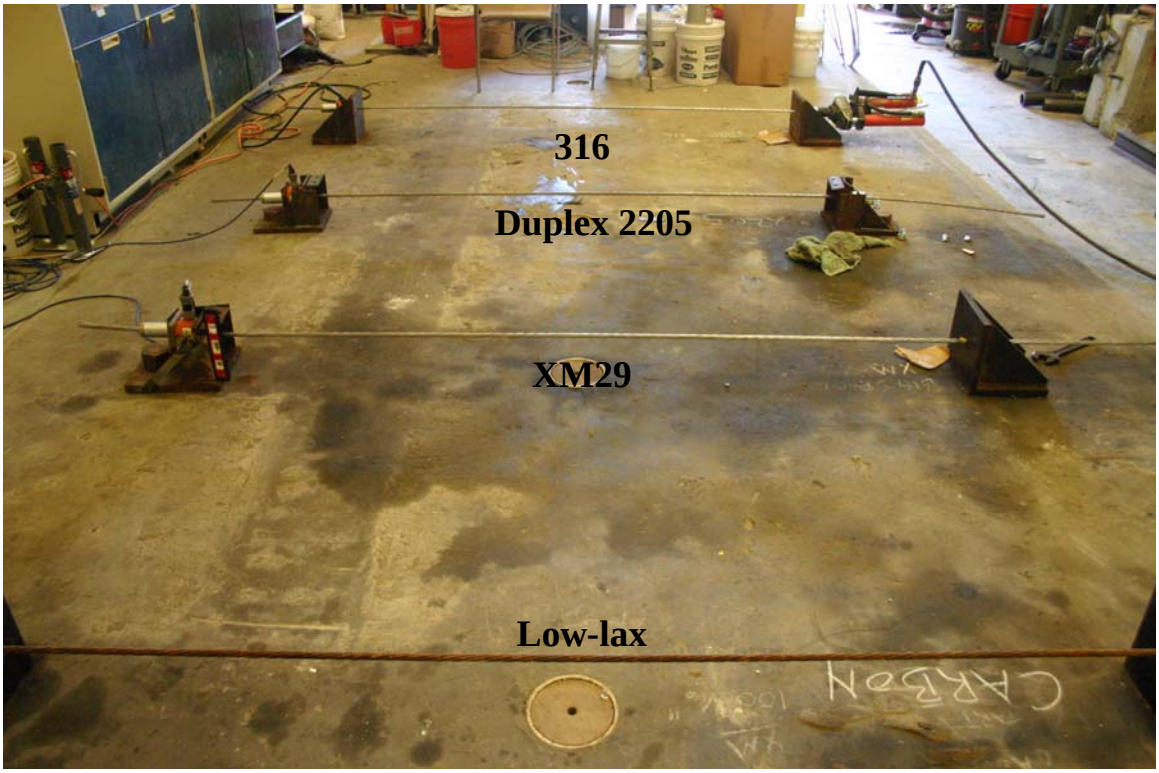

Figure 4.17 Relaxation test setup with all 4 materials.

4.2.3 Initial Relaxation Testing

The target stressing load was determined based on FDOT standard drawings for a 14 inch square pile and the associated load in each strand. For the 12 strand configuration planned for the prototype piles, a target maximum load of 21 kips was applied to the strands to determine percent relaxations for each material. Figure 4.18 shows the results of the initial relaxation testing. The top graph shows the load loss for each strand versus log time once strain was locked in. The bottom graph shows the relaxation (or percent loss) versus log time for each material. The tests were run for approximately 200 hours and extrapolated to 1000 hours to provide ASTM relaxation values.

Results from initial relaxation testing compared well with Moser (2011) for the 316. Moser predicted stress relaxations at 1000 hours for 316 of 2.4% and testing showed low-lax carbon steel and 316 at 1.5%. Both tests were at approximately 70% ulitamate load. The Carbon and Duplex 2205 were test below the 70% ultimate load and is not comparable to Moser. Recall, ASTM A416 allows a 3.5% relaxation at $0.80f_u$ and 2.5% relaxation at $0.70f_u$ at 1000 hours for strands. The 316 and XM-29 stainless steel strands resulted in higher than the allowable relaxation, with the 316 strand controlling at 7.25% loss.

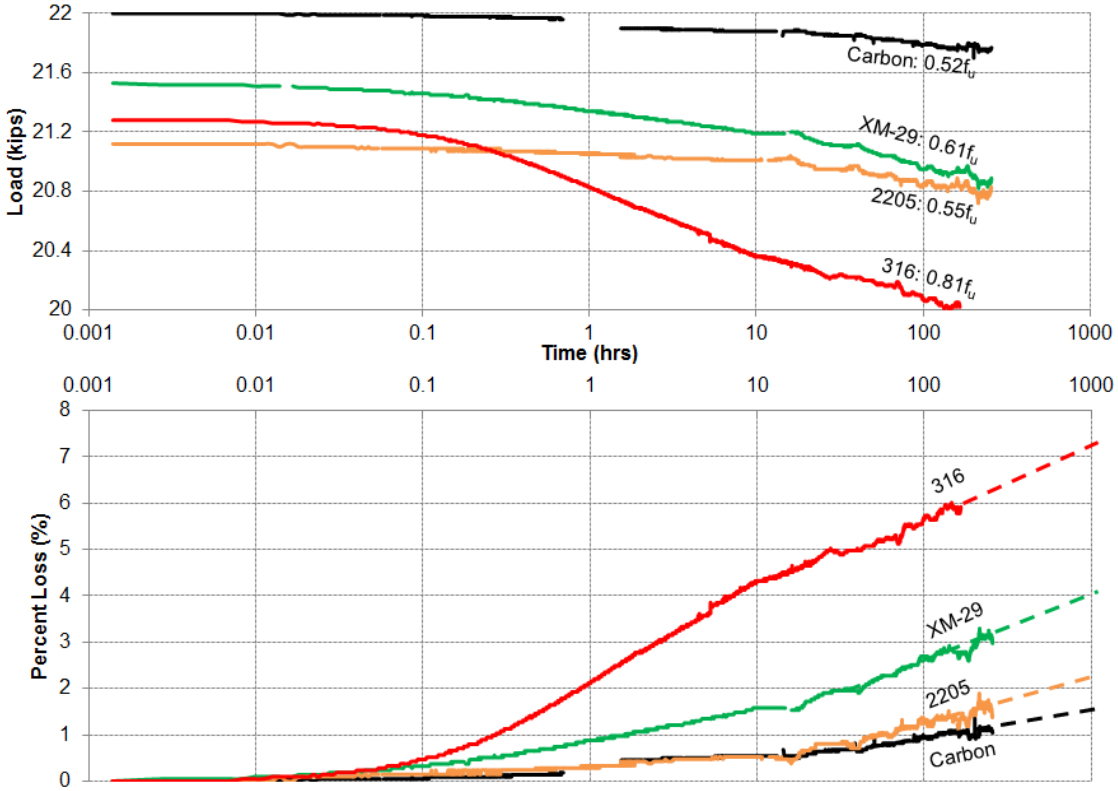

Figure 4.18 Initial relaxation test results.

The temperature was monitored to verify the temperature did not deviate during testing per ASTM standards of ±3°C from initial temperature. Figure 4.19 shows the measured temperature during the relaxation testing. The graph shows that the temperature did not exceed the maximum and minimum allowed temperatures per ASTM from initial testing.

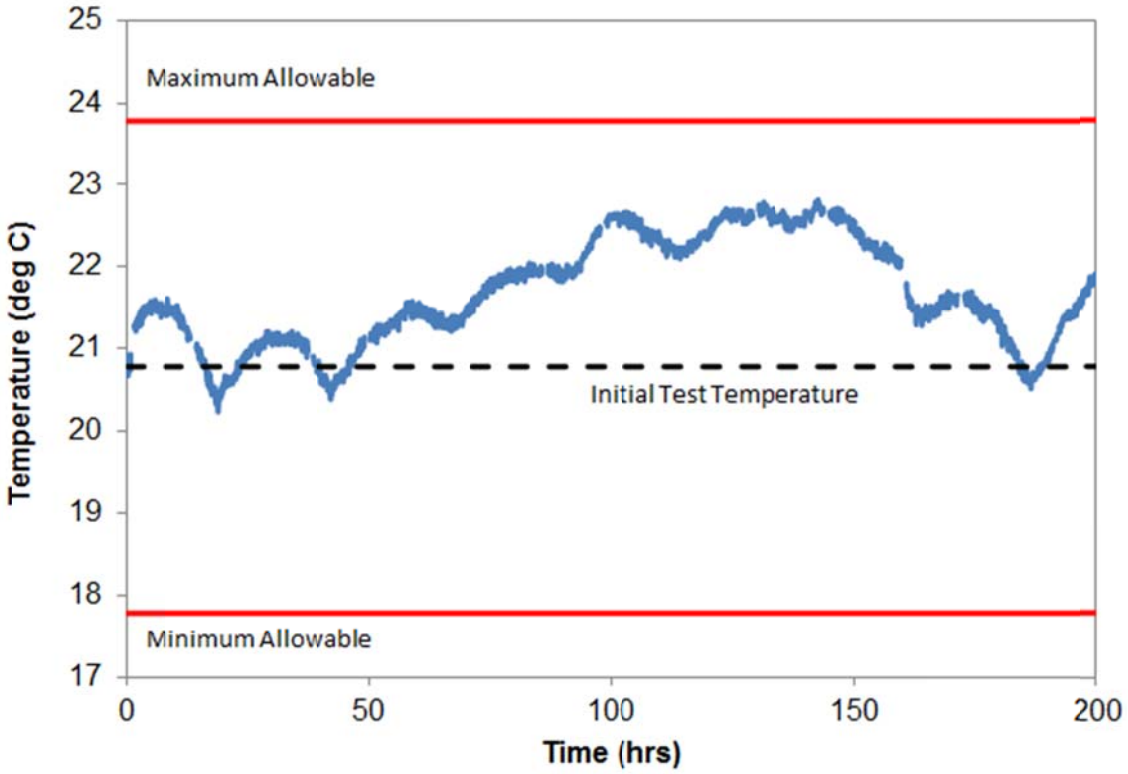

Figure 4.19 Temperature measurements during relaxation testing.

4.2.4 Combating Relaxation Losses

While the relaxation of the grade 316 stainless steel strands did not meet ASTM A416 relaxation criterion, an extensive series of trials was carried out on 316 to determine the best means of reducing relaxation losses over time and still maintain a reasonable field/production protocol. This included: (1) standard ASTM testing where the load was applied to the strand and strain maintained (Standard Loading), (2) standard loading subsequently reloaded after 20 hours to regain any initial losses, and (3) cyclic loading, hold and reloading after 20 hours. Based on these results, low-lax carbon steel, Duplex 2205, and XM29 were then tested by the best means of reducing relaxation losses. Table 4.3 shows the type of testing and number of tests for each material evaluated.

Table 4.3 Number of tests performed for each loading scenario.

Material	Standard Loading	Std Loading w/ Reloading @ 20hrs	Cyclic Loading w/ Reloading @ 20hrs
low-lax	3	0	2
Duplex 2205	3	0	2
XM29	3	0	2
316	3	2	3

316. A series of relaxation tests was conducted on 316 to determine an effective way of combating excessive losses. Figure 4.20 illustrates sample test data showing the loading sequence prior to maintaining and monitoring relaxation losses. Figure 4.21 shows the overall load history of the each relaxation test for 316 versus log time. Each test was terminated at approximately 200 hours. From these plots, the blue curve shows a standard test method for strands by loading to the desired level and maintaining constant strain. The black curve is similar to the standard method but with a reloading after 20 hours to regain initial losses. The orange plot shows cyclic load prior to relaxation testing and a reload after 20 hours.

Figure 4.22 shows the load relaxation versus log time with reloading of the two specimens discussed above. Figure 4.23 plots the analysis of the relaxation data extrapolated to 1000 hours. The analysis shows 316 to be between 7% and 8% regardless of the initial loading sequence. However, after a 20 hour reload, relaxation losses were reduced to 3.5% and 5% for the cyclic and standard loading sequence, respectively.

Figure 4.24 shows the measured temperature during the relaxation testing of the 316. The graph shows that the temperature did not exceed the maximum and minimum allowed temperatures per ASTM from initial testing.

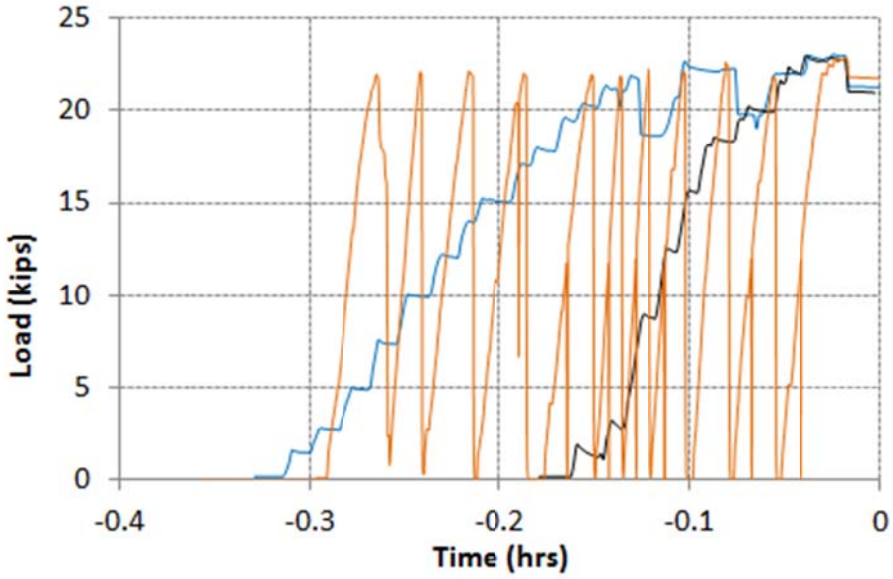

Figure 4.20 Loading cycles prior to start of relaxation testing for 316.

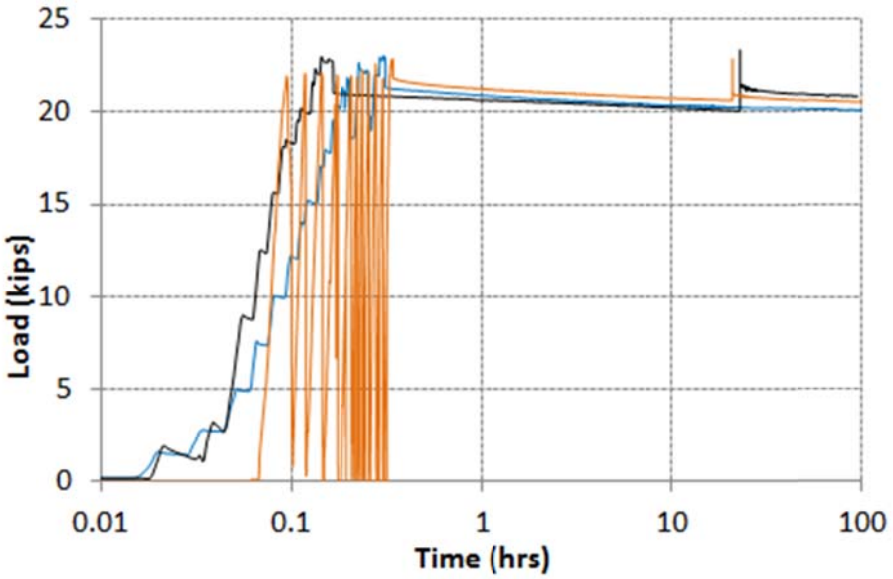

Figure 4.21 Loading history for 316.

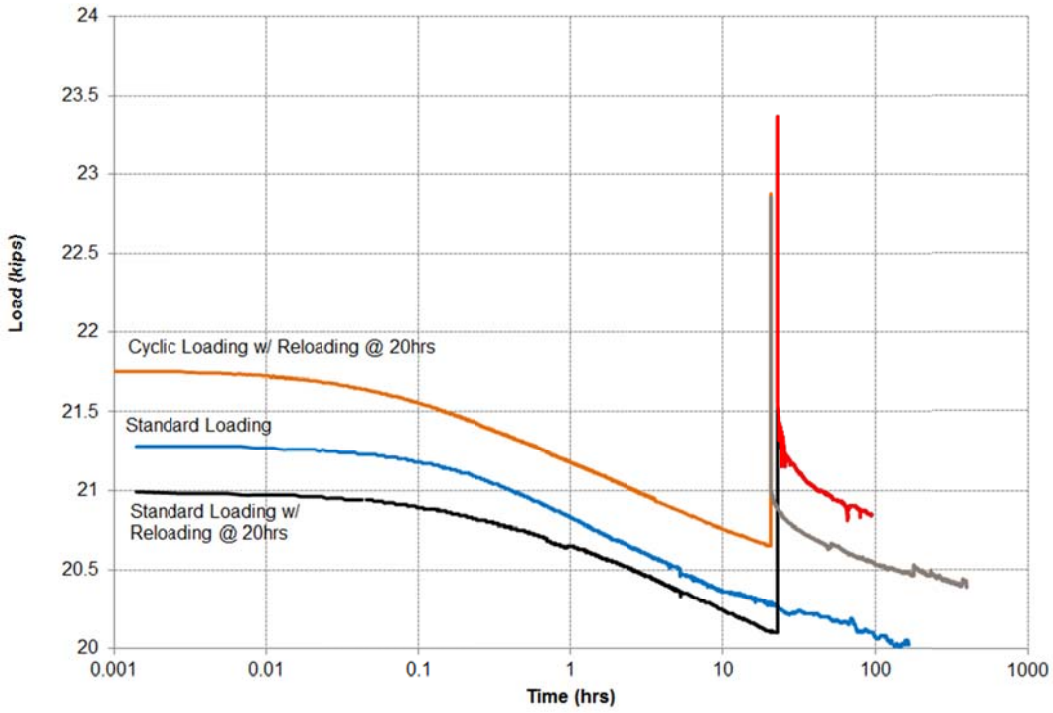

Figure 4.22 Relaxation test data for grade 316 stainless steel strands.

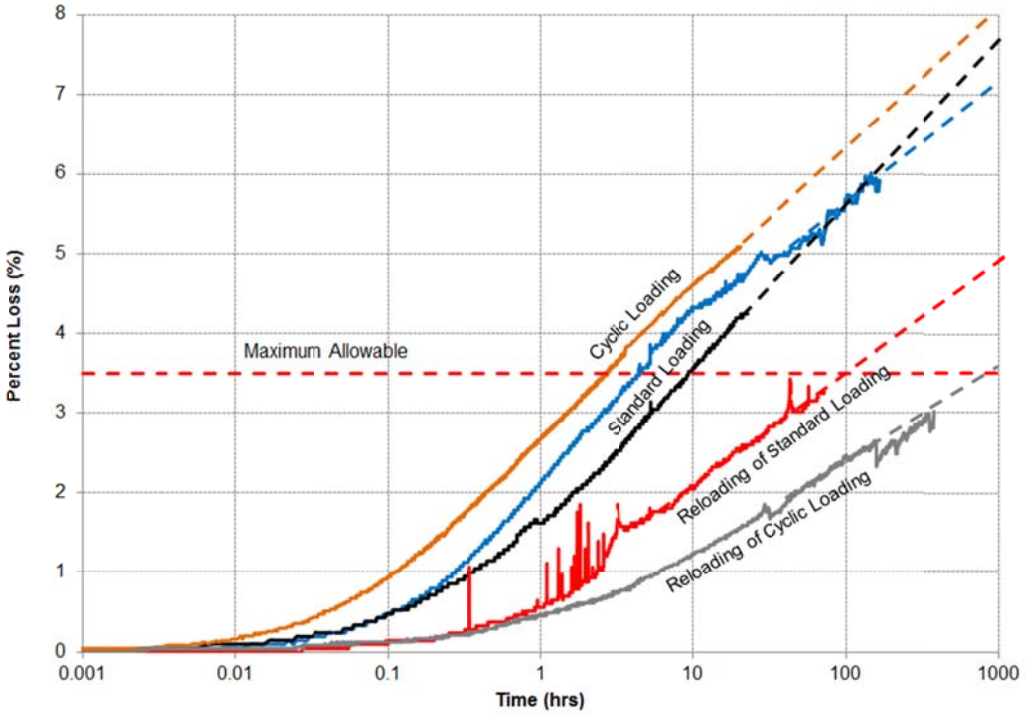

Figure 4.23 Relaxation test results for grade 316 stainless steel strands.

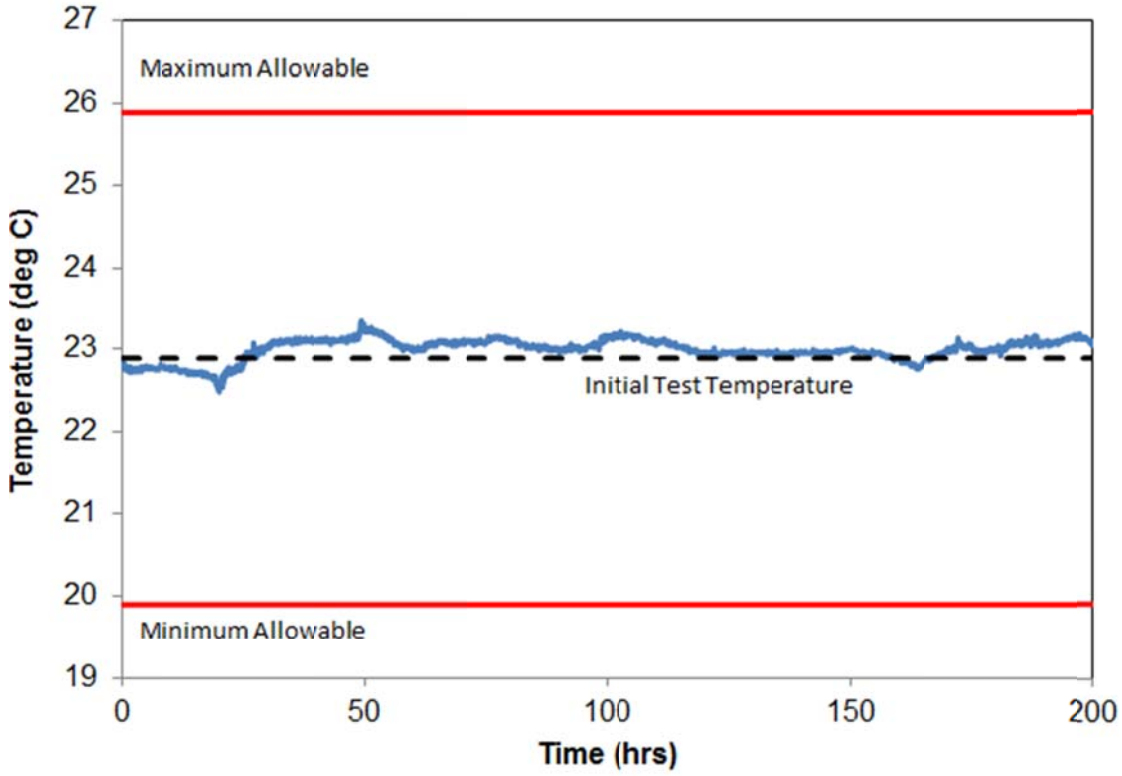

Figure 4.24 Temperature measurements during 316 relaxation testing.

Low-lax carbon steel. After completing the series of relaxation tests on 316, it was determined that initial cyclic loading with reloading after 20 hours provided the best means to combat relaxation losses. Therefore, low-lax carbon steel, Duplex 2205, and XM29 were tested using standard ASTM methods and cyclic loading with reloading after 20 hours. No tests were performed using standard loading and reloading after 20 hours for these materials.

Figure 4.25 illustrates sample test data showing the loading sequence prior to maintaining and monitoring relaxation losses for the low-lax carbon steel strand. Figure 4.26 shows the overall load history of the each relaxation test for Low-lax carbon steel versus log time. Each test was terminated at approximately 200 hours. Figure 4.27 shows the load relaxation data versus log time for the low-lax carbon steel. Figure 4.28 shows the relaxation for low-lax carbon steel extrapolated to 1000 hours. The modified test method using cyclic loading and reloading after 20 hours reduced the relaxation of low-lax carbon steel from 2.5% to 1.5% at 1000 hours.

Figure 4.29 shows the measured temperature during the relaxation testing of the low-lax carbon steel. The graph shows that the temperature did not exceed the maximum and minimum allowable temperatures per ASTM from initial testing.

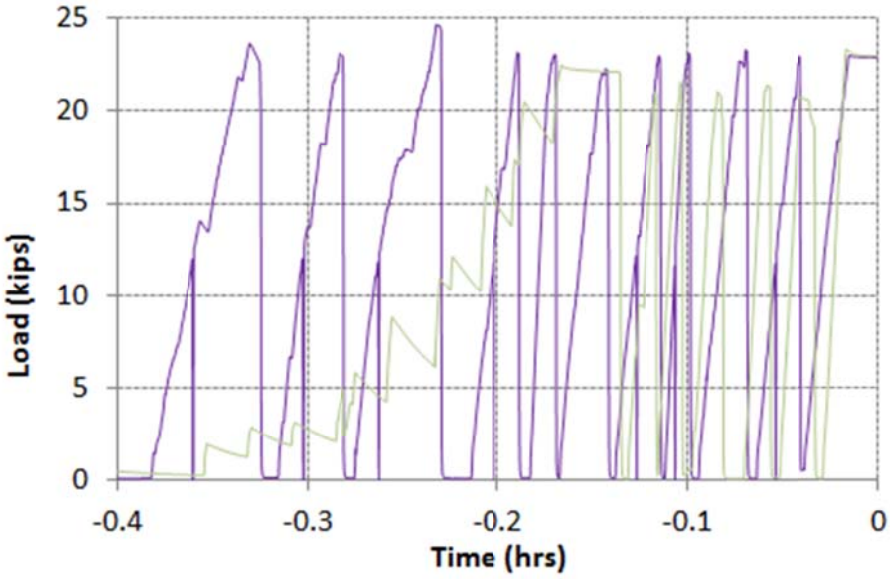

Figure 4.25 Loading cycles prior to start of relaxation testing for low-lax carbon steel.

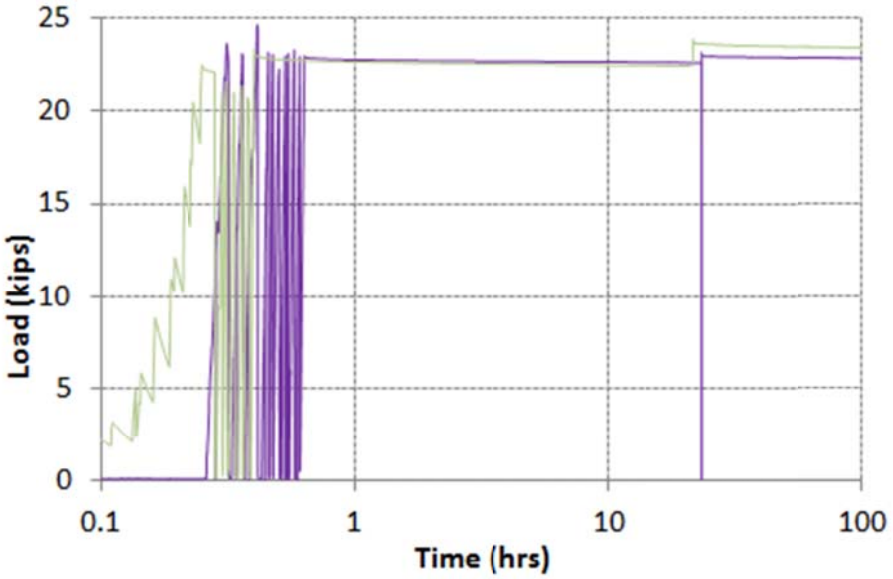

Figure 4.26 Loading history for low-lax carbon steel.

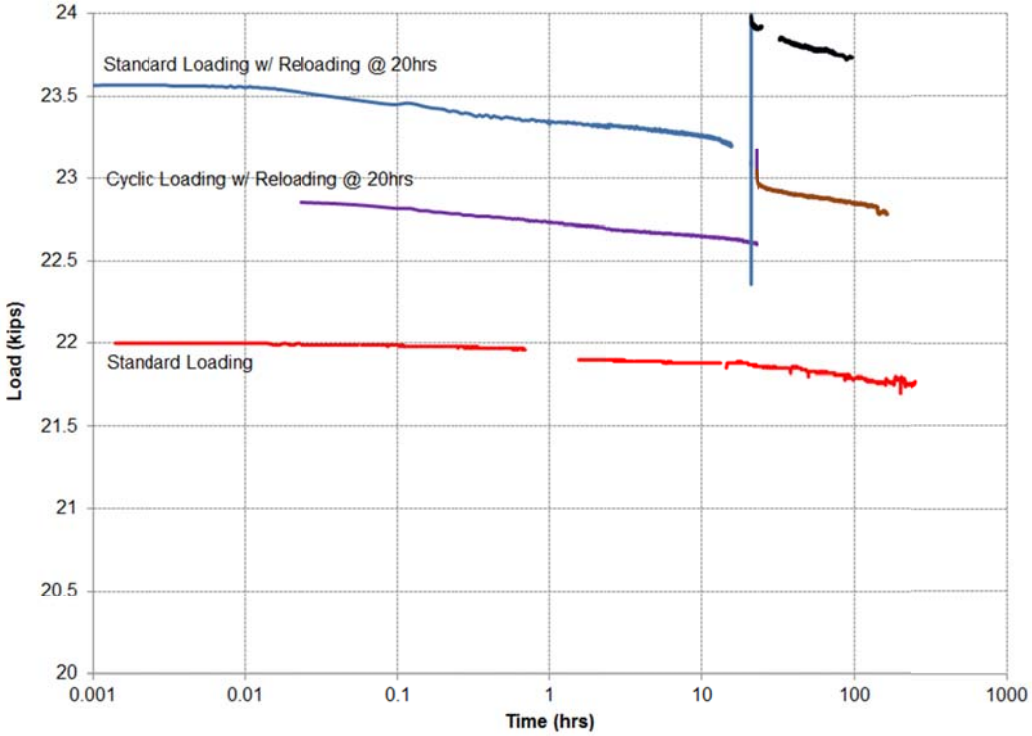

Figure 4.27 Relaxation test data for low-lax carbon steel strands.

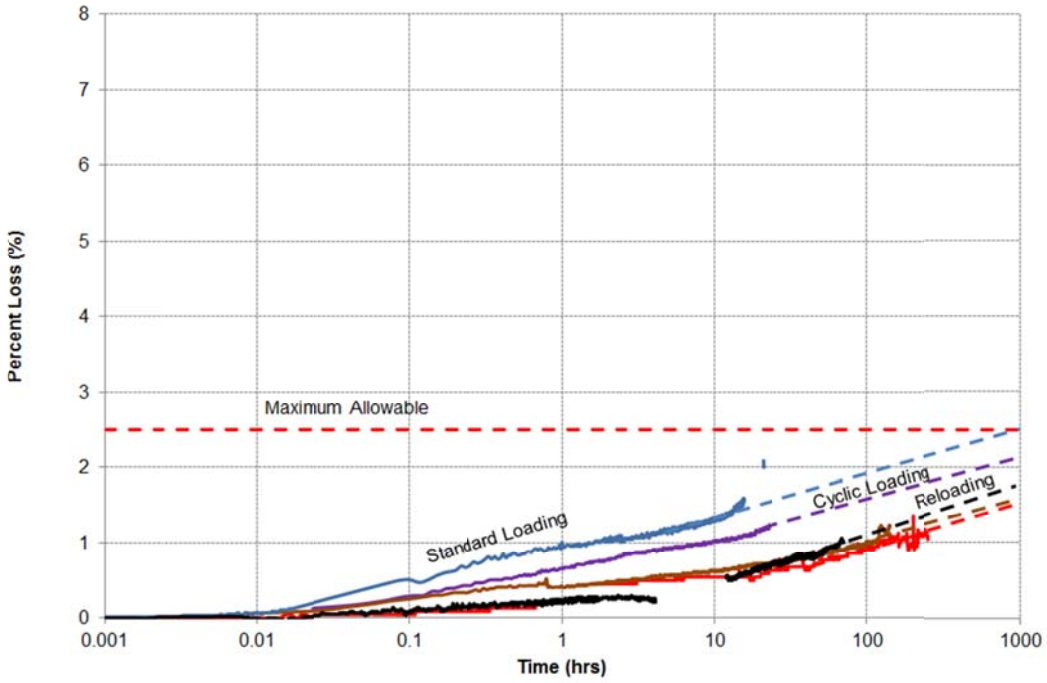

Figure 4.28 Relaxation test results for low-lax carbon steel strands.

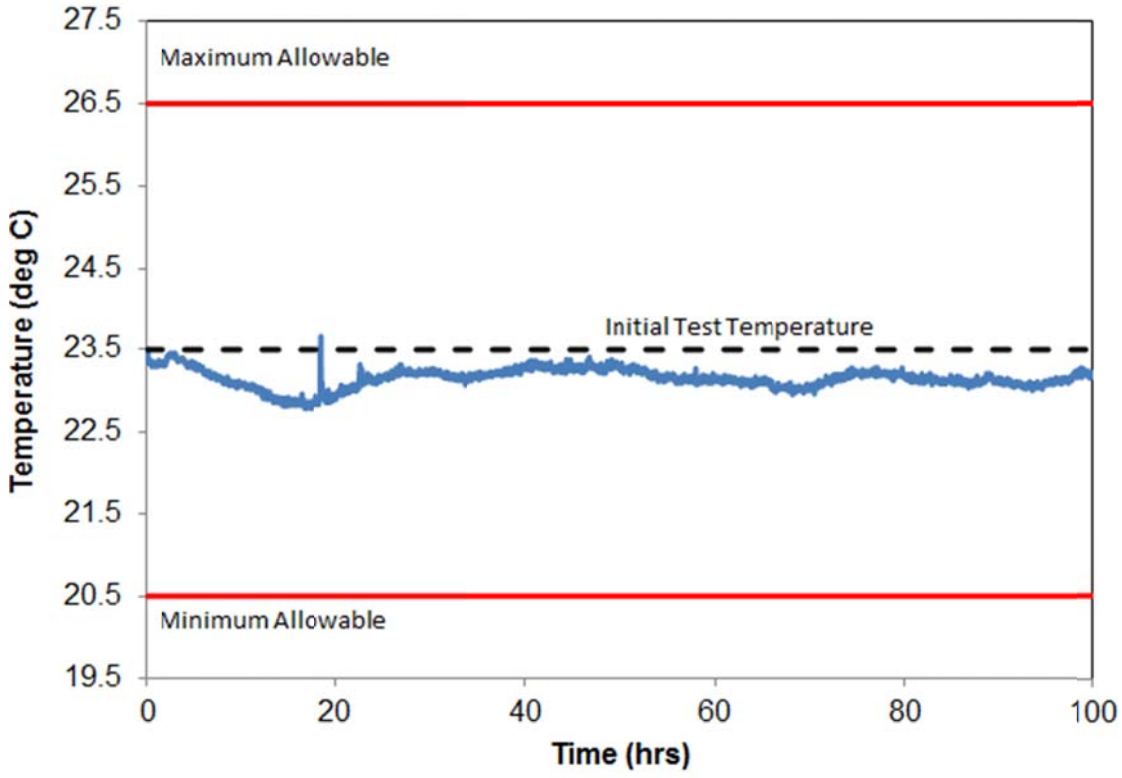

Figure 4.29 Temperature measurements during 316 relaxation testing.

XM29. Figure 4.30 illustrates sample test data showing the loading sequence prior to maintaining and monitoring relaxation losses for the XM29 strand. Figure 4.31 shows the overall load history of the each relaxation test versus log time. Each test was terminated at approximately 200 hours. Figure 4.32 shows the load relaxation data versus log time while Figure 4.33 shows the relaxation for XM29 extrapolated to 1000 hours. The modified test method using cyclic loading and reloading after 20 hours reduced the relaxation of XM29 from 6.5% to 4.5% at 1000 hours. Despite the effectiveness of cyclic loading and reloading of 316 stainless steel strand, this method did not reduce the relaxation of XM29 to allowable standards for a low-relaxation strand.

Figure 4.34 shows the measured temperature during the relaxation testing of the XM-29. The graph shows that the temperature did not exceed the maximum and minimum allowable temperatures per ASTM from initial testing.

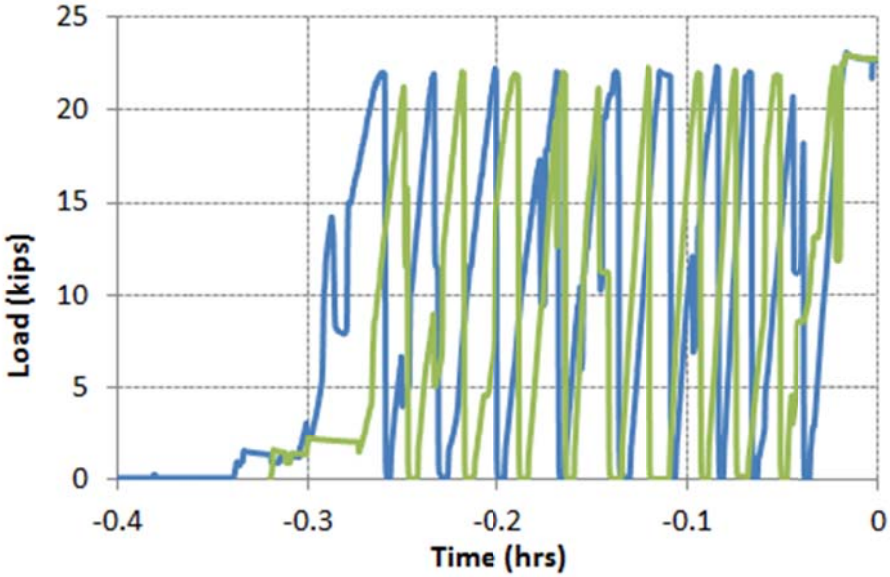

Figure 4.30 Loading cycles prior to start of relaxation testing for XM29.

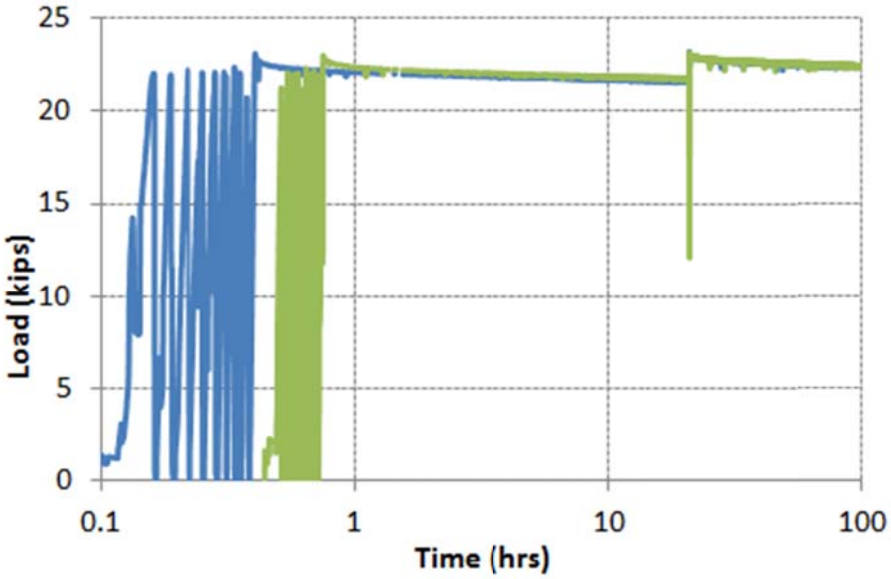

Figure 4.31 Loading history for XM29.

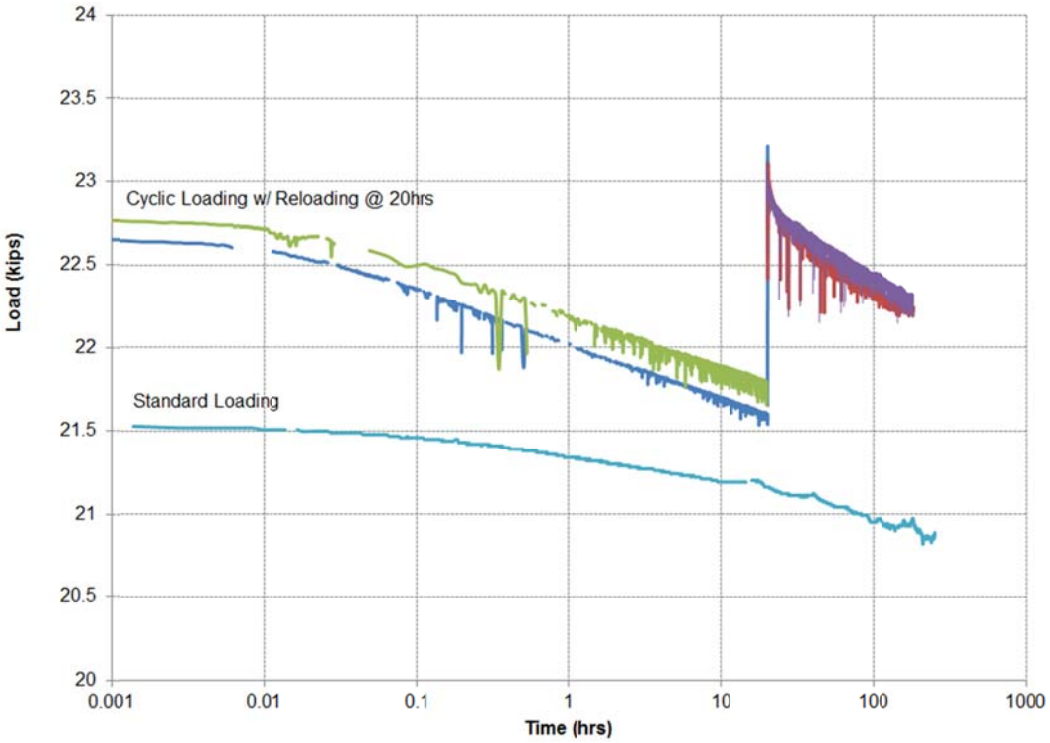

Figure 4.32 Relaxation test data for XM-29 strands.

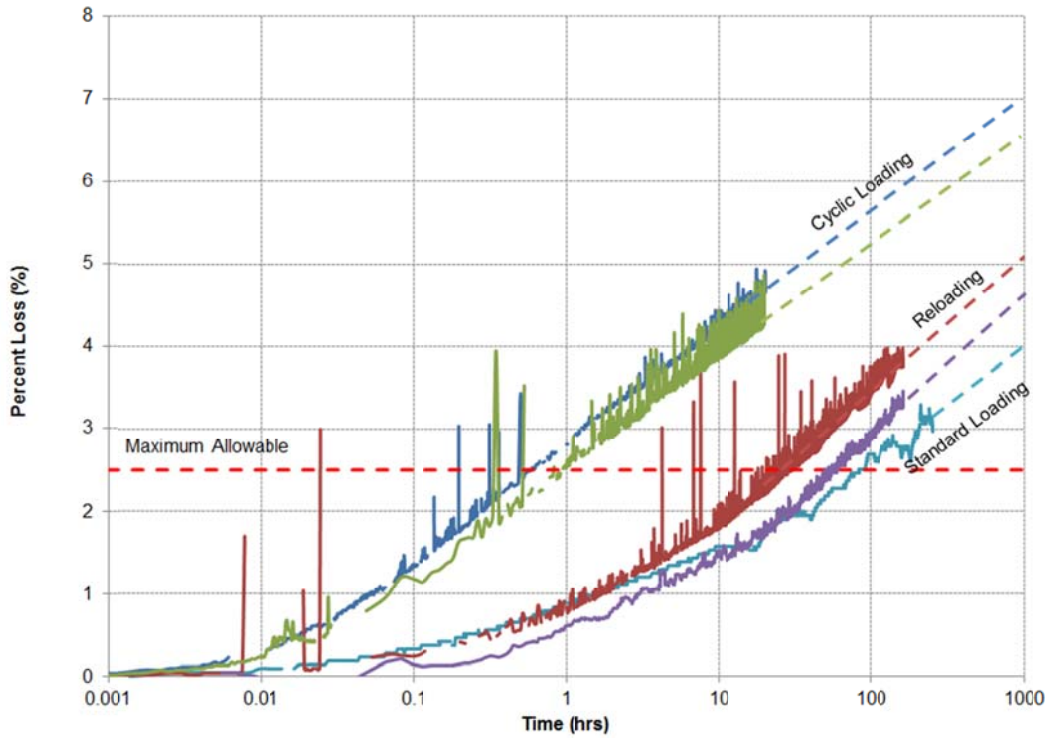

Figure 4.33 Relaxation test results for XM-29 strands.

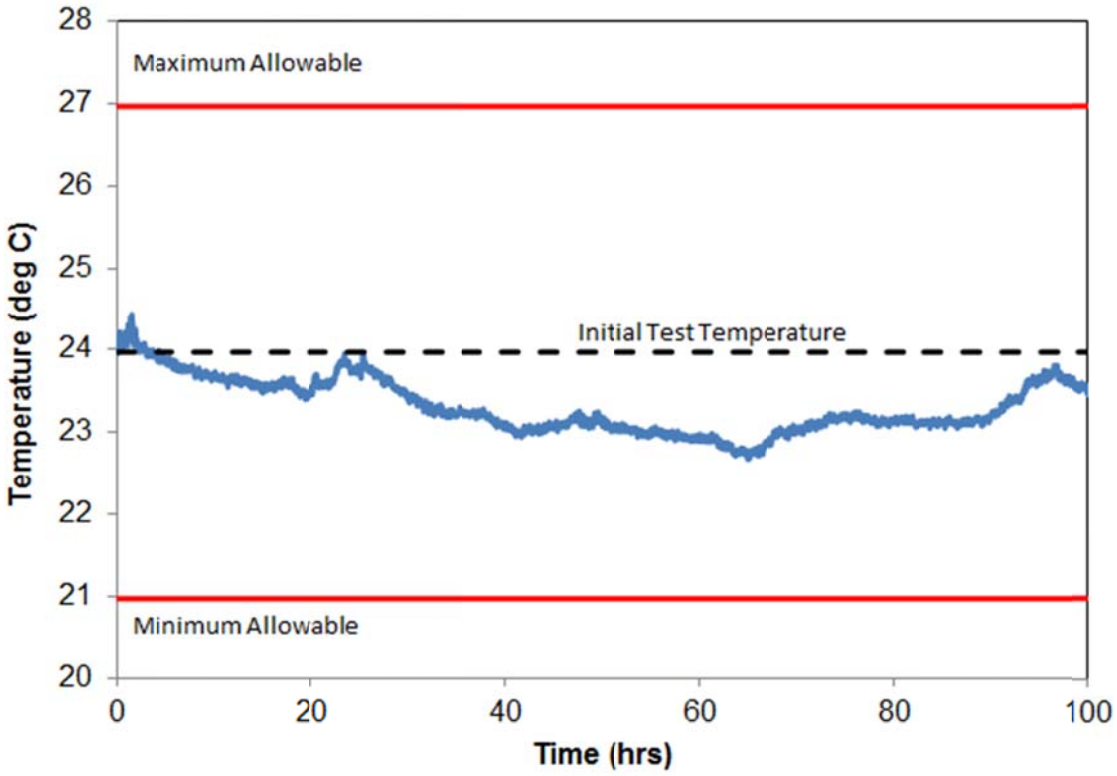

Figure 4.34 Temperature measurements during XM29 relaxation testing.

Duplex 2205. Figure 4.35 illustrates sample test data showing the loading sequence prior to maintaining and monitoring relaxation losses for the Duplex 2205 strand. Figure 4.36 shows the overall load history of the each relaxation test versus log time. Each test was terminated at approximately 200 hours. Figure 4.37 shows the load relaxation data versus log time while Figure 4.38 shows the relaxation for Duplex 2205 extrapolated to 1000 hours. The modified test method using cyclic loading and reloading after 20 hours reduced the relaxation of Duplex 2205 from 2.5% to 1.5% at 1000 hours.

Figure 4.39 shows the measured temperature during the relaxation testing of the Duplex 2205. The graph shows that the temperature did not exceed the maximum and minimum allowable temperatures per ASTM from initial testing.

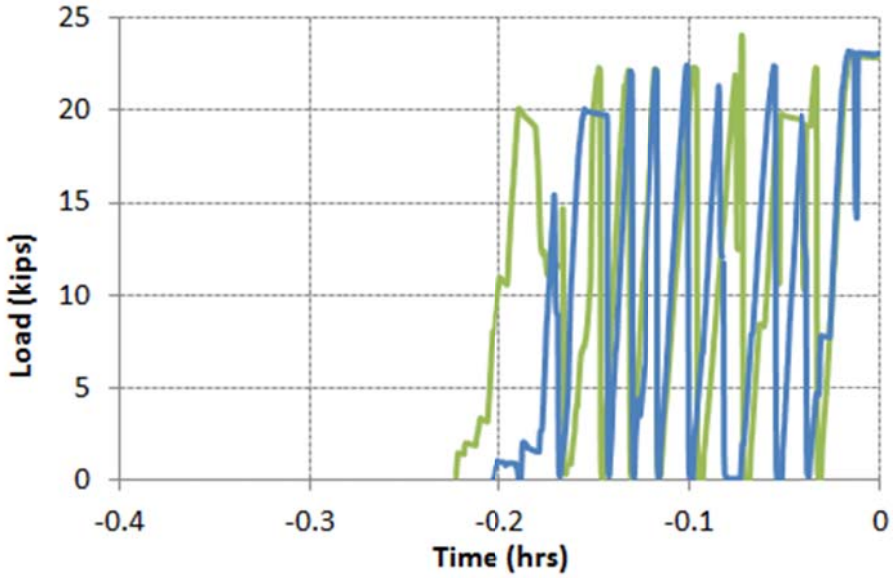

Figure 4.35 Loading cycles prior to start of relaxation testing for Duplex 2205.

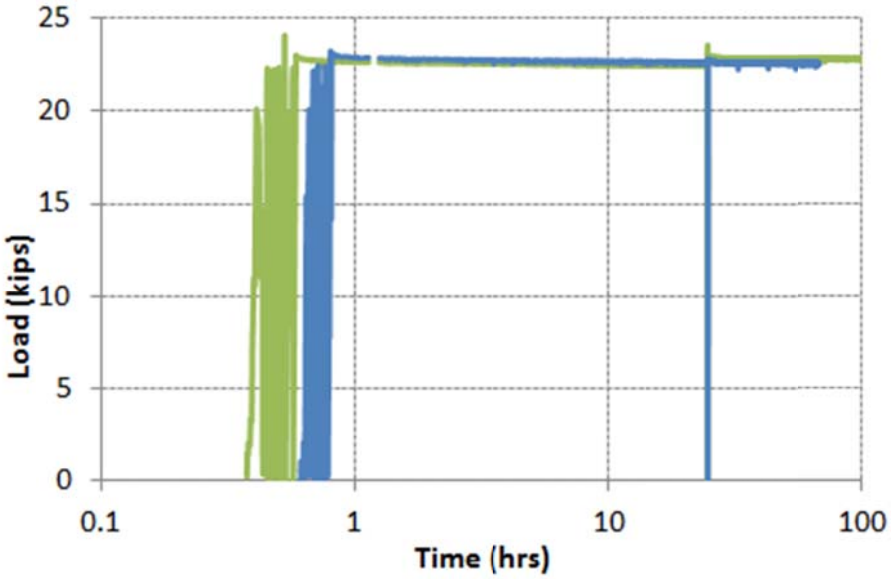

Figure 4.36 Loading history for Duplex 2205.

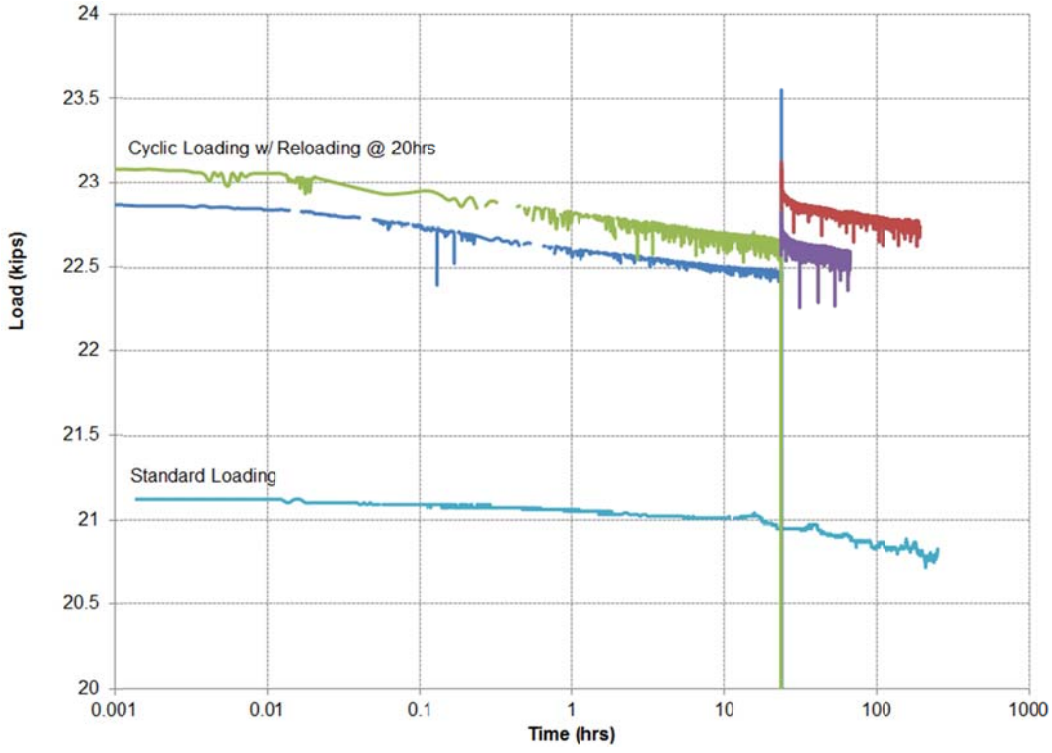

Figure 4.37 Relaxation test data for Duplex 2205 strands.

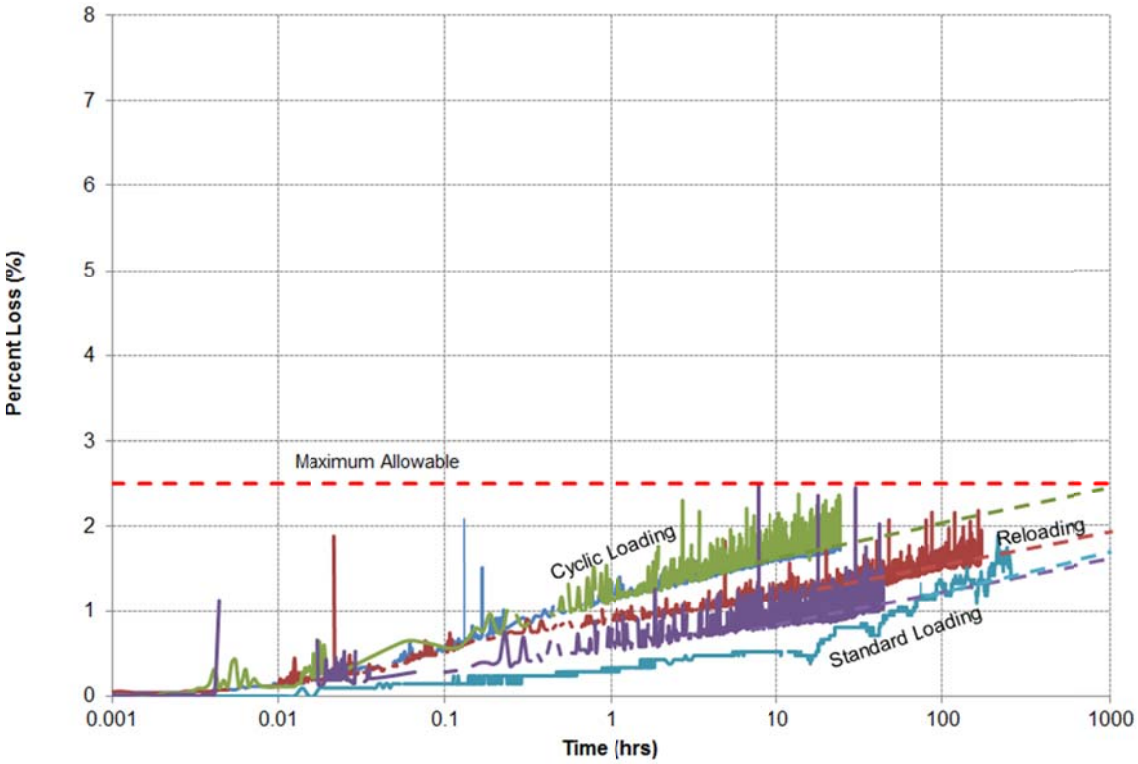

Figure 4.38 Relaxation test results for Duplex 2205 strands.

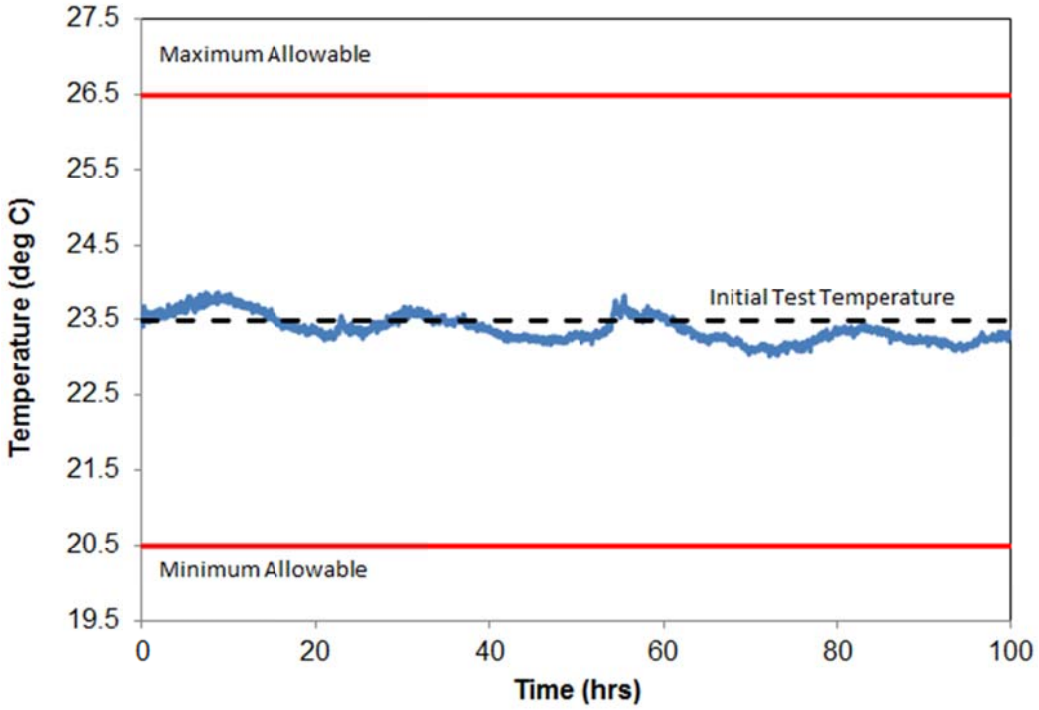

Figure 4.39 Temperature measurements during Duplex 2205 relaxation testing.

Modified loading protocols showed effective reduction in relaxation for various strand materials. However, field cyclic loading may be impractical for production pile fabrication. Therefore a minimum number of cycles should be established based on the laboratory findings. Figure 4.40 shows the stress-strain curve for the 316 cyclic loadings prior to the sustained relaxation testing. The plot shows an increase in stiffness after the first cycle and subsequence cycles are similar in stiffness. Figure 4.41 shows the calculated modulus for each material (low-lax carbon steel, Duplex 2205, XM29, and 316) as a function of load cycle. These results suggest the strands reached a stable modulus after 2 full loading cycles, however all sustained testing conducted in this study followed 10 cycles. As a result, field testing discussed in Chapter 5 also followed that procedure.

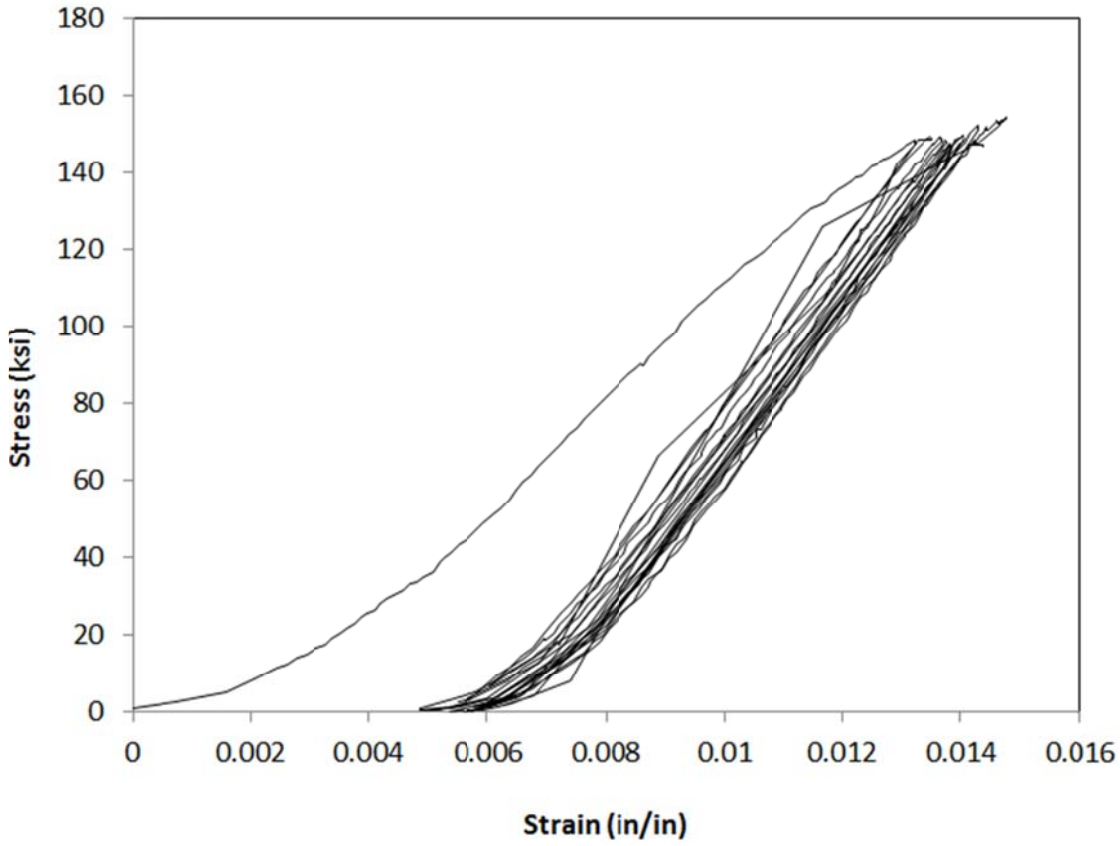

Figure 4.40 Stress-strain history for the 316 cyclic loading.

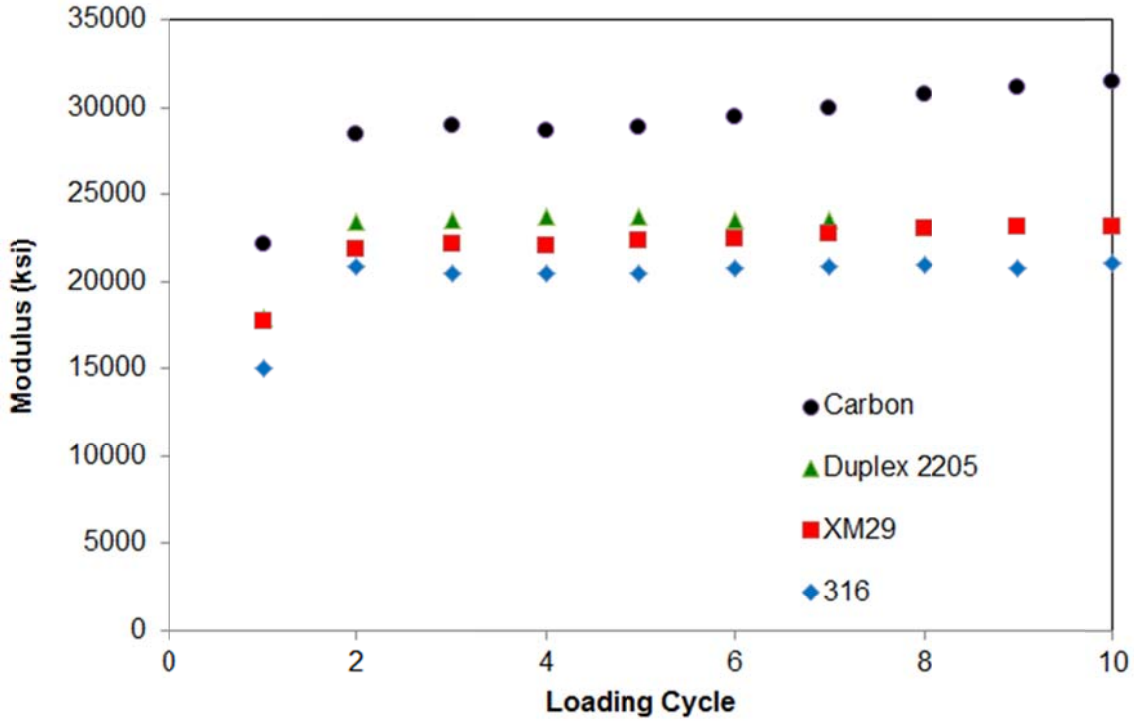

Figure 4.41 Calculated modulus for each load cycle during cyclic loading.

Chapter 5: Full Scale Pile Casting / Transfer Length

Investigation into the effects of using stainless steel strand on transfer length proceeded with the construction of four full-scale piles (square 14in x 75ft ea.), wherein each pile was instrumented and monitored during de-tensioning to record the strain distribution.

5.1 Preparations for Full Scale Pile Casting

5.1.1 Materials

For this portion of the study, investigation focused on the Duplex 2205, XM-29, and 316 grades of stainless steel. Grade 316 was chosen for its availability and its successful use as reinforcing material. The XM-29, like the Duplex 2205, has both high strength and corrosion resistance. It stands apart as the only stainless steel product currently used in prestressing applications; however, it cannot be relaxed using traditional methods. The Duplex 2205 has the strength, the corrosion resistance and the ability to be relaxed, but is not routinely available. Individual piles were cast using each of the three grades of stainless steel, along with a control pile cast using low-relaxation carbon steel. Table 5.1 summarizes the four types of strand used.

Table 5.1 Strand Properties

Strand Material	Ultimate Tensile Strength (ksi)	Strand Diameter (in)	Cross Sectional Area (in^2)	Allowable Load (80% Ultimate)
Carbon Steel – Low-Lax	288	0.506	0.1564 in^2	33.8 k
Stainless Steel – XM-29	241	0.513	0.1527 in^2	28.1 k
Stainless Steel – 316	191	0.490	0.1467 in^2	21.1 k
Stainless Steel – 2205	240*	0.500	0.1608 in^2	30.9 k

*nominal value per manufacturer

Where stainless steel was used for strand material, it was also used for the spiral ties, tie wire and embedded strain gage bars to prevent galvanic corrosion between the metals. Mild steel, in contact with the stainless steel, acts as a sacrificial anode, thus inhibiting corrosion of the stainless steel. Preventing this by using similar metals allows for a conservative assessment of the corrosion behavior of the strands. It is not, however, necessary to use the same grades of stainless steel, only that the potential difference between the two metals is minimal. Therefore availability and cost dictated the selection of stainless steel for spirals and strain gage bars, and grades 304 and 2205 steels were chosen, respectively. A list of materials is provided in Table 5.2.

Table 5.2 Materials List

Item	Manufacturer	Location	Amount Purchased
XM-29 Strand	Insteel	Sanderson, Florida	1500 ft
316 Strand	National Strand	Houston, Texas	2000 ft
2205 Strand	Sumiden	Dickson, Tennessee	2000 ft
304 Spiral Wire			2000 ft
Splice Chucks	Prestress Supply	Lakeland, Florida	72 chucks
304 Stainless 18 gauge Tie Wire	Comet Supply	cometsupply.com	10 – 3.5lb rolls
316 Stainless Rebar	Salit Stainless	Niagra Falls, New York	32 ft
Surface Strain Gages	Texas Instruments	College Station, Texas	96 gages
Bonded Foil Strain Gages	Vishay Measurements Group	Wendell, North Carolina	32 gages
Concrete	Preferred Materials	Tampa, Florida	20 cubic yards
Epoxy	Red Head Adhesive Anchoring System	Tampa, Florida	88 fluid oz

5.1.2 Casting Bed

A square 14 in. x 400 ft. casting was selected to cast all four 75 ft. piles in-line with each other. Although the bed was mostly ready for casting as-is, the header plates had to be modified. The most common strand configuration for a 14 in. pile is eight ½ in. strands stressed to 31 k each (248 k total). This force, however, is beyond the capacity of all three stainless steel grades, thus in order to achieve the same overall effective prestress, a 12 strand configuration was planned, with each strand stressed to 21 k (252 k combined). To accommodate this strand pattern, additional holes were drilled in the header plates. Figure 5.1 shows the casting bed selected for the project and the modifications made.

Figure 5.1 400ft prestressing bed (left); drilling modification to header plates (top rt); 12 strand pattern superimposed on 8 strand header plate (bot rt).

5.1.3 Spirals

Grade 304 stainless steel was chosen for the spiral material based on availability which was delivered in a single spool of 0.2031 in. wire (Figure 5.2). Because the material was stronger than the mild steel typically used, commonly available equipment could not easily bend the wire without damaging the equipment. Therefore the wire was taken to a specialty fabricator in Miami, FL in order to form the wire into spirals for the 14 in. strand configuration. FDOT standard specifications for 14 in. piles require the spirals be 8 in. square wherein a total of 174 turns was estimated for each pile. The fabricated spirals are shown in Figure 5.2.

Figure 5.2 Grade 304 stainless steel wire used for spirals (as-received, left) and fabricated into spirals (right).

5.1.4 Embedded Strain Gages

Transfer length determination most commonly looks at the strain distribution along the length of the pile. For this, strain gages are typically surface mounted. A side-line objective for this study was to also enable the monitoring of strains within the pile if and when the piles are driven subsequent to the project conclusion. Bonded surface gages used for transfer length determination are not robust enough to be used for driving applications as the gages would be stripped off the pile as they pass against the soil/concrete interface. As a result, sister bar strain gages were prepared using stainless steel rebar for the eventual embedment in the piles during casting.

The sister bar gages were made from 36in long 316SS #3 rebar turned in a lathe to remove the deformations and to provide a smooth bonding surface for CEA-06-062UT-350 resistive-type foil gages. Two gages (2 resistive elements per gage) were mounted on each bar and wired in a full bridge Wheatstone bridge configuration. Figure 5.3 shows the gages equipped with the foil gages and the protective adhesive-type heat shrink tubing.

5.2 Construction and Instrumentation

Data collected for this phase of the project involved a labor intensive field component of pile construction coupled with instrumentation and monitoring.

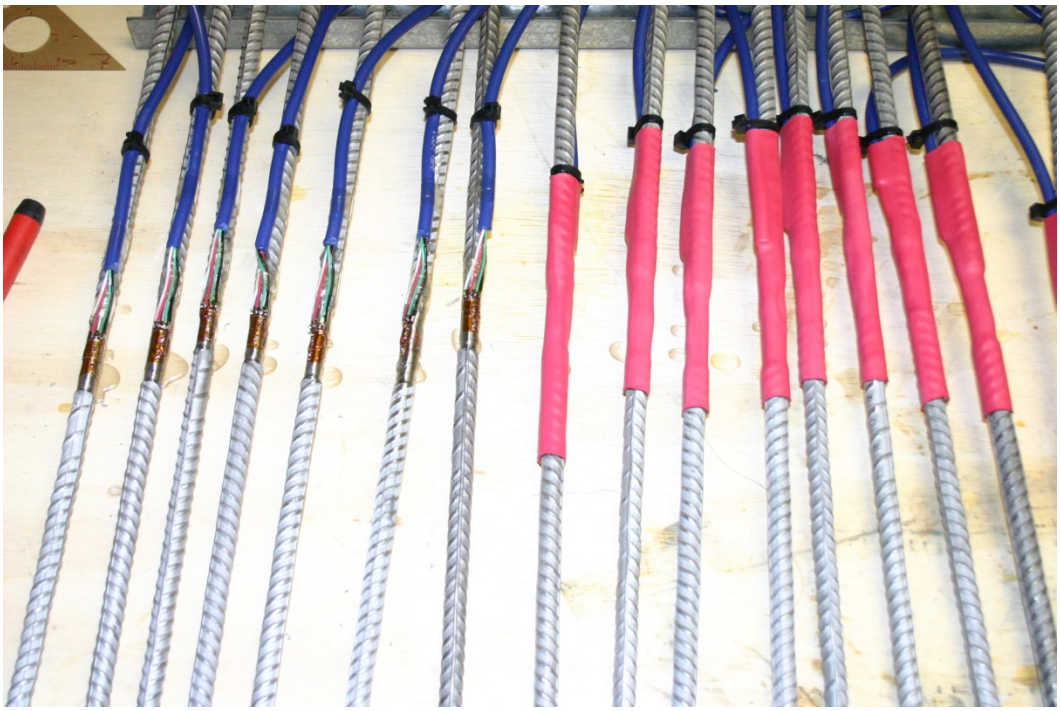

Figure 5.3 Stainless steel sister bar gages prepared for embedment.

5.2.1 Construction of Pile Specimens

The first stage of construction consisted of cutting each set of strands to length, running them through the header plates, and splicing them together using splicing chucks. By splicing the strands end to end and casting the piles in line with each other, each strand stressing event occurs simultaneously and identically for all for piles. As the splicing chucks allow for only a short segment of strand to be inserted, special attention had to be paid to the cut ends of strands. Many of the wires tended to unravel after cutting, thus hindering their use with the splicing chucks. This was particularly true with the XM-29 strand, but was mitigated by securing the strands with hose clamps or tape prior to cutting (Figure 5.4). Recall similar measures were taken during tension testing discussed in Chapter 4.

Once cut, the strands were fed through spirals (Figure 5.5) and the separation headers (Figure 5.6). Logistically, care must be taken to prevent the strands from crossing in the bed. Prior to insertion into the splicing chucks, each end was then wrapped with tie wire and the hose clamp removed. The tied end was inserted into the splice cut by manually placing the wedge clamps over the tie wire restraint (Figure 5.7). Figure 5.8 shows the strands being coupled/threaded together and Figure 5.9 shows the fully laid out strands prior to stressing.

Figure 5.4 All twelve hose clamp-restrained strands cut to length.

Figure 5.5 Spiral reinforcement placed over cut strands.

Figure 5.6 Each strand threaded through the appropriate hole in the pile header blocks.

Figure 5.7 Tie wire restrained strand (left); manually inserted in splicing chuck (right).

Figure 5.8 Ends of each strand material coupled by splicing chucks.

Figure 5.9 Spliced strand corridor between adjacent piles with different strand material.

Load cells were placed on the four corner strands at the dead end, as shown in Figure 5.10. This provided confirmation of jacking forces and allowed for continuous monitoring after tensioning to provide both relaxation and de-tensioning information.

Figure 5.10 Load cells inserted between chucks and bed header plates.

Each strand was pulled to remove slack to check the strand layout. All pile headers were measured to confirm pile length.

5.2.2 Stressing

In line with the results from laboratory relaxation testing, the strands were cyclically stressed to mechanically relax the steel before final stressing and concreting. Each strand was stressed to near full load (~21 k) and relaxed ten times (without a chuck). Upon reaching the tenth cycle, chucks were placed on the strands and they were stressed to full design load (21 k) and left alone for approximately 24 hours. During the holding period some movement of the strand was expected although minimal. However, in order to expedite construction, all spirals were stretched out to their appropriate layout on the first day in accordance with FDOT standard specifications for 14in piles. Spirals were restrained from movement by stringing all spirals together with stainless steel tie wire (Figure 5.11). Embedded sister bar strain gages were installed 2 diameters (28in) from the pile ends for future applications (Figure 5.12). These gages were mounted at mid-height (neutral axis), one on each side (2 gages per end, 4 gages per pile total). Figure 5.13 shows the stress jack and operator performing the stress cycles.

Figure 5.11 Spirals restrained by continuous stainless steel tie wire.

Figure 5.12 Embedded sister bar gages installed at mid height, 28in from each end.

Figure 5.13 48in stroke hydraulic jack used to cycle and bring strands to design load.

Figure 5.14 shows the order of stressing as well as the position and color coding of the load cells. Figure 5.15 shows the cyclic loading measured by the four load cells on the corner strands again color-coded to the Figure 5.14 layout. The stressing sequence was also used to identify individual strands and load cells herein. Final stressing took place the following day to recover any load lost to relaxation during that time. Table 5.3 lists the elongation of the strands after initial stressing and final stressing.

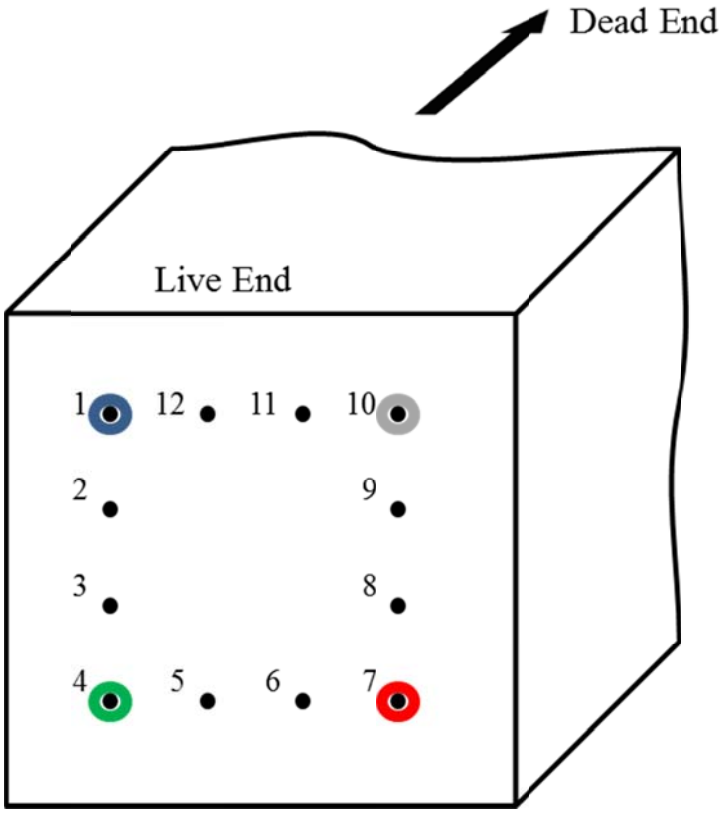

Figure 5.14 Stressing sequence and load cell locations.

Table 5.3 Strand elongations after stressing

Strand	Elongation after initial stressing (in.)	Additional elongation after final stressing (in.)	Total elongation (in.)
1	23.4	1.6	25.0
2	23.6	1.9	25.5
3	24.3	1.6	25.9
4	23.5	1.5	25.0
5	23.5	1.6	25.1
6	23.5	1.6	25.1
7	24.0	1.3	25.3
8	23.5	1.3	24.8
9	23.1	1.9	25.0
10	24.0	0.5	24.5
11	24.0	1.0	25.0
12	23.5	0.5	24.0

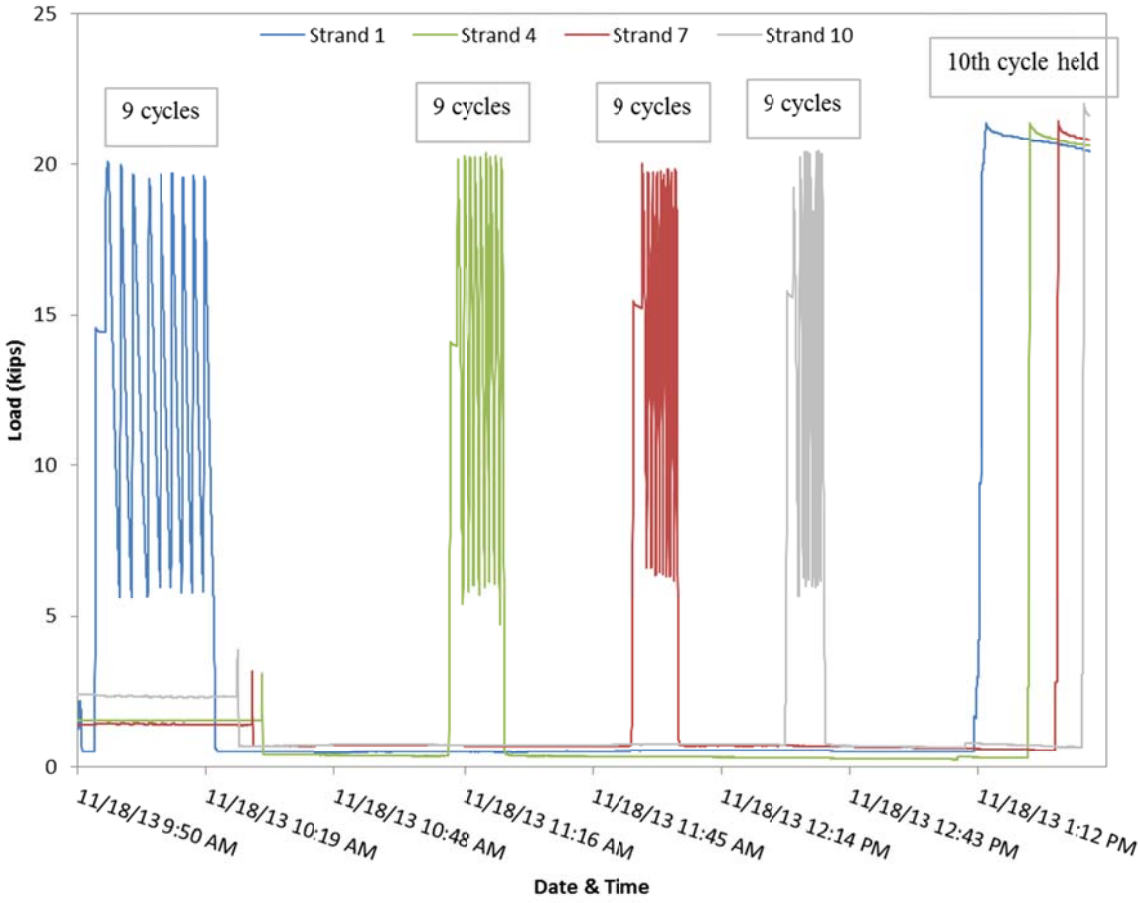

Figure 5.15 Initial stress cycles.

Conveniently, the 48in stroke jack used in the field was long enough to achieve the target elongation (24-25in) without complicated use of steps in the process that would be caused by a shorter stroke jack (a concern early-on in the lab phase). However, the hydraulically-unassisted jack relaxation upon removal of the hydraulic pressure was slow for the first couple of strands, so relaxation was assisted by direct hydraulic activation of the retracting mode of the jack. This is evident in the time to cycle the strands shown in Figure 5.15. Operator performance can also be noticed to have increased with more experience with field cycling.

5.2.3 Concreting

Subsequent to final stressing, the casting bed was rubbed with form oil and concrete was placed. Form oil was not sprayed indiscriminately over the casting bed and strands in order to prevent any unwanted variability in bond behavior between piles / strand material. Concrete was placed directly from the truck chute and was vibrated in the bed (Figure 5.16). One slump test was performed upon arrival of each truck (2 total) and 8 cylinders were cast from the beginning and end of each truck. Care was taken not to allow any cold joints to form in the piles, therefore when the second pile was completely

poured any remaining concrete in the first truck was not used to start the third pile. Mix design, delivery tickets, and test results are provided in Appendix A.

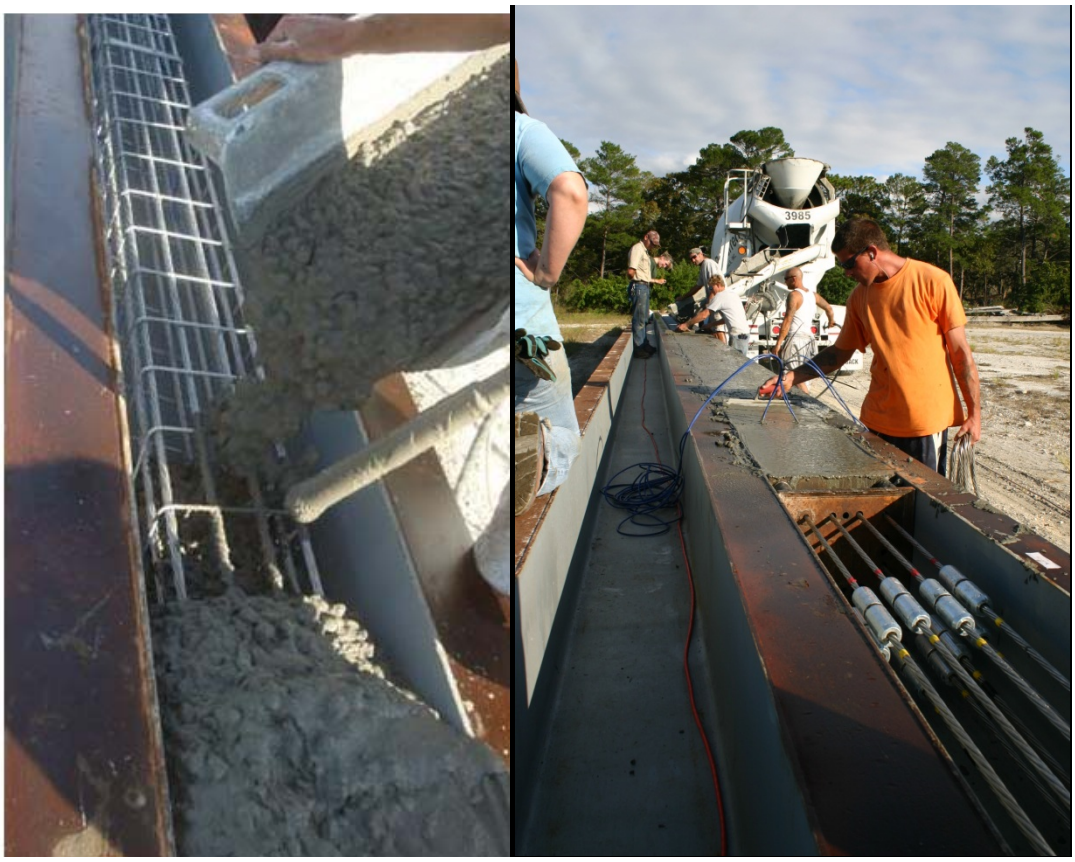

Figure 5.16 Concrete placement and finishing.

5.3 Instrumentation and Monitoring

Data from the load cells was continuously collected throughout the stressing, re-stressing, concreting, curing, and de-tensioning (Figures 5.17a through 5.17f). These graphs show the stress cycles (Figure 5.15) as well as the restressing to the target stressing force of 21kips (Figure 5.17b and c). The amount of load lost in the first strand (Figure 5.17a) can be attributed to some relaxation but more prominently the elastic shortening of the casting bed which is shown as steps / drops in load corresponding to each strand being stressed. The total loss in load cell from the subsequent 11 strands was approximately 640lbs. The computed stiffness of Strand #1 obtained from the measured load and strand elongation (20.7kips / 23.33in = 0.89 kip/in) provides a convenient method to compute the elastic shortening of the bed from the subsequent 11 strands. Therein, a 640lb loss in Strand #1 (0.64kips) divided by 0.89k/in is 0.72 inches. For 12 strands however, the bed shortens additionally to make a total bed shortening 12/11 times 0.72in, or 0.79in.

Following completion of the initial stressing of all strands, elastic shortening of the bed ceased but additional losses due to relaxation of the strands continued (Figure 5.17b).

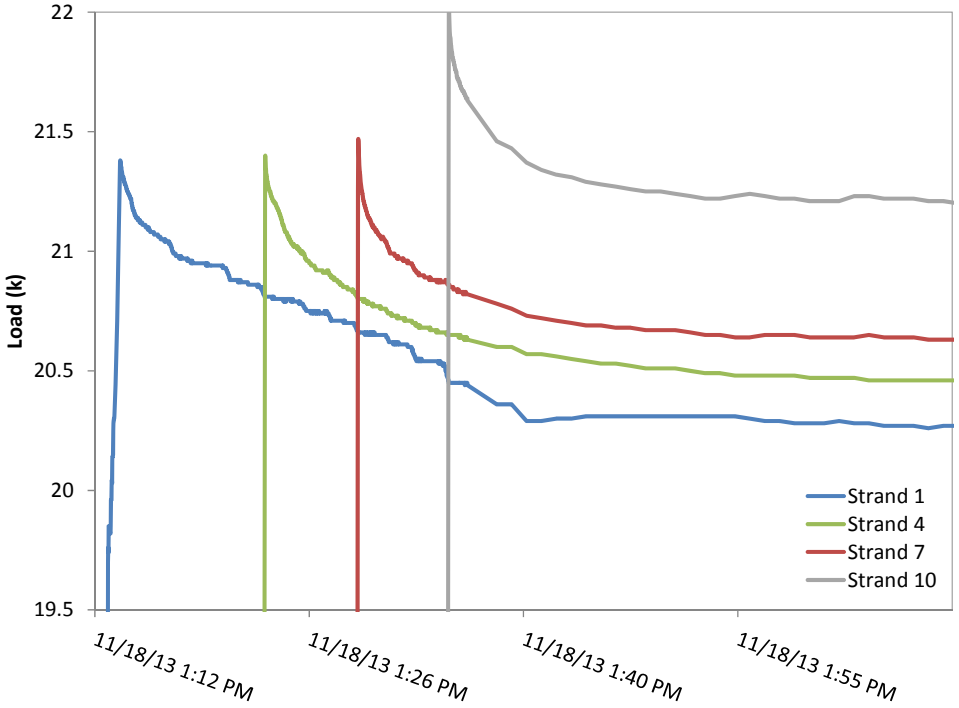

Figure 5.17a Timeline from load cell data after final cycle of initial stressing (Day 1)

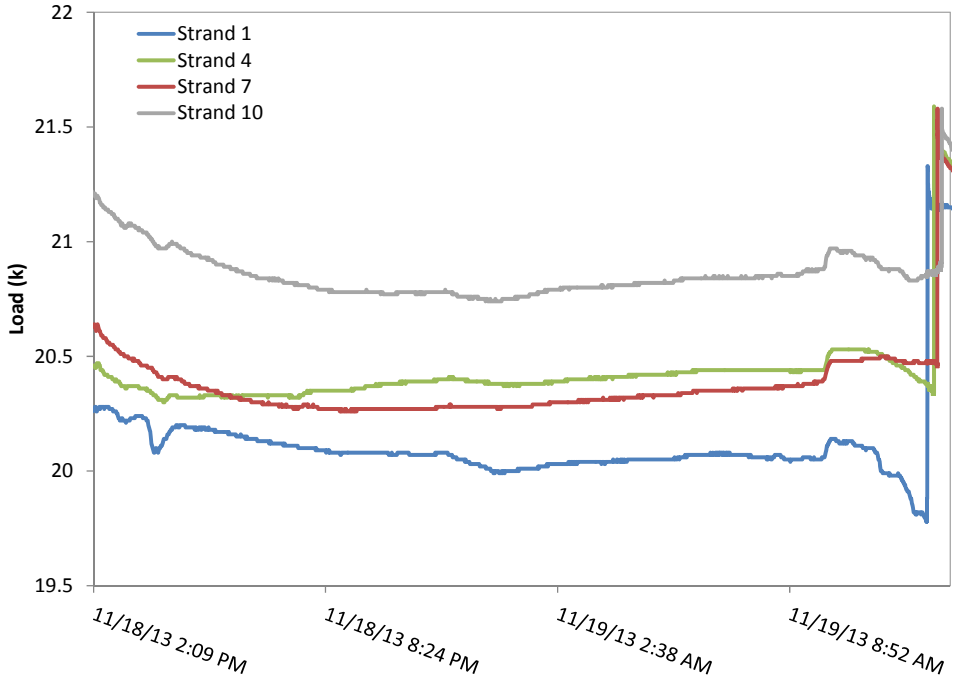

Figure 5.17b Timeline from load cell data between initial and final stressing (Day 1-2)

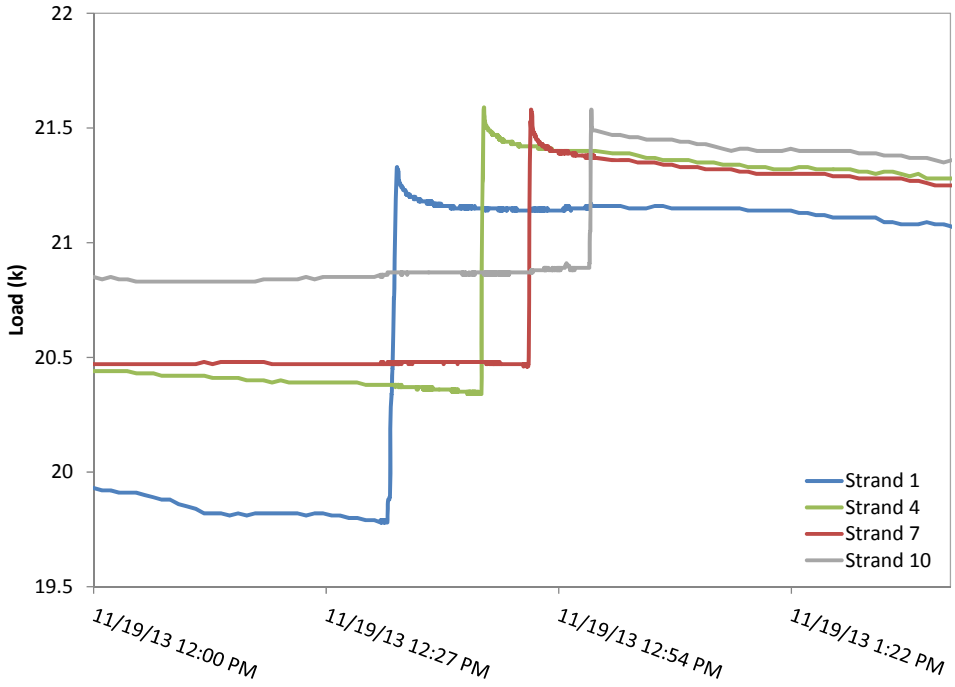

Figure 5.17c Timeline from load cell data final stressing (Day 2)

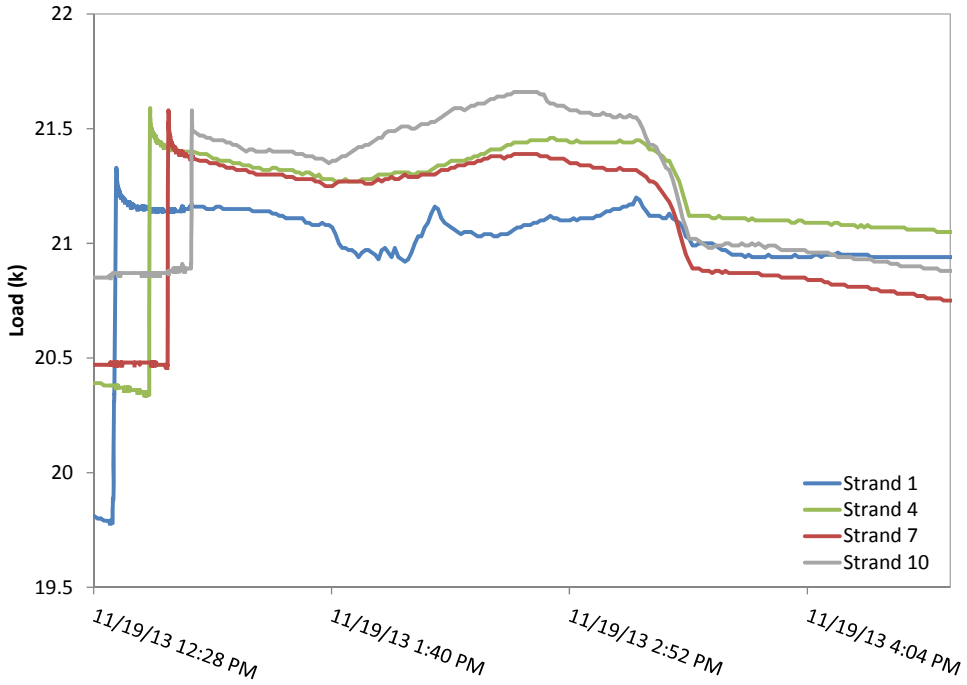

Figure 5.17d Timeline from load cell data during final stressing and concreting (Day 2)

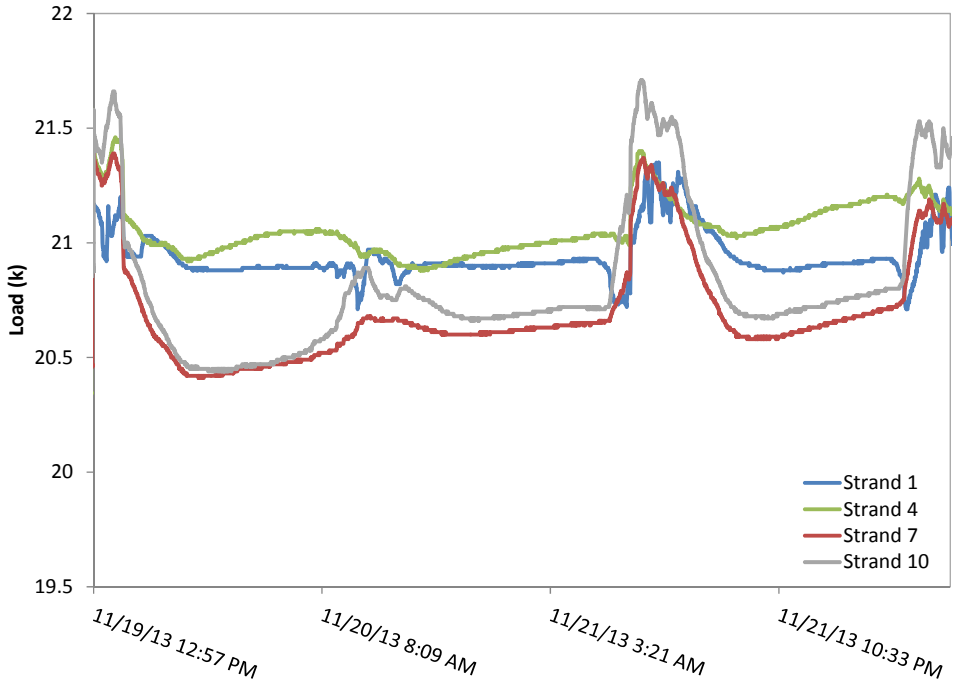

Figure 5.17e Timeline from load cell data during concrete curing (Days 2-5)

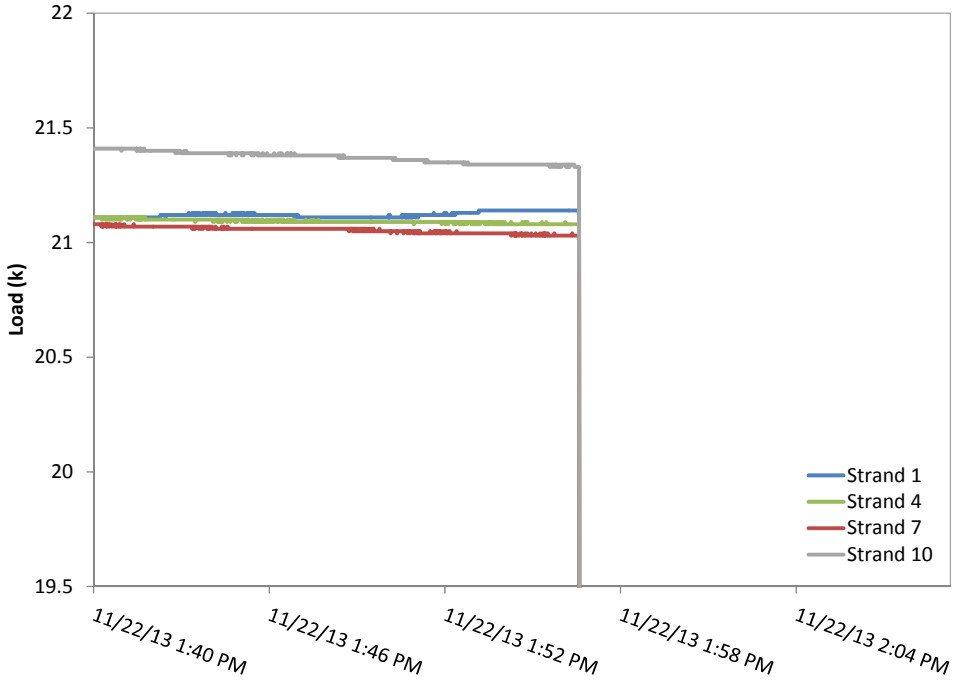

Figure 5.17f Timeline from load cell data during de-tensioning (Day 5)

The load cell readings are provided in Table 5.4 for discrete times of interest including: initial load after 10th cycle, load after all strands initially loaded, lowest load shown overnight within first 24hrs, load just before prestressing, load during re-stressing, load after all strands were re-stressed, and the load just prior to de-tensioning.

Table 5.4 Load cell data at various times during the fabrication process.

Load in kips						
		Strand 1	Strand 4	Strand 7	Strand 10	Avg.
11/18 1:13 – 1:35 PM	Jacking force on 10^{th} cycle of initial stressing	21.4	21.4	21.5	22.1	21.6
11/18 1:42 PM	Just after completion of all initial stressing	20.3	20.6	20.7	21.3	20.7
11/18 8:15 PM	Minimum load due to relaxation after initial stressing	20.1	20.4	20.3	20.8	20.4
11/19 12:27 PM	Just before re-stressing	19.8	20.4	20.5	20.9	20.4
11/19 12:35 – 12:58 PM	Jacking force at re-stressing	21.3	21.6	21.6	21.6	21.5
11/19 1:40 PM	Just before concreting	21.1	21.3	21.3	21.4	21.2
11/22 1:55 PM	Just before de-tensioning	21.1	21.1	21.0	21.3	21.1

Further review of this data showed that the effective modulus of the four strands in series could be computed from the actual load measured and the elongation of that strand. As modulus values from testing are most sensitive to displacement (strain) measurements, long samples lengths provide the most reliable results. In this case the sample was a composite of four materials and the gage length was 400ft. The prorated strand area (based on length and area of each strand type) was used to compute the composite modulus of the four strand system using the following equations:

$$E_{composite\ field} = \frac{Load_{measured}/a_{composite}}{elongation/L_{total}}$$

where

$$a_{composite} = \frac{a_{316}L_{316} + a_{2205}L_{2205} + a_{XM29}L_{XM29} + a_{lowlax}L_{lowlax}}{L_{total}}$$

Using the areas for each material given in Table 4.2 and field lengths of each strand (85ft for each of the stainless steel piles and 145 for the low-lax carbon steel), the composite modulus was found to be 27,600ksi. A predicted value was also computed using a similar approach from laboratory relaxation data values of modulus (from Figure 4.40), where the composite modulus was prorated on the basis of lengths to obtain 26,800ksi.

$$E_{composite\ predicted} = \frac{E_{316}L_{316} + E_{2205}L_{2205} + E_{XM29}L_{XM29} + E_{lowlax}L_{lowlax}}{L_{total}}$$

By averaging the load in the four corner strands from load cell data, the overall trend of load versus time can be reviewed (Figures 5.18a – 5.18c). The temperature of the air directly above the bed was also recorded and shown in these figures. From these graphs, the response from varying temperature can be seen to be partly responsible for variations in load over the 96hr field testing timeframe. Over the first 24hrs (Figure 5.18b), strand cooling from rapid air temperature changes inversely affect the load, while the gradual changes from day to night appear to be more proportional.

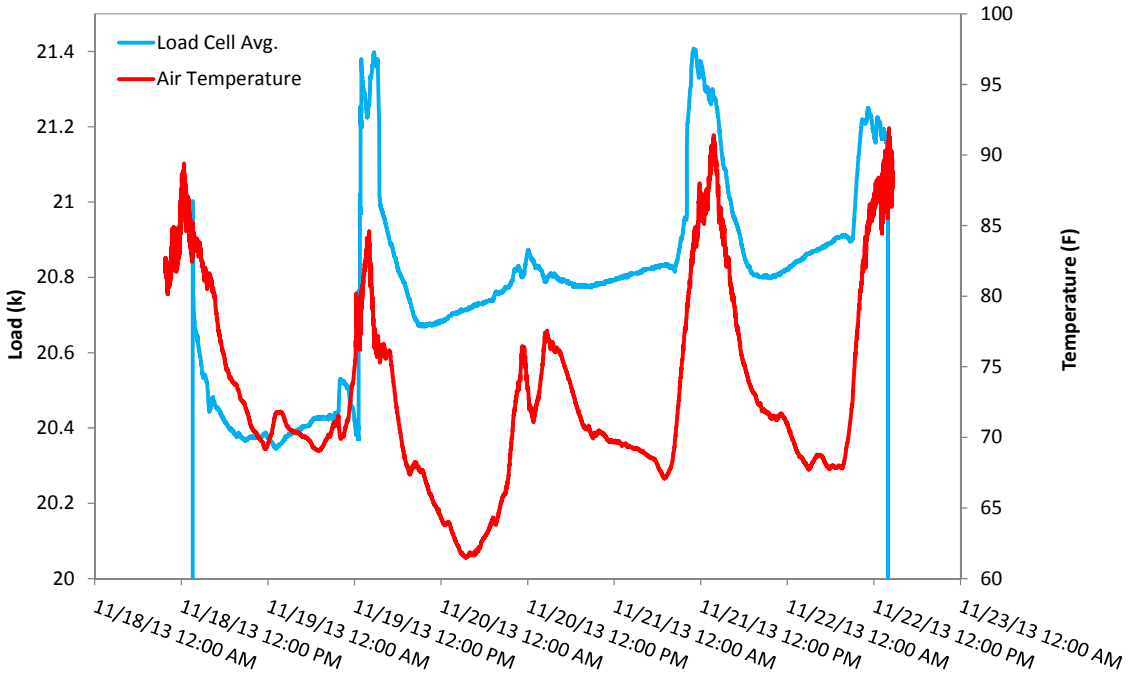

Figure 5.18a Average load and air temperature over the 96hr field testing time frame.

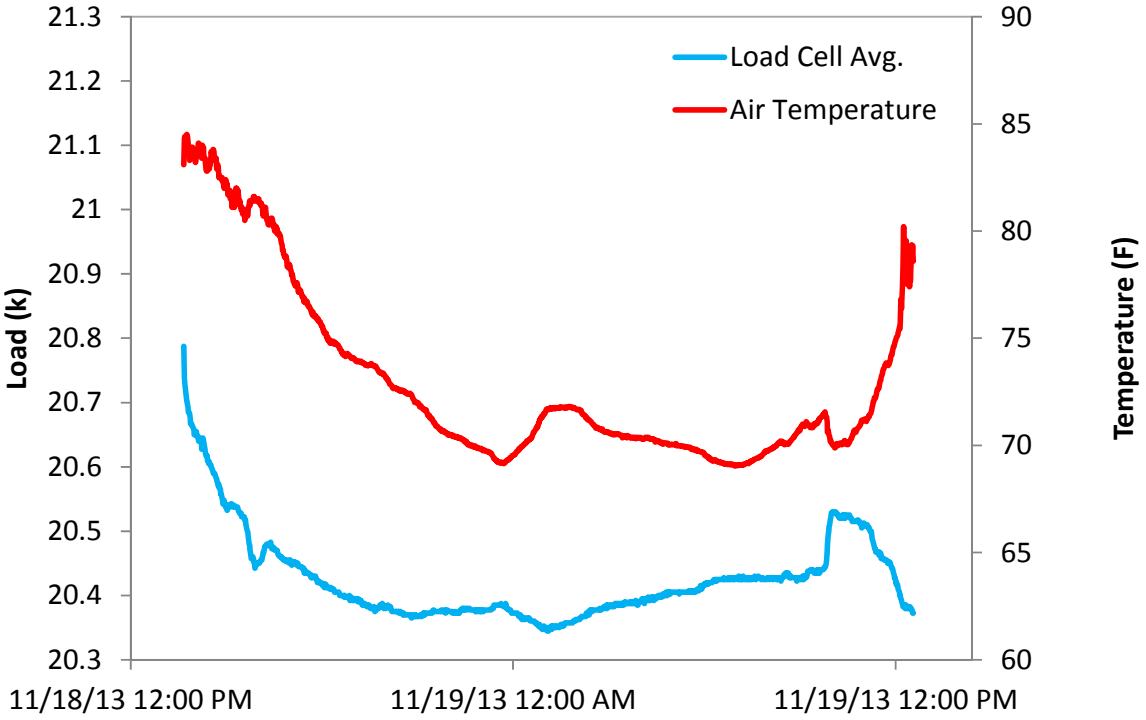

Figure 5.18b Average load and air temperature over the first 24hrs of field testing (prior to concreting).

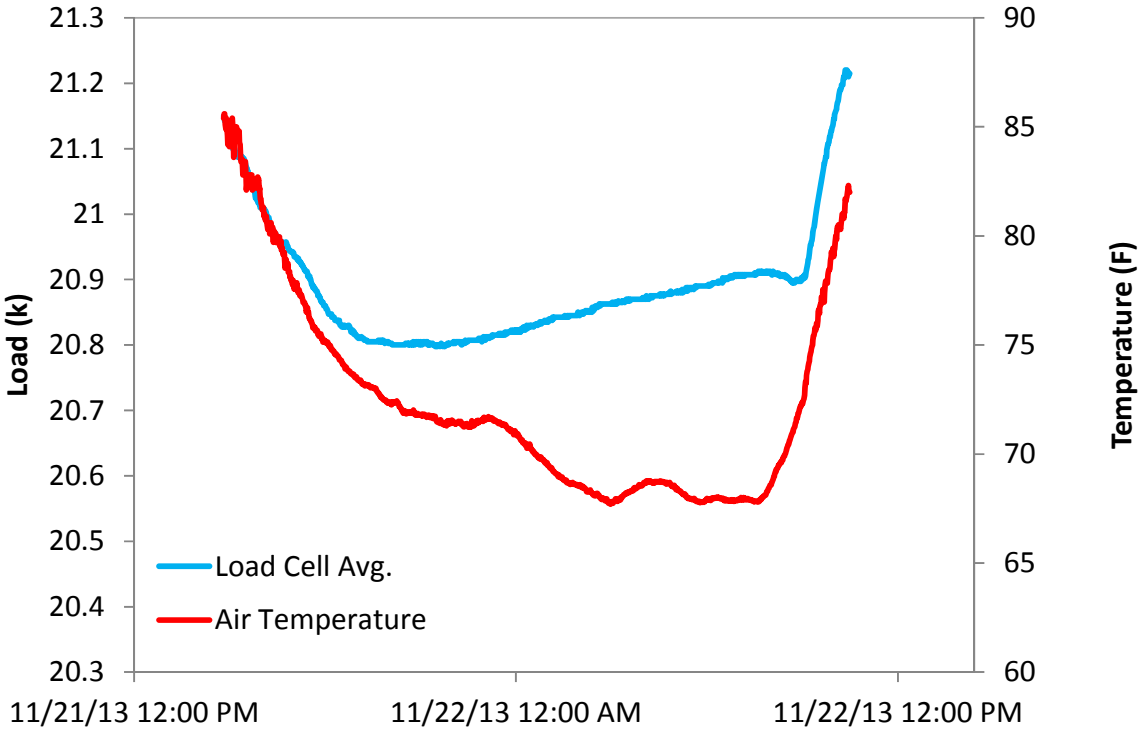

Figure 5.18c Average load and air temperature over the last 24hrs of field testing (cured concrete).

An increasing trend in strand force can also be seen that is independent of the observed temperature variations. This trend is speculated to be caused by shrinkage forces that if left too long without de-tensioning can develop to levels higher than the tensile strength of the concrete.

5.3.1 Surface mounted gages

Along with the load cell installation and monitoring discussed above, an elaborate surface gage program was implemented to show the transfer length upon de-tensioning. This involved mounting surface gages, connecting all gages to computerized data collection systems, and monitoring during de-tensioning (cutting the strands). This has traditionally been an accepted mechanism to determine the transfer length which shows the point at which no additional strain is noted. In effect, a sufficient length of bond is required to withstand the full strand force which in this case was 21kips. In this regard, a strand loaded to a higher load would conceivably need a longer embedment to develop that force and vice versa. The surface gage layout used for all piles is shown in Figure 5.19.

For this project 60mm long, 120ohm, resistive type strain gages (Figure 5.20) were epoxy bonded to the concrete surface. In general, the process entails: (1) grinding the concrete surface smooth, (2) cleaning the surface of all loose debris and dust, (3) placing a layer of paste-consistency epoxy on the concrete and embedding the gage into epoxy. Figures 5.19 - 5.22 show the overall surface gage program components and process.

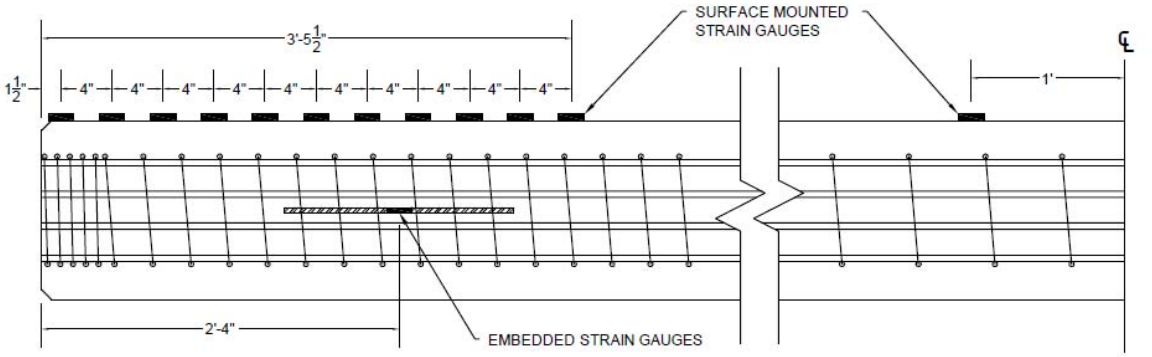

Figure 5.19 Instrumentation layout for each end of every pile.

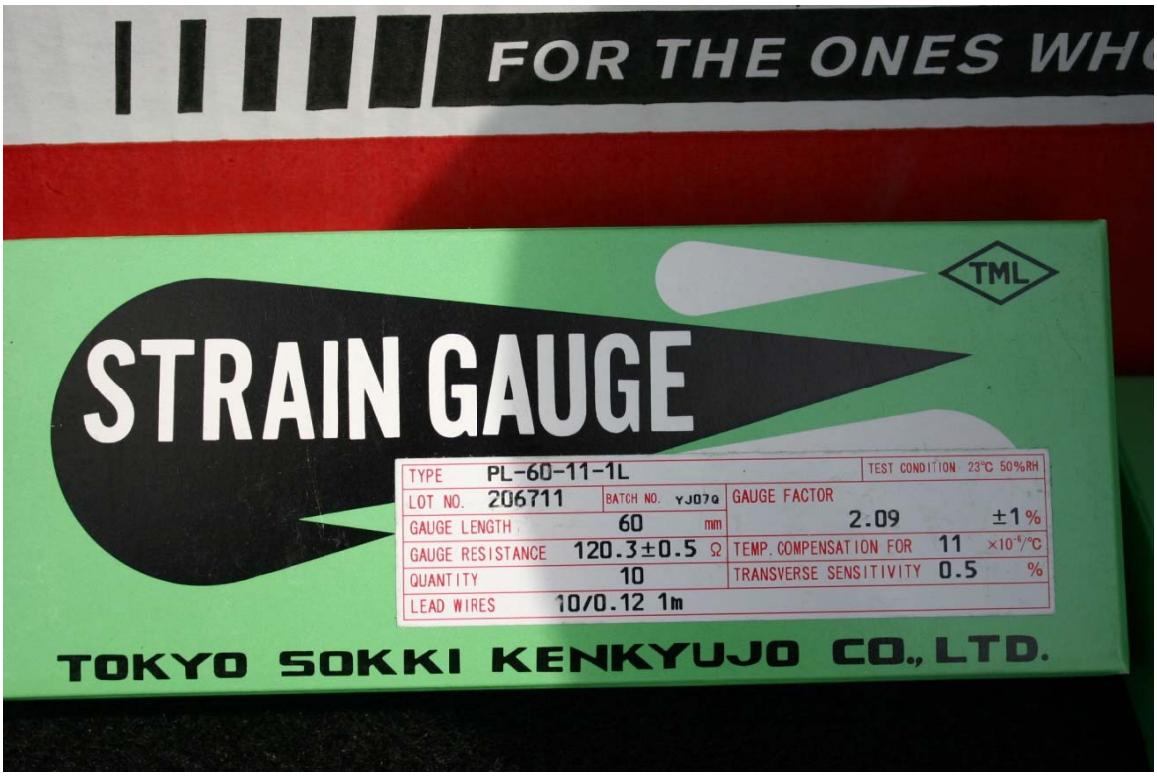

Figure 5.20 60mm strain gage selected for surface mounting.

Figure 5.21 Construction grade epoxy paste.

Figure 5.22 Grinding pile (top left); gage layout (top right); embedding gages in epoxy (bot left); and finished instrumentation (bot right).

5.3.2 Data Collection Wiring and Setup

To minimize wire lengths and the associated costs, each pile was assigned a dedicated high speed data collection system. Each pile had 11 surface strain gages near each end on 4 inch centers (40in total length) starting 1.5 inches from the ends and two strain gages mounted near the center to serve as an indication/confirmation of the full transferred strain. When coupled with the four embedded strain gages, each pile had 28 strain gages wired back to the data collection system. This translated into lead wires spanning from the end of each pile back to the center of the pile where the computerized systems were positioned or approximately 1000ft of lead wire per pile. Figure 5.23 shows the gages being connected and an overview of the long lead wires.

Figure 5.23 Surface gage wiring back to data collection systems.

All computer systems (Figure 5.24) were synchronized in time and strain gage electrical offsets were removed prior to de-tensioning. In all, five computerized data collections systems were used: one connected to each of the four piles and a fifth attached to the load cells which continuously monitored for the duration of the tensioning and de-tensioning time frame (approximately 96hrs). The de-tensioning/cutting sequence is shown in Figure 5.25 which was selected from FDOT specifications. Figure 5.26 shows the cutting process performed with an oxy-acetylene torch. As the low-lax carbon steel pile was closest to the live end where cutting occurred first, the surface strains were most pronounced during that cutting process as shown in Figure 5.27. The center gage shows the highest amount of possible strain, although some bed friction may still have resided which was eliminated once the next open corridor was cut.

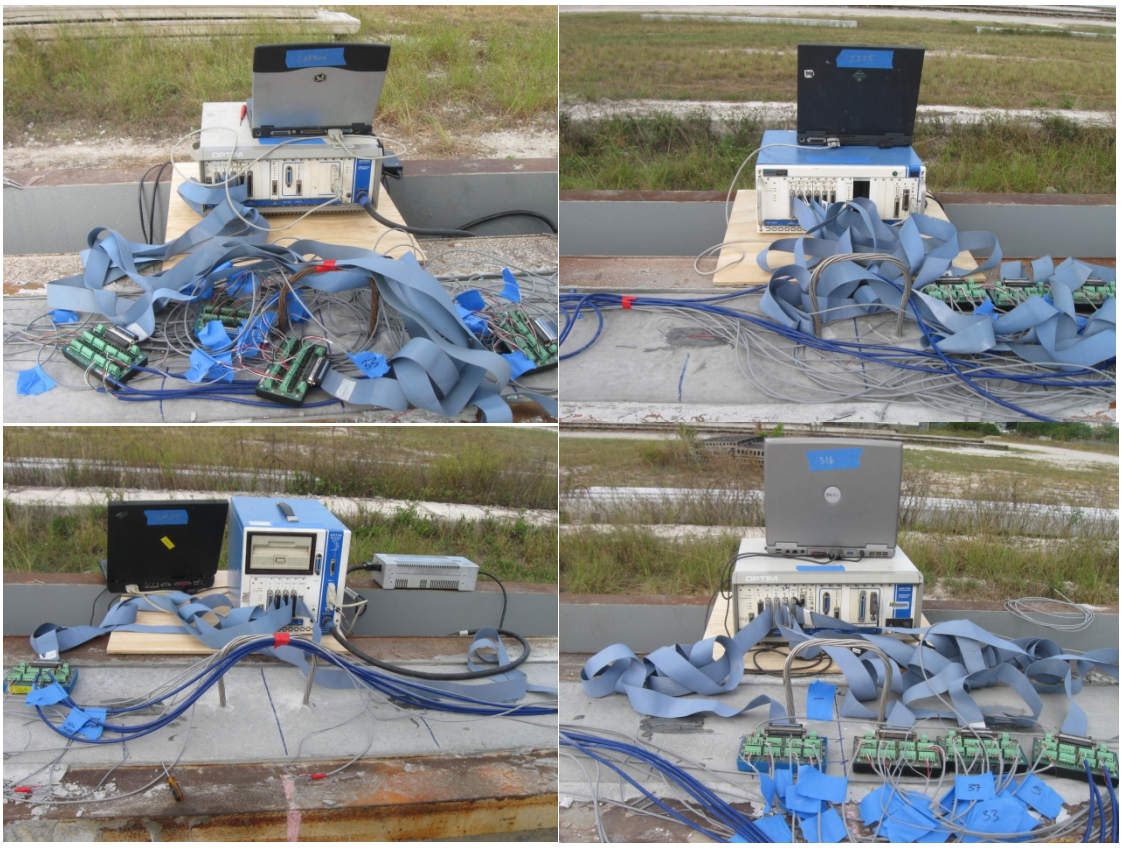

Figure 5.24 Data collection systems for each pile (top left: Carbon, top right: 2205, bottom left: XM-29, bottom right: 316).

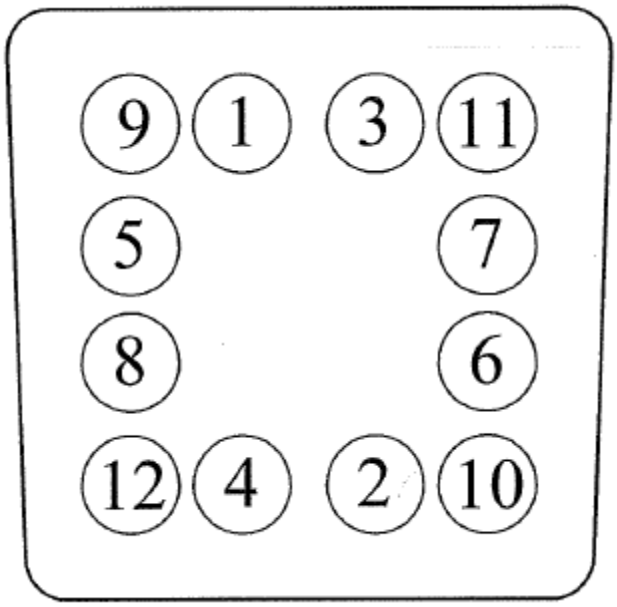

Figure 5.25 De-tensioning sequence for 12-strand piles.

Figure 5.26 De-tensioning performed by cutting strands with a torch.

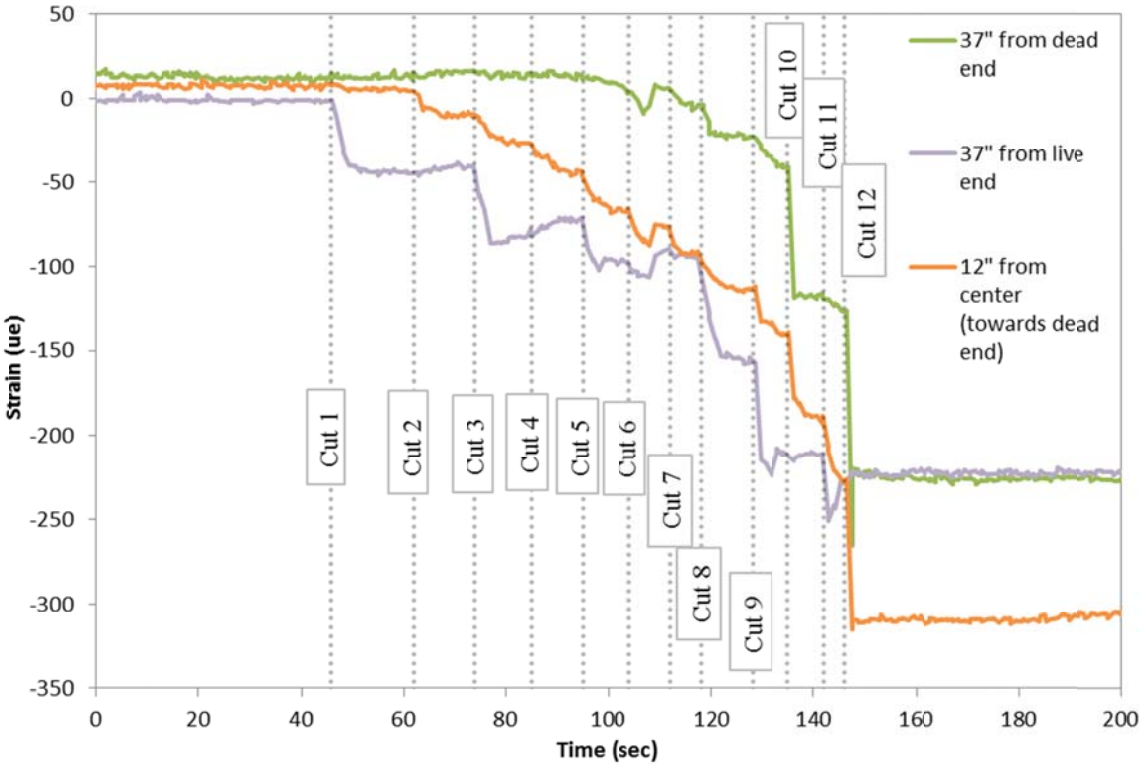

Figure 5.27 Strain vs. time during de-tensioning for selected surface strain gages on the low-lax carbon pile during first cuts (live end).

Full de-tensioning of the entire bed proceeded cutting from the live to dead end thereby fully releasing the low-lax carbon steel pile first followed by the 2205, XM-29 and then the 316 pile. Figure 5.28 shows the center of pile strain and the dead end load cell readings as a gradual increase in strain as the bed was fully released. As expected the load cells closely mimic the strain response in the closest pile to the dead end (316). The dashed black lines denote the times when cutting each of the five corridors between or beside the piles initiated. The entire process took approximately 10 minutes.

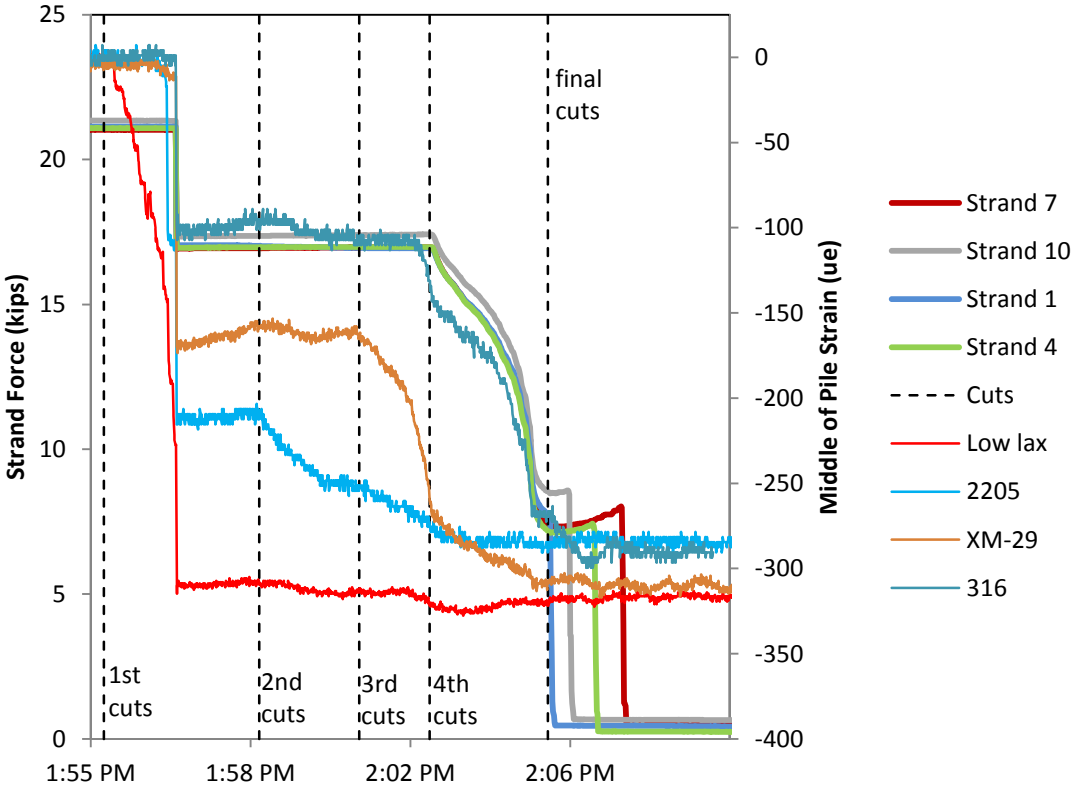

Figure 5.28 Gradual load transfer into piles from live to dead end as each pile is cut loose from both ends.

As expected strains within the pile were lowest at the pile ends and increased with distance from the ends. Figures 5.29a - 5.29d show the raw strain gage data vs. time for each of the low-lax, 2205, XM-29 and 316 piles, respectively. Figures 5.30a - 5.30d show the strain gage data as a function of surface position time for each of the low-lax, 2205, XM-29 and 316 piles, respectively. And finally, Figures 5.31a - 5.31d show the linear regression of the strain gage data vs. position for each of the low-lax, 2205, XM-29 and 316 piles, again respectively.

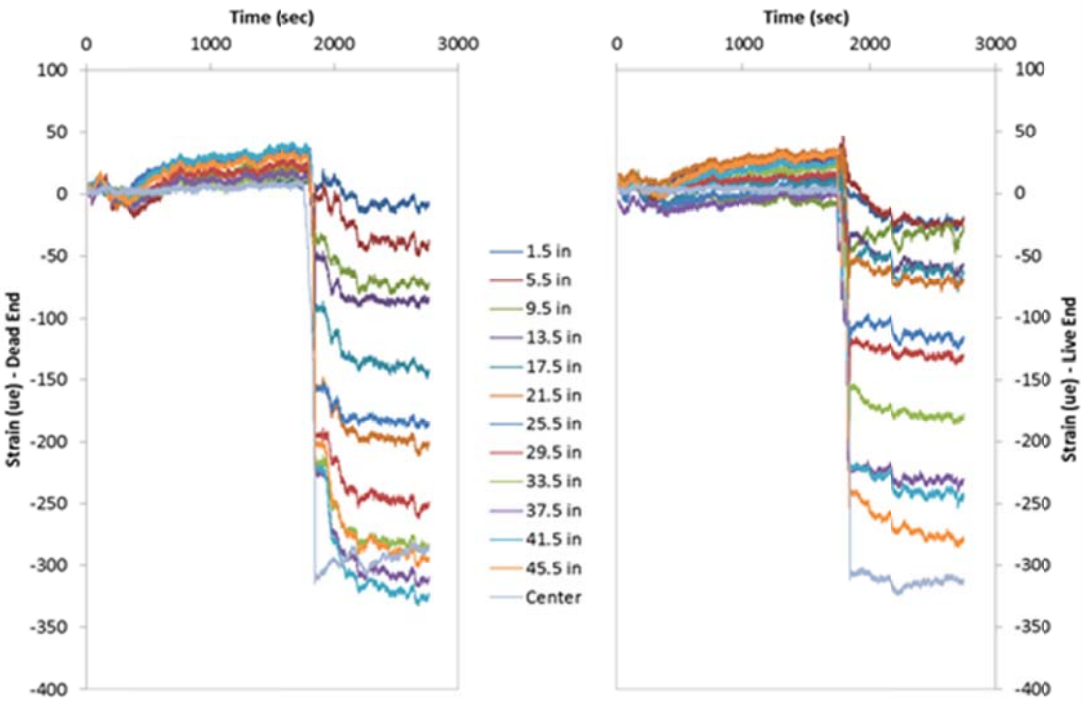

Figure 5.29a Strain gage response during cutting for low-lax carbon steel pile.

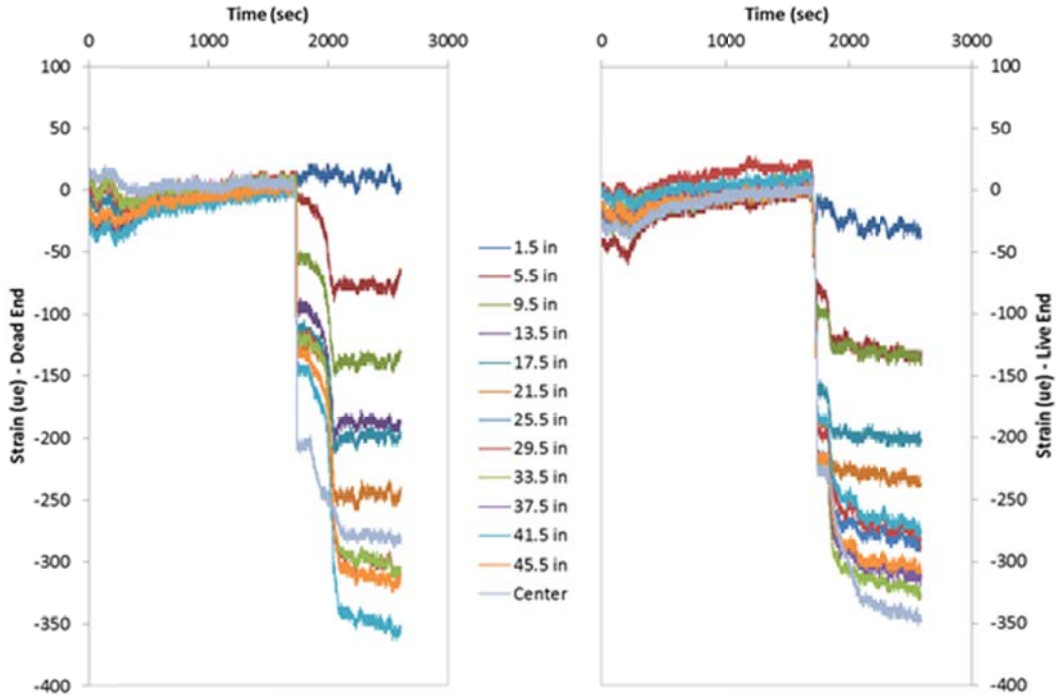

Figure 5.29b Strain gage response during cutting for 2205 stainless steel pile.

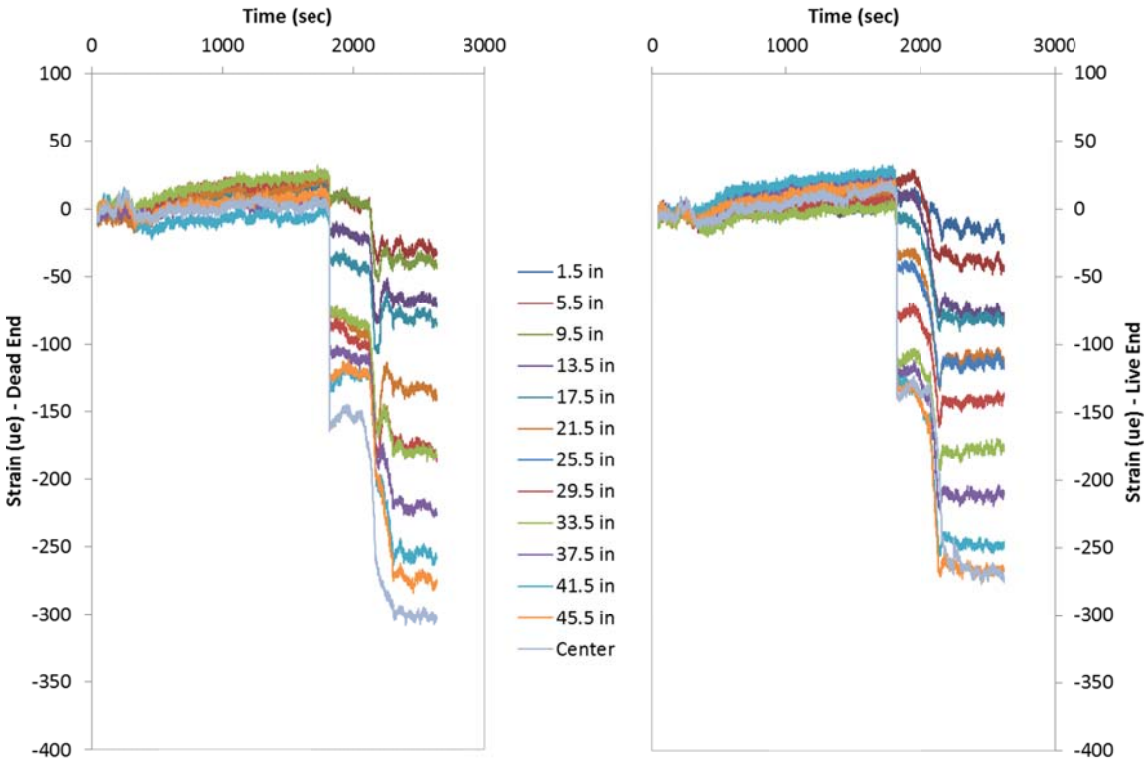

Figure 5.29c Strain gage response during cutting for XM-29 stainless steel pile.

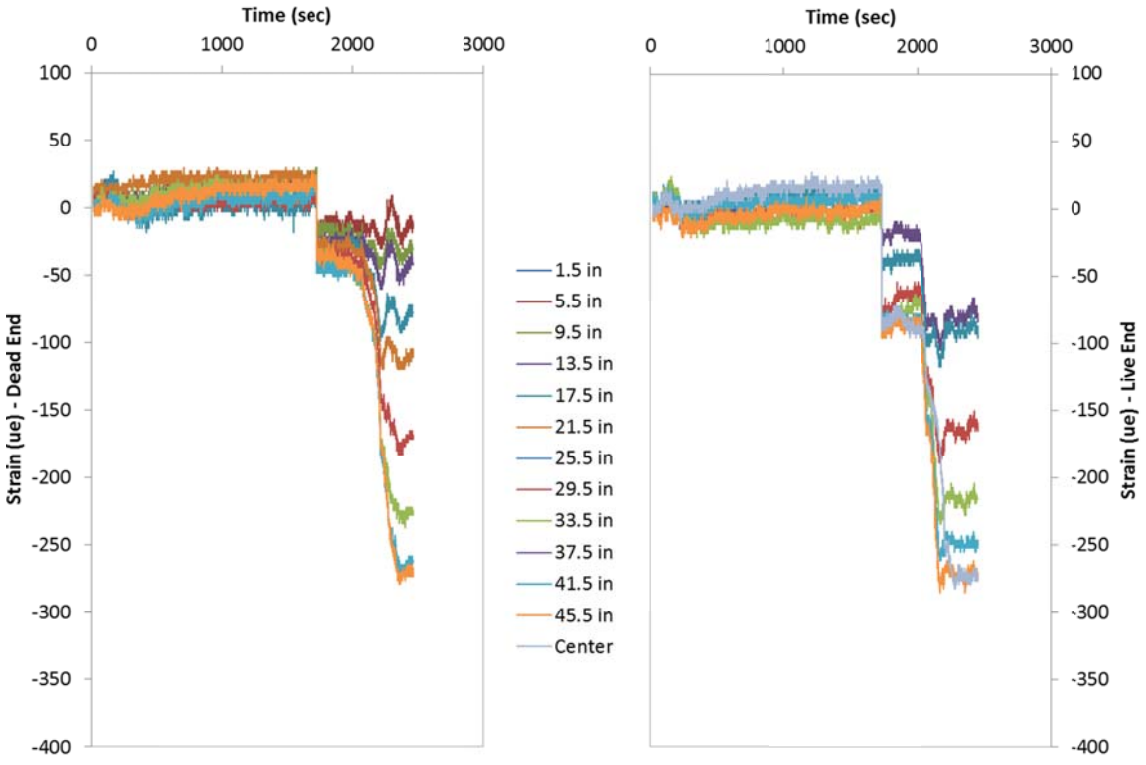

Figure 5.29d Strain gage response during cutting for 316 stainless steel pile.

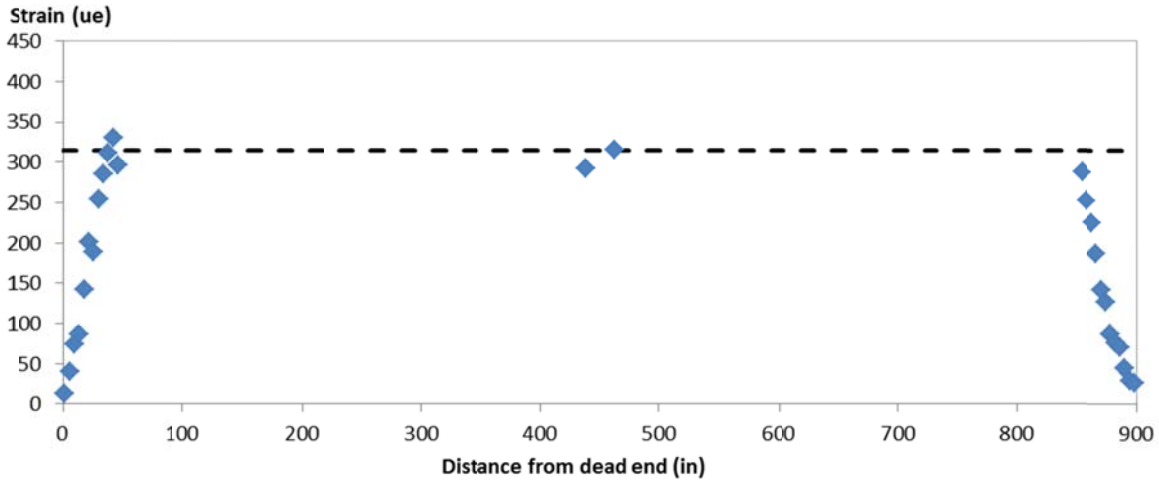

Figure 5.30a Strain vs. position along pile (low-lax carbon steel pile)

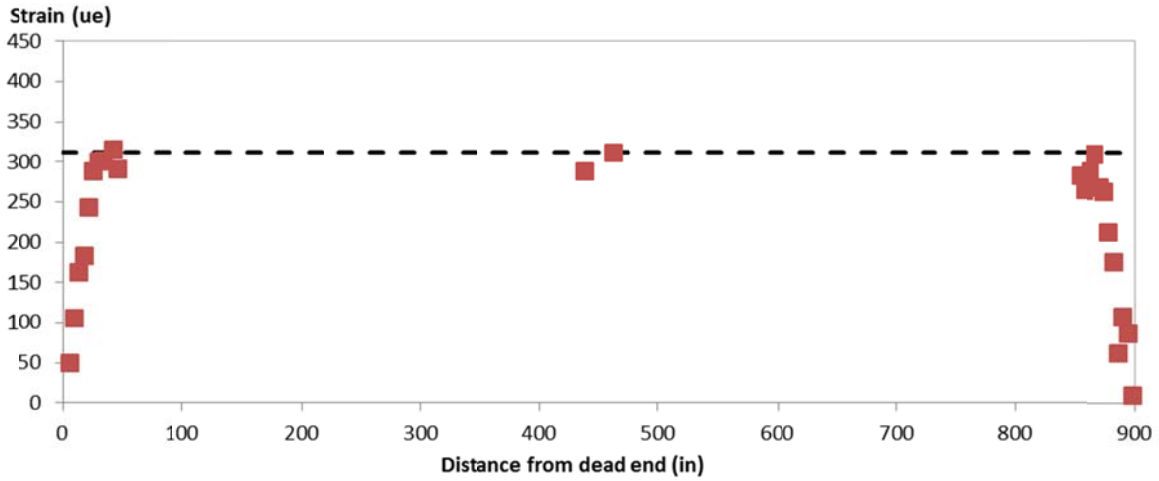

Figure 5.30b Strain vs. position along pile (2205 stainless steel pile)

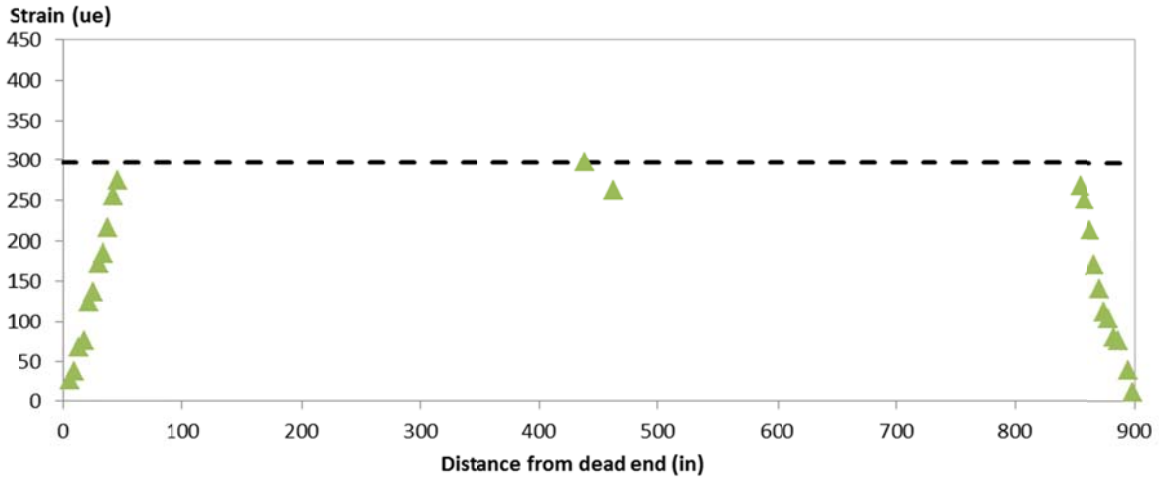

Figure 5.30c Strain vs. position along pile (XM-29 stainless steel pile)

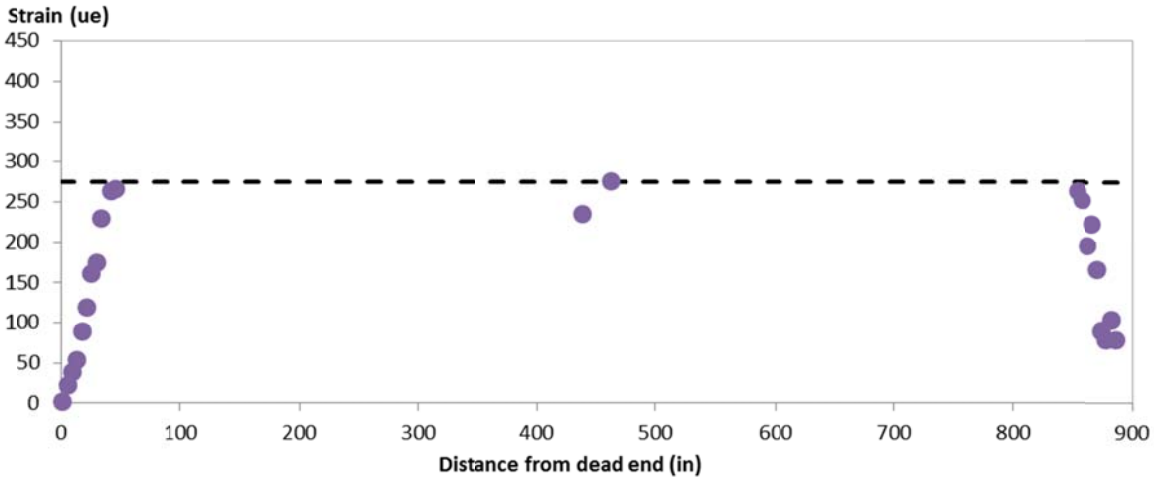

Figure 5.30d Strain vs. position along pile (316 stainless steel pile)

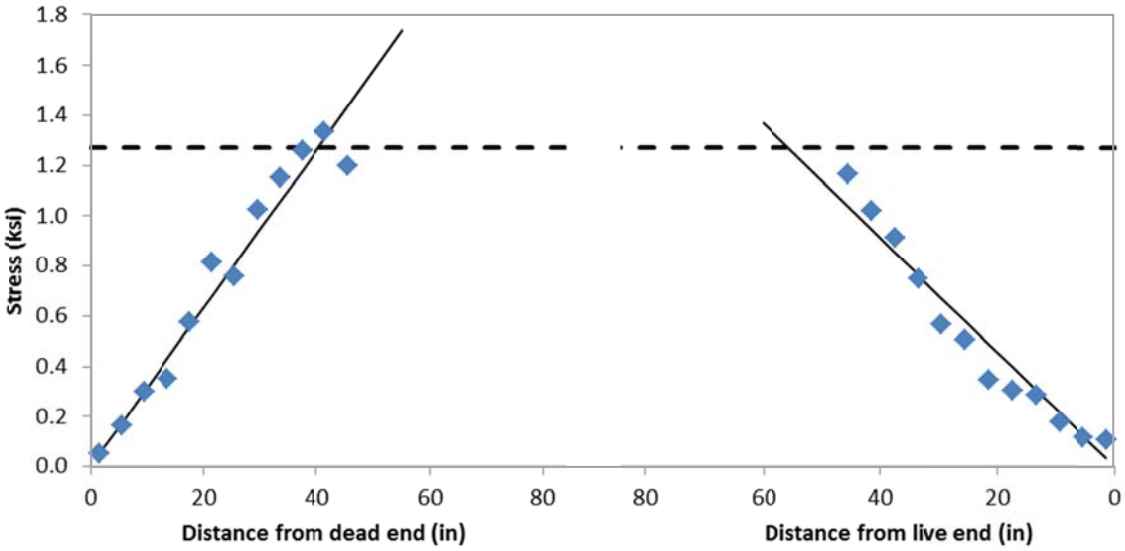

Figure 5.31a Linear regression of strain in transfer zones (low-lax carbon steel pile)

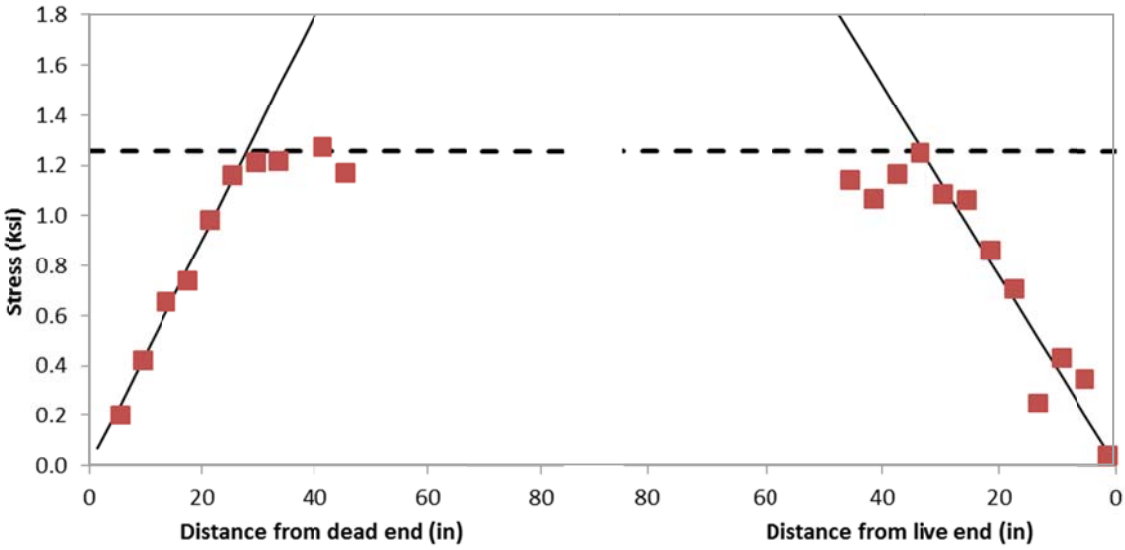

Figure 5.31b Linear regression of strain in transfer zones (2205 stainless steel pile)

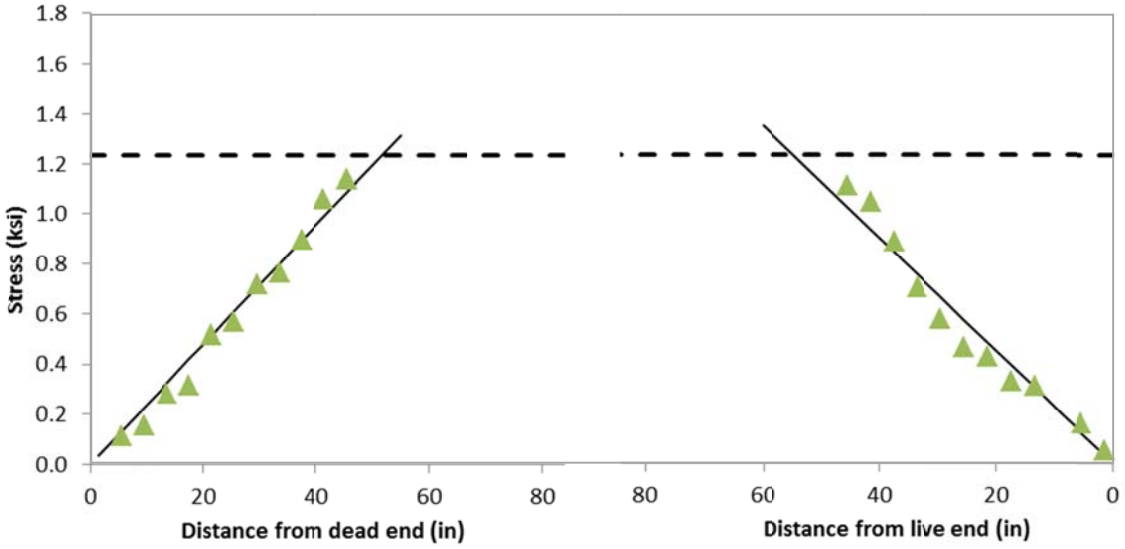

Figure 5.31c Linear regression of strain in transfer zones (XM-29 stainless steel pile)

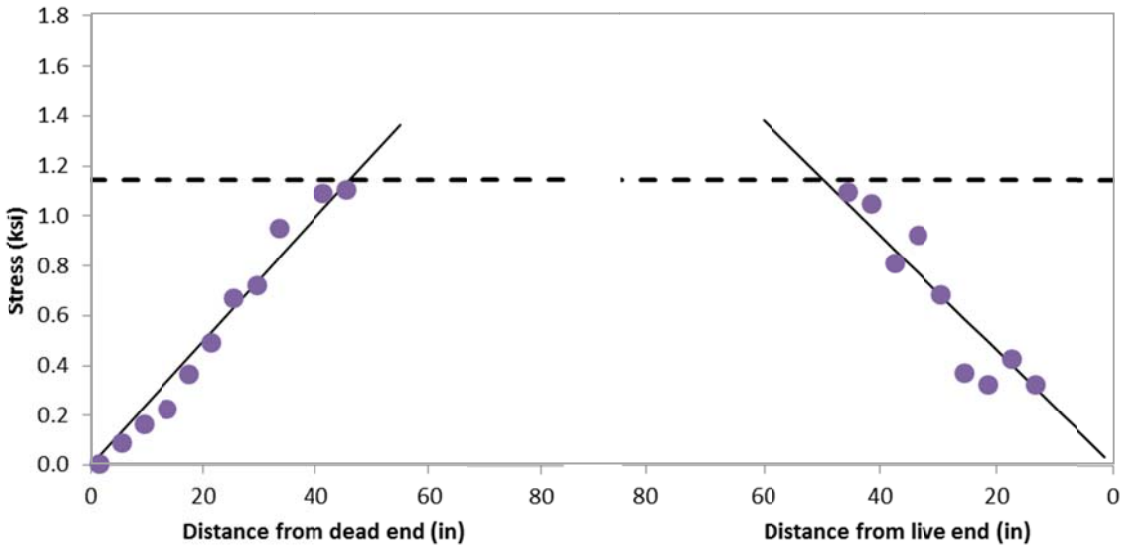

Figure 5.31d Linear regression of strain in transfer zones (316 stainless steel pile)

Using the concrete strength from the delivery trucks associated with each pile, the strain distributions shown above were converted to concrete stress and plotted in Figure 5.32. The effective prestress was in general proportional to the modulus of the steel wherein the low-lax carbon steel achieved the highest values followed by the 2205, XM-29, and 316 piles.

In relation to the AASHTO code value for transfer length of 30in (60 times diameter of strand), the observed average transfer lengths ranged from 30.5in to 52.6in as shown in Table 5.5. This translates into values of 60 to 101 times the diameter of the strand. However, there were no observed detrimental effects in transfer length as a result of using the stainless steel strands selected for this study. In fact, the 2205 showed a marked reduction in transfer length that may be in part explained by the slightly larger area, $0.161in^2$, when compared to the rest which were $0.156in^2$, $0.153in^2$, and $0.147in^2$ for the low-lax, XM-29 and 316, respectively (Table 4.2).

Table 5.5 Effective prestress and transfer length

Pile I.D.	E strand (Figure 4.40)	max strain	f 'c	Unit wt.	E conc.	Effective prestress	Transfer length		
							Live	Dead	Avg.
	ksi	ue	psi	pcf	ksi	ksi	in.	in.	in.
Low-Lax	28,900	315	5753	137.5	4036	1.27	40.3	55.7	48.0
2205	23,500	312	5753	137.5	4036	1.26	27.9	33.1	30.5
XM-29	22,100	297	6015	137.9	4145	1.23	51.5	53.8	52.6
316	20,500	276	6015	137.9	4145	1.14	46.0	49.5	47.8

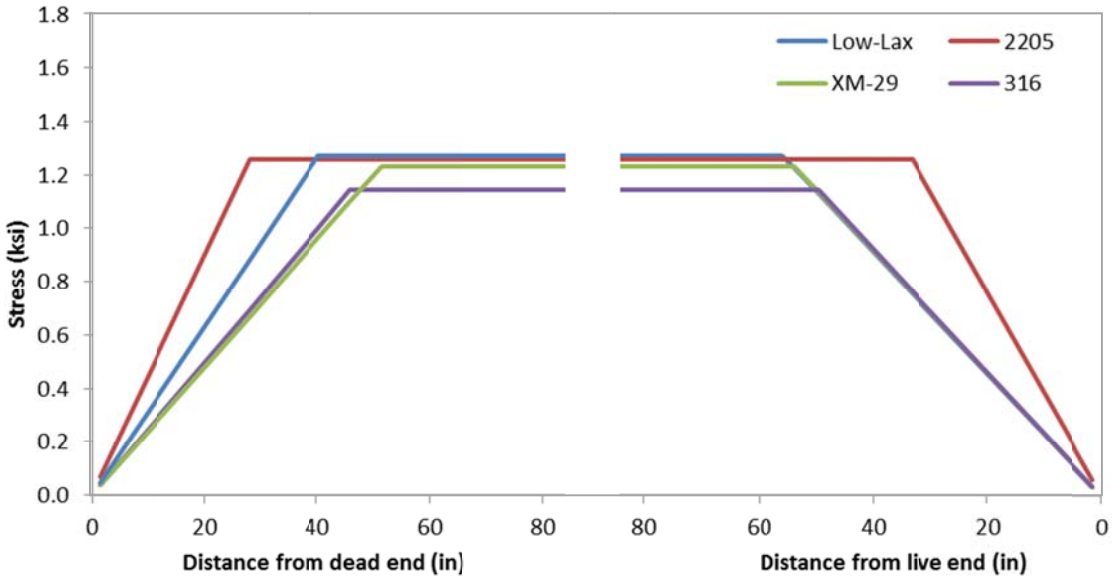

Figure 5.32 Regressed strain distributions for each pile

Chapter 6: Conclusions

In Florida, approximately two thirds of the 5500 bridges reside in marine environments making corrosion damage one of the main sources of service life reduction. Most of this damage pertains to substructural elements (e.g. piles or drilled shafts, footings, and columns). Therein, the service life of these elements is, in part, dictated by the time required to corrode the steel once chloride ions are at the surface of the steel (concrete quality being a similarly important factor).

Stainless steel materials have a higher tolerance to chloride ions and therefore can be expected to extend the service life of marine structures. For prestressed piles, however, the high strength requirements for prestressing strands make many stainless steel grades inadequate and in most cases are not available in strand form. Further, if the strength of the stainless steel is increased through cold working or similar, heightened concerns arise regarding the possibility of stress corrosion cracking (SCC). This study investigated the corrosion and structural performance of three candidate stainless steel materials with the goal of identifying a possible solution that uses stainless steel for prestressed concrete piles suitable for Florida marine environments.

The three candidate stainless materials selected for evaluations were an austenitic Grade 316 stainless steel, a low nickel but high manganese alloy known as XM-29, and a duplex (austenitic / ferritic) alloy known as 2205. The primary components of this study included: (1) screening for potential SCC development in single wire specimens, (2) documenting the tensile strength and relaxation properties of 7-wire strands, and (3) the transfer length determination from the fabrication and testing of full scale prestressed piles. Given the virtually infinite alloy combinations from which to choose, the candidate materials were largely selected on the basis of their availability in strand form.

6.1 Corrosion Tests

The results suggest that duplex high-strength stainless steel 2205 performed better overall than the other two alloys. While 2205 performed second best in the Phase 1 tests, it had clearly superior performance in the Phase 2, anodic polarization stage tests, which involved high severity and were also conducted in an environment more representative of conditions in concrete. The results of testing in the initial stage of Phase 2 were nevertheless encouraging in that none of the three alloys exhibited any signs of SCC in an environment that simulated heavily Cl- contaminated concrete pore water at a highly accelerating temperature regime. Although these findings are preliminary in nature and should be supplemented by the results of longer time exposures, it suggests that the concrete pore water environment protects the stainless steel to a level that may extend service life for all the candidate stainless steel materials tested.

6.2 Relaxation Tests

Relaxation tests showed that the as-received stainless strand materials are not relaxed to

an acceptable level for immediate use in prestressed applications. This is not surprising given the standard practice for relaxing strand material is induction heating that makes use of the magnetic permeability of normal carbon steels. The lower to near zero magnetic permeability of stainless steels exclude the use of induction furnaces for this purpose. However, mechanical relaxation in the form of cyclic stressing was found to reduce losses to commonly accepted levels with the exception of the XM-29 which showed very little improvement. In all cases, the act of cycling the strand increased the apparent modulus significantly thereby removing compliance associated with the strand configuration.

As the ultimate goal of setting relaxation limits is to reduce long-term losses in effective prestress, the tolerable amount of relaxation may be subject for review on a case by case basis. In the case of XM-29, for instance, the exact same strand material produced in Sanderson, FL, has been accepted for use and is now in use in the Pearl Harbor Submarine Silencing Facility (as discussed in Chapter 2).

6.3 Transfer Length Testing

Aside from the corrosion resistance and mechanical properties of the stainless steel materials, the surface smoothness was also noted as a point of concern as it pertains to bond with the concrete. Both development length and transfer length can be affected in this regard, but for prestressing applications, transfer length is most important. For this study, full scale piles were cast with each of the three candidate stainless steel materials and one with Grade 270 low-lax carbon steel. Results showed no adverse effects from the use of any of the stainless steel strand products used in this study. In one case (2205), a reduction in transfer length was observed. When compared to code specified values (60 times the diameter of the strand; 60d), the actual values ranged from 60d to 101d. The 316, XM-29 and Grade 270 low-lax carbon steel all showed similar transfer lengths at approximately 100d.

6.4 Design of Prestressed Piles using Stainless Steel

The design of prestressed structural elements and specifically piles is dependent on the mechanical properties of the strands, concrete strength and level of effective prestress. With regards to using stainless steel strands, these properties are relevant for setting limits for the stressing operation, calculating prestress losses, evaluating ductility, and estimating ultimate capacity.

As the stainless steel materials are weaker than standard Grade 270 low-lax carbon steel, additional strands are required to offset the loss in combined load. For instance, the 14in square demonstration piles cast in this study used 12 strands instead of the more commonly-used 8-strand pattern. That determination was made on the basis of the weakest strand material used (316) and because all piles were cast simultaneously end-to-end, in-series (all had identical strand forces). However, fewer strands could have been used for the stronger 2205 and XM-29 piles if those piles could have been cast separately from the weaker 316. Further, as no degradation in bond was noted as a result

of the smoother stainless steel surface, the design hinges simply on required total force and ultimate strength of the strand.

Figure 6.1 shows the required number of strands, strand pattern, jacking forces, effective prestress and clear spacing between strands for 14in, 18in, and 24in square piles. Therein, any of the three stainless steel materials used in this study can be used.

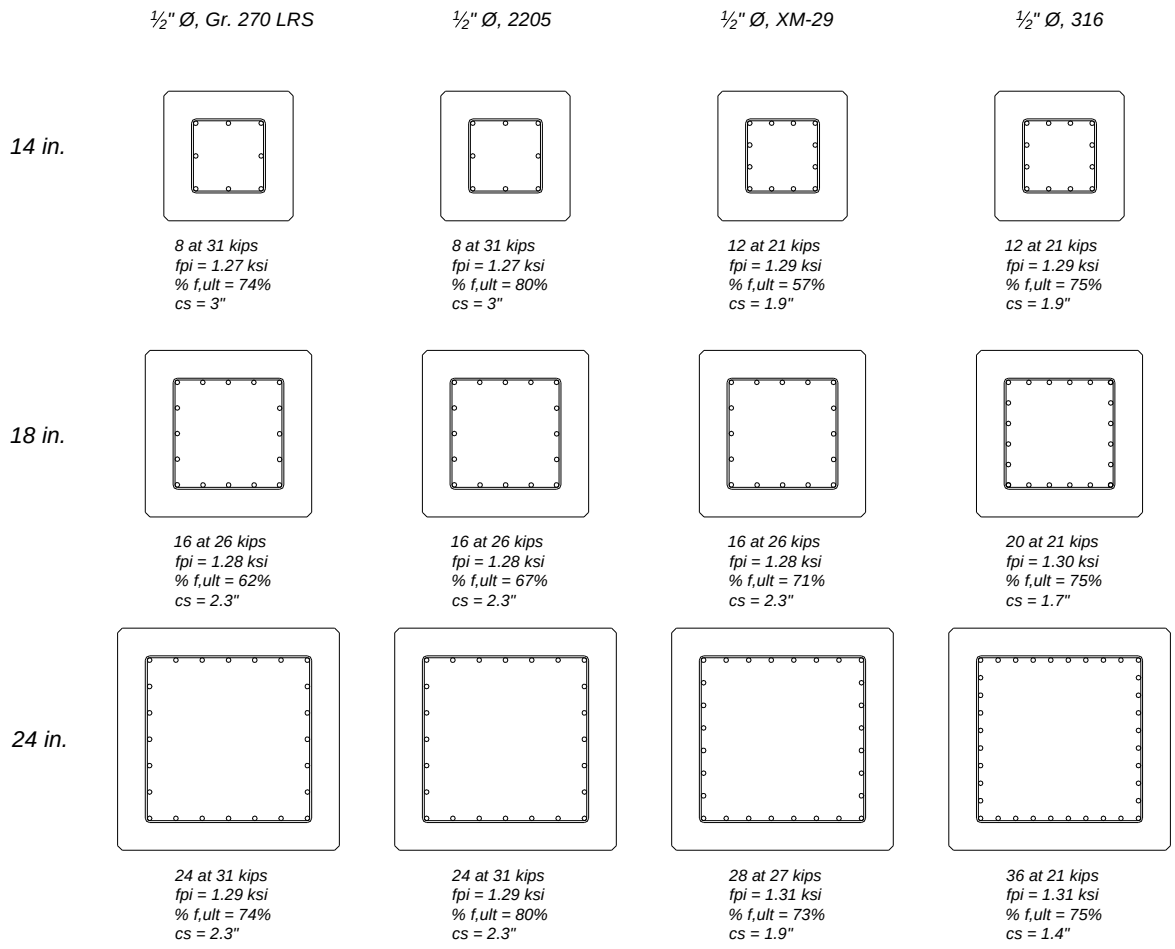

Figure 6.1 Pile strand patterns, jacking forces, and effective prestress for the various strand materials used in this study.

6.5 Cost Effectiveness

Given the higher cost of stainless steels relative to carbon steels, it is immediately apparent that piles cast with stainless steel reinforcement will have a higher initial cost. The rationale for considering stainless steels stems from to need to extend the service life

of bridges preferably without the need for periodic repairs. In so doing, the potential to decrease costs exists when the time value of monies is considered.

The cost of stainless steel strands for this project ranged from $2.7/ft for Grade 316 to $3/ft for the duplex 2205. As the 2205 was a special order, it is more likely that the $2.7/ft is a more reasonable estimate of costs as 316 is commonly used and readily available. Regardless and despite the slight increase in cost, 2205 uses only 24 strands compared to 36 strands required when using Grade 316 (Figure 6.1). In this way, the 2205 is an obvious choice when comparing solely between stainless products (this does not account for the reduced labor costs associated with prestressing with fewer strands).

Grade 270 low-lax carbon steel general costs on the order of $0.79/ft for US manufactured strands. These costs were used to provide a life cycle comparison (Appendix C). This analysis showed that the present day value of a pile cast with Grade 270 low-lax carbon steel strands (repaired at 50 and 75yrs from corrosion damage) would cost 10% more than a pile cast with 2205 strands. Table 6.1 provides a comparison of Grade 316, 2205 and Grade 270 carbon steel pile costs.

Table 6.1 Present day value of 75ft piles with various grades of steel and life spans.

Strand Material	Initial cost	75yr life span	100yr life span
Grade 270 low-lax carbon steel	$6,231.75	$11,508.22	$15,456.17
Grade 316 Stainless steel	$12,612.75	$12,612.75	$16,362.70
Duplex 2205 Stainless steel	$9,957.75	$9,957.75	$13,707.70

6.5 Summary

The findings of this study suggest that use of higher strength grades of stainless steel (2205 and XM-29) as a reinforcing material in prestressed piles is a cost effective alternative to plain carbon steel reinforcing strands. These results account for structural capacity, long-term relaxation, corrosion resistance, and field fabrication aspects of prestressed piles. Increased cost effectiveness is likely to ensue as use of stainless strands becomes more prevalent. However, the cost of nickel largely drives the cost of stainless steels and as it is a naturally mined mineral, unforeseen market swings may have undesirable outcomes.

This project concluded with four 75ft piles cast with different strand materials that can and should be used to further explore the field performance of stainless steel reinforced piles. This might include driving performance and cracked section corrosion testing.

References

- AASHTO (2010). "AASHTO LRFD Bridge Design Specifications," 5th ed., American Association of State Highway and Transportation Officials, Washington, DC, Article 5.11.4.1.
- AK Steel (2007). "Product Data Bulletin - Hot-Rolled Steel", Product Catalog Sheet from AK Steel Corporation.
- Alyousif, O. M, and Nishimura, R. (2006). "The Effect of Test Temperature on SCC Behavior of Austenitic Stainless Steels in Boiling Saturated Magnesium Chloride Solution", Corrosion Science, Volume 48, Pages 4283-4293, May.
- Baumeister, T. and Marks, L. (1958). "Standard Handbook for Mechanical Engineers", 7th Edition, McGraw-Hill, New York, NY.
- Cui, F. and Sagüés, A. (2006). "Exploratory Assessment of Corrosion Behavior of Stainless Steel Clad Rebar", Corrosion, Volume 62 No. 9, Pages 822-838, September.
- Cui F. and Sagüés A. (2006). "Exploratory Assessment of Corrosion Behavior of Stainless Steel Clad Rebar - I: Experimental", *Corrosion*,Vol. 62, p.822.
- Davis, J.R. (1994). "ASM Specialty Handbook Stainless Steels", ASM International, Materials Park, OH, December.
- Faller, M. and Richner, P. (2003). Journal: Materials and Corrosion-werkstoffe Und Korrosion - MATER CORROS, vol. 54, no. 5, pp. 331-338.
- FDOT (2013). "Master Pay Item List," Florida Department of Transportation. http://www.dot.state.fl.us/specificationsoffice/Estimates/BasisofEstimates/
- Fernandez, J. (2011). "Stress Corrosion Cracking Evaluation of Candidate High Strength Stainless Steels for Prestressed Concrete", University of South Florida, Tampa, FL, December.
- FGE (2009). Gray Mullins personal voice and email communication with Foundation & Geotechnical Engineering, LLC. Plant City, FL.
- Hurley M. and Scully J., (2006). "Threshold Chloride Concentrations of Selected Corrosion-Resistant Rebar Materials Compared to Carbon Steel" *Corrosion*, Vol. 62, p.892.
- Hartt, W. H., Powers, R. G., Leroux, V. and Lysogorski, D. K. (2004). "A Critical Literature Review of High-Performance Corrosion Reinforcement in Concrete Bridge Applications", Federal Highway Administration Report, FHWA-HRT-04-093 (located at http://www.fhwa.dot.gov), July.
- Insteel Wire Products (2013). http://www.insteel.com/ quote prepared for project
- Iversen, A. and Prosek, T. (2007). "Atmospheric stress corrosion cracking of austenitic stainless steels in conditions modeling swimming pool halls," Eurocorr 2007, EFC, Freiburg im Breisgau, Germany, Paper No. 1142.
- Jenkins, J. F. (1987). "Validation of Nitronic 33 in reinforced and prestressed concrete" Naval Facilites Engineering Command, Jacksonville, FL
- McDonald, D., Sherman, M., Pfeifer, P. and Virmani, P. (1995). Stainless Steel Reinforcing as Corrosion Protection. Concrete International, Vol. 17, No. 5, pp. 65-70.
- Mindess, S, Young, F. and Darwin, D. (2003). Concrete, 2nd Edition, Prentice-Hill, Englewood Cliffs, NJ.

- Naaman, A. (2012). *Prestressed concrete analysis and design*, Techno Press 3000, Ann Arbor, MI.
- NBI (2007). "National Bridge Inventory ," US Dept of Transportation, Federal Highway Admission. http://www.fhwa.dot.gov/bridge/nbi.cfm May.
- National Strand (2013). http://nationalstrand.heicowiregroup.com/ quote prepared for project
- Moser, R. J. (2011). "High-strength stainless steels for corrosion mitigation in prestressed concrete: development and evaluation". Ph. D dissertation, Georgia Institute of Technology, Atlanta, GA, April, 330 pages.
- Moser, R.J. (2013). "Preliminary studies of high-strength stainless prestressing steels". ACI SP 291-6, pp. 95-104, Farmington Hills, MI.
- Powers, R., Lasa, I., Duncan, M. (2001). "Evaluation of Galvonic Battery Power Supply for Cathodic Protection", Florida Department of Transportation Corrosion Research Laboratory, Gainesville, Florida.
- Sagüés, A., Kranc, S.C., Presuel-Moreno, F., Rey, D., Torres-Acosta, A. and Yao, L. (2001). "Corrosion Forecasting for 75-Year Durability Design of Reinforced Concrete", Florida Department of Transportation Final Report BA502 (located at http://www.dot.state.fl.us), December.
- Sanchez, J., Fullea, J. and Andrade, C. (2007). "Stress Corrosion Cracking Mechanism of Prestressing Steels in Bicarbonate Solutions", Advances in Construction Materials, Part V, Pages 397-404.
- Sumiden Wire (2013). http://www.sumidenwire.com/ quote prepared for project
- Weast, R. C. (1973-74) "Handbook of Chemistry and Physics", 54th Edition, Published by CRC Press, Boca Raton, FL.
- Wikipedia (2009). http://en.wikipedia.org/wiki/Stainless_steel#cite_note-0 Accessed December 20, 2013.
- Wire World (2009). http://wireworldinc.com/product4.htm Accessed September 17, 2009.
- Wu, Y. and Nürnberger, U. (2009). "Corrosion-technical Properties of High-Strength Stainless Steels for the Application in Prestressed Concrete Structures", Materials and Corrosion, Volume 60, Number 10, p. 771-780.

PMI# 8659912C

CONCRETE MIX DESIGN

Class: V | Mix Design Number: 01-1025-01 | Minimum Strength: 6500 psi

FDOT Approval Date: 04/07/2011 | Hot Weather? Yes | Issuer's Name: Sean Masters PE

Status: APPROVED | Slip Form?: No | Project #:

Producer : Preferred Materials Corp. | Plant #:

Source of Materials

Product / Product Name	Quantity		Producer / Plant #	QPL # / Spec:	SSD	FM	Geological Type
Cement: Type II Cement	750	LB	AMERICAN CEMENT COMPANY CMT40	AASHTO M 85 - Type II	3.15		
Fly Ash: Class F Fly Ash	180	LB	SEPARATION TECHNOLOGIES-BIG BEND FA30	ASTM C 618 - Class F	2.43		
Coarse Aggregate: # 57 Stone	1523	LB	CEMEX 87089		2.42		Limestone
Fine Aggregate: Silica Sand	989	LB	VULCAN MATERIALS COMPANY 16659		2.63	2.21	Silica Sand
Air Ent Admixture: AEA92 S	0.5	OZ	EUCLID CHEMICAL CO.	S924-0023 AASHTO M 154 - AEA			
Type D Admixture: Eucon WR	93	OZ	EUCLID CHEMICAL CO.	S924-0307 AASHTO M 194 - Type D			
Type F Admixture: Plastol 6200 EXT	23.3	OZ	EUCLID CHEMICAL CO.	S924-0568 AASHTO M 194 - Type F			
Water: Water for Concrete	38.00	GA					
Water: Water for Concrete	316.5	LB					

Specification Limits

Slump (Target Slump: 7 Inches)	5.50 to 8.50	inches
Air Content	1.00 to 5.00	percent
W/CM Ratio	Less than or equal to 0.34	LB per LB
Temperature	Less than or equal to 100	degree F
Compressive Strength	Greater than or equal to 6500	avgpsi

Aggregate Correction Factor: 0.5

Comments:

Coarse aggregate substitution 87089 for 12521
Fine aggregate substitution 16659 for 03677
3% air used to achieve Theo. yield of 27cf

Producer Data

W/CM Ratio	0.34	LB per LB
Theoretical Yield	27.00	CF
Temperature		degree F
Slump		inches
Density	139.2	LBperCF
Chloride Content	0.083	LB per CY
Air Content		percent
Agg Corr Factor	0.5	percent

Mix Designer:	First Name	Last Name
	James	Reeves

Conc_Mix-10.rpt 04/04/11 slb

Figure A.1 Concrete mix design.

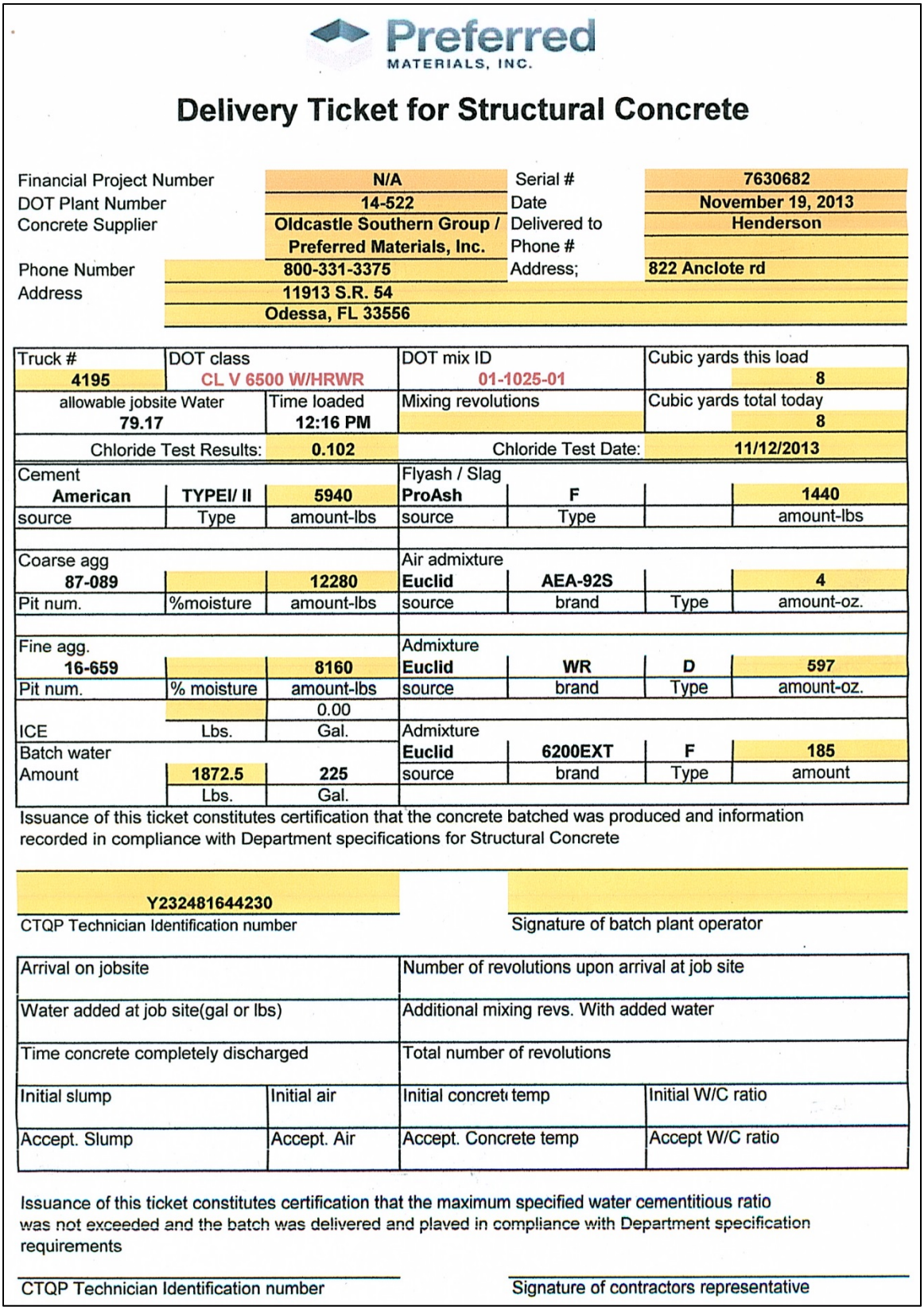

Preferred MATERIALS, INC.

Delivery Ticket for Structural Concrete

Financial Project Number	N/A	Serial #	7630682
DOT Plant Number	14-522	Date	November 19, 2013
Concrete Supplier	Oldcastle Southern Group / Preferred Materials, Inc.	Delivered to	Henderson
		Phone #	
Phone Number	800-331-3375	Address;	822 Anclote rd
Address	11913 S.R. 54 Odessa, FL 33556		

Truck #	DOT class	DOT mix ID	Cubic yards this load
4195	CL V 6500 W/HRWR	01-1025-01	8
allowable jobsite Water: 79.17	Time loaded: 12:16 PM	Mixing revolutions	Cubic yards total today: 8
Chloride Test Results: 0.102		Chloride Test Date: 11/12/2013	

Cement			Flyash / Slag			
American	TYPEI/ II	5940	ProAsh	F		1440
source	Type	amount-lbs	source	Type		amount-lbs
Coarse agg			Air admixture			
87-089		12280	Euclid	AEA-92S		4
Pit num.	%moisture	amount-lbs	source	brand	Type	amount-oz.
Fine agg.			Admixture			
16-659		8160	Euclid	WR	D	597
Pit num.	% moisture	amount-lbs	source	brand	Type	amount-oz.
		0.00				
ICE	Lbs.	Gal.	Admixture			
Batch water			Euclid	6200EXT	F	185
Amount	1872.5	225	source	brand	Type	amount
	Lbs.	Gal.				

Issuance of this ticket constitutes certification that the concrete batched was produced and information recorded in compliance with Department specifications for Structural Concrete

Y232481644230
CTQP Technician Identification number

Signature of batch plant operator

Arrival on jobsite		Number of revolutions upon arrival at job site	
Water added at job site(gal or lbs)		Additional mixing revs. With added water	
Time concrete completely discharged		Total number of revolutions	
Initial slump	Initial air	Initial concrete temp	Initial W/C ratio
Accept. Slump	Accept. Air	Accept. Concrete temp	Accept W/C ratio

Issuance of this ticket constitutes certification that the maximum specified water cementitious ratio was not exceeded and the batch was delivered and played in compliance with Department specification requirements

CTQP Technician Identification number

Signature of contractors representative

Figure A.2 Delivery ticket for first truck (piles: lox-lax & 2205).

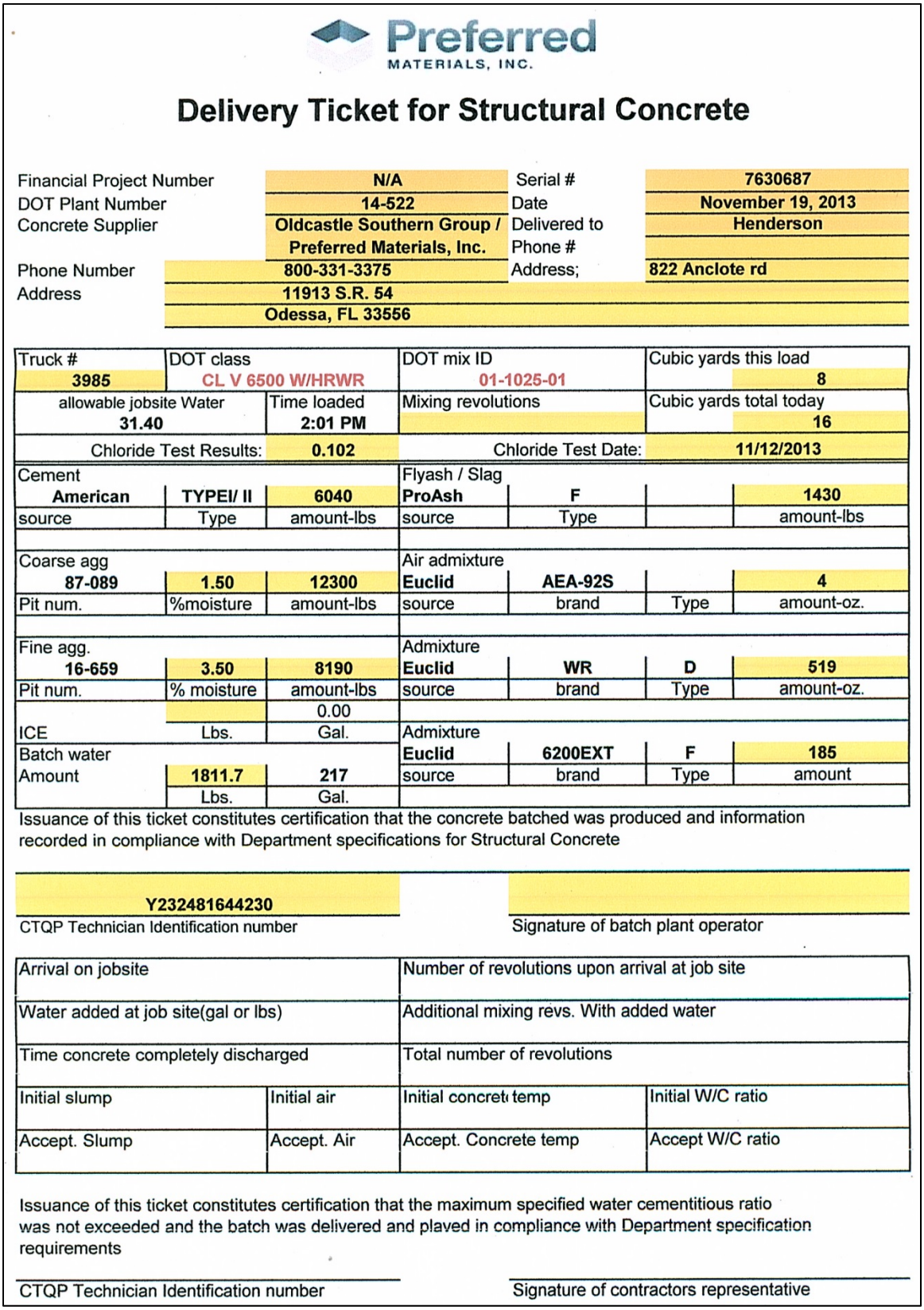

Preferred MATERIALS, INC.

Delivery Ticket for Structural Concrete

Financial Project Number	N/A	Serial #	7630687
DOT Plant Number	14-522	Date	November 19, 2013
Concrete Supplier	Oldcastle Southern Group / Preferred Materials, Inc.	Delivered to	Henderson
		Phone #	
Phone Number	800-331-3375	Address;	822 Anclote rd
Address	11913 S.R. 54 Odessa, FL 33556		

Truck #	DOT class		DOT mix ID			Cubic yards this load	
3985	CL V 6500 W/HRWR		01-1025-01			8	
allowable jobsite Water	Time loaded		Mixing revolutions			Cubic yards total today	
31.40	2:01 PM					16	
Chloride Test Results:	0.102		Chloride Test Date:			11/12/2013	
Cement			Flyash / Slag				
American	TYPEI/ II	6040	ProAsh	F		1430	
source	Type	amount-lbs	source	Type		amount-lbs	
Coarse agg			Air admixture				
87-089	1.50	12300	Euclid	AEA-92S		4	
Pit num.	%moisture	amount-lbs	source	brand	Type	amount-oz.	
Fine agg.			Admixture				
16-659	3.50	8190	Euclid	WR	D	519	
Pit num.	% moisture	amount-lbs	source	brand	Type	amount-oz.	
		0.00					
ICE	Lbs.	Gal.	Admixture				
Batch water			Euclid	6200EXT	F	185	
Amount	1811.7	217	source	brand	Type	amount	
	Lbs.	Gal.					

Issuance of this ticket constitutes certification that the concrete batched was produced and information recorded in compliance with Department specifications for Structural Concrete

Y232481644230	
CTQP Technician Identification number	Signature of batch plant operator

Arrival on jobsite		Number of revolutions upon arrival at job site	
Water added at job site(gal or lbs)		Additional mixing revs. With added water	
Time concrete completely discharged		Total number of revolutions	
Initial slump	Initial air	Initial concrete temp	Initial W/C ratio
Accept. Slump	Accept. Air	Accept. Concrete temp	Accept W/C ratio

Issuance of this ticket constitutes certification that the maximum specified water cementitious ratio was not exceeded and the batch was delivered and played in compliance with Department specification requirements

CTQP Technician Identification number	Signature of contractors representative

Figure A.3 Delivery ticket for second truck (piles: XM-29 & 316).

Table A.1 Concrete cylinder compressive strengths at time of de-tensioning.

	Cylinder Size	Age	Cylinder 1 Compressive Strength (psi)	Cylinder 2 Compressive Strength (psi)	Average Compressive Strength (psi)
Truck 1	4x8 in.	3 days	5126	6381	5753
Truck 2	4x8 in.	3 days	5778	6252	6015

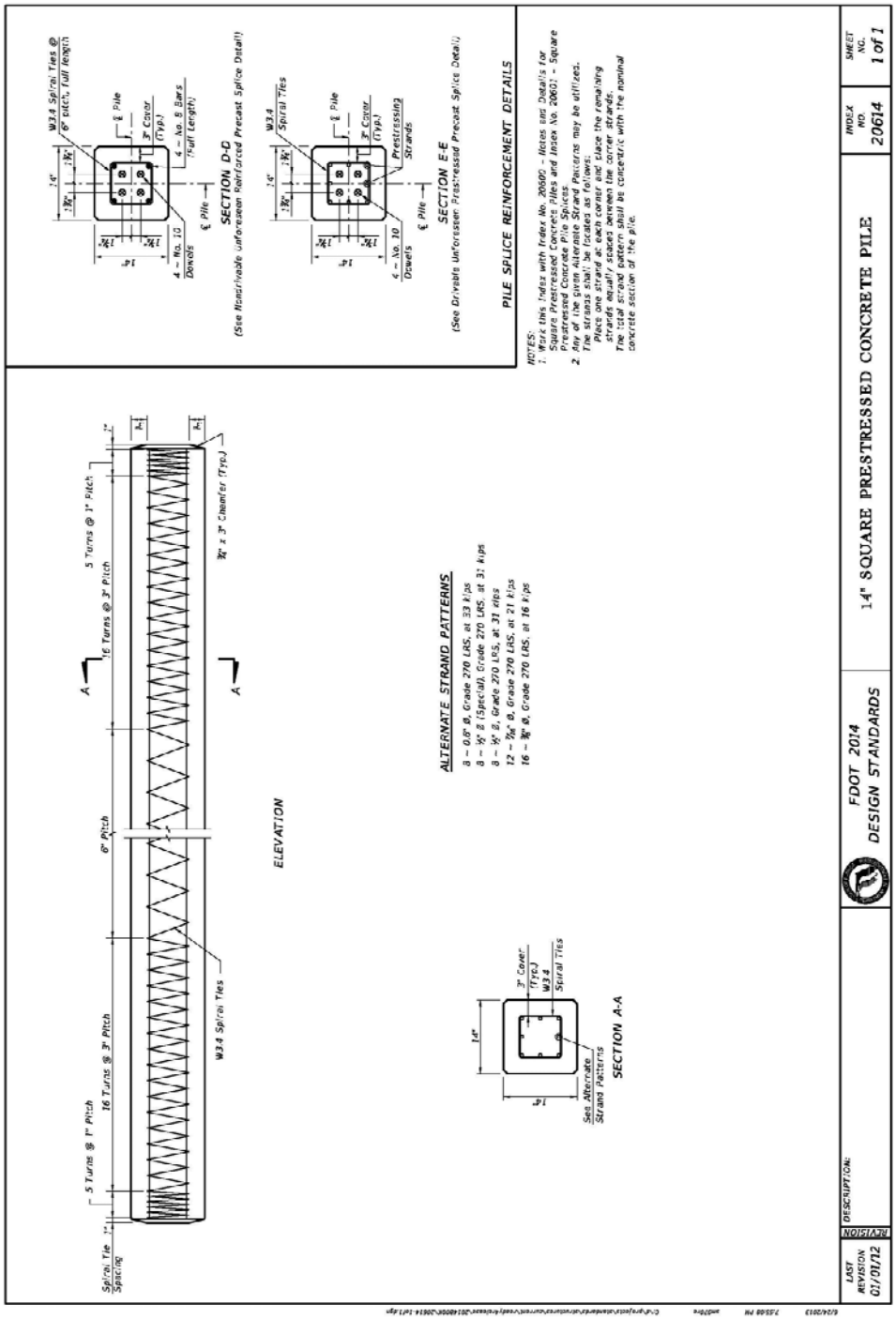

Figure B.1 14 in. square pile (FDOT index 20614)

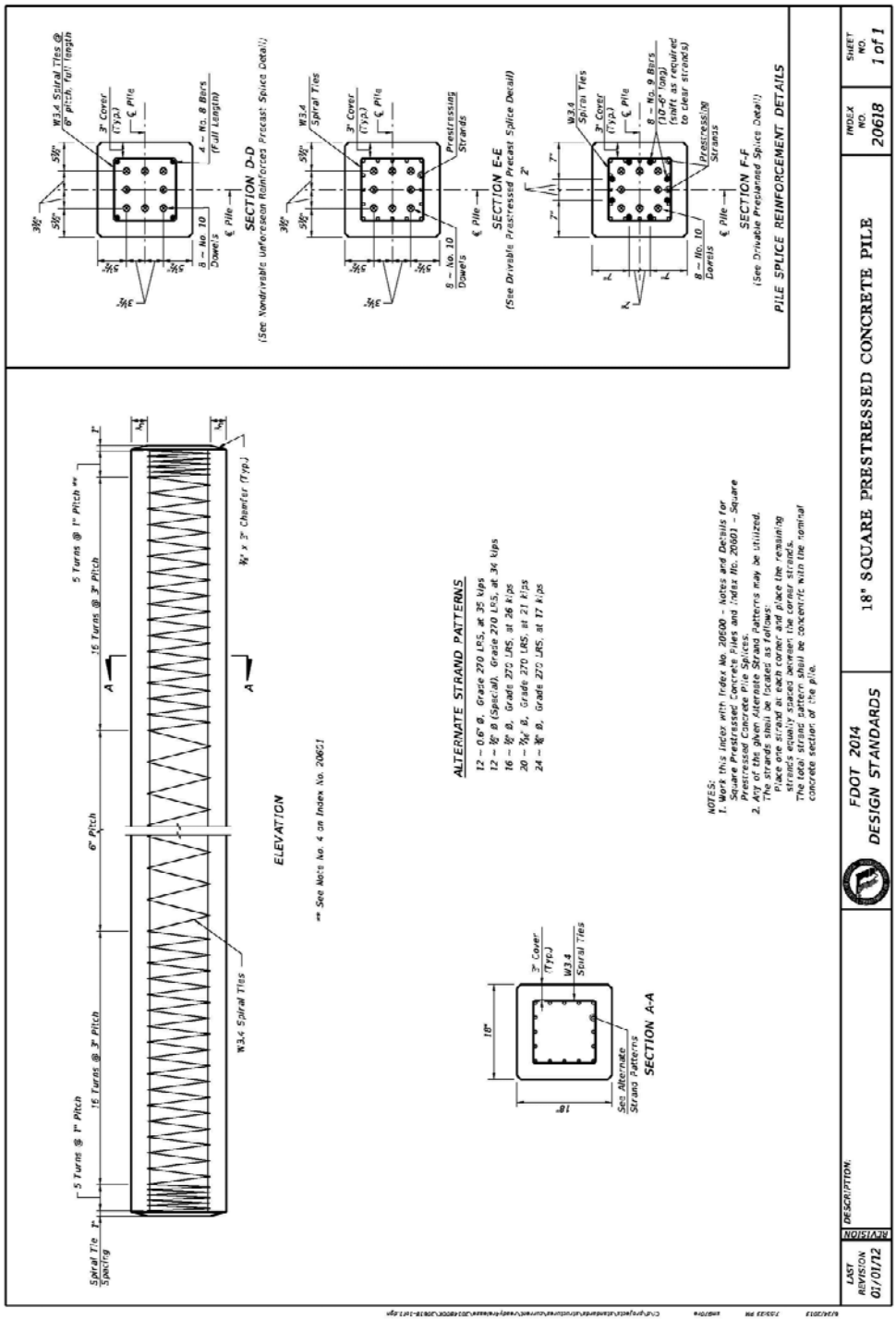

Figure B.2 18 in. square pile (FDOT index 20618)

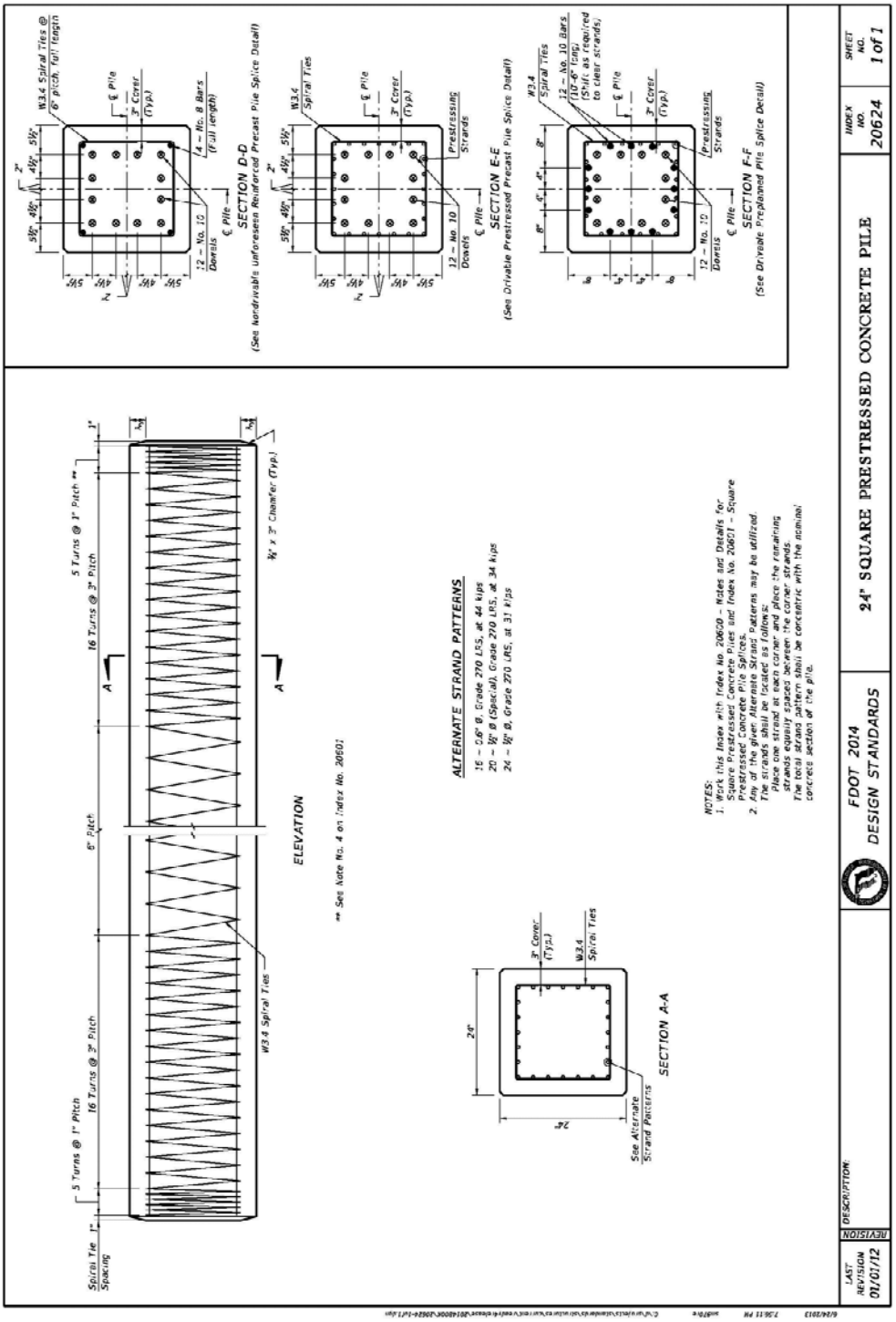

Figure B.3 24 in. square pile (FDOT index 20624)

Appendix C: Life Cycle Cost Comparison

According to FDOT Master Pay Item records the current price of prestressed concrete piling 24" square is $80.93 per foot (FDOT, 2013). The average price of plain carbon prestressing strand currently used is seventy-nine cents per foot while the average price of stainless prestressing strand is $2.95 per foot (Insteel, 2012; Sumiden, 2012; National Strand, 2012). One foot of a 24" square pile typically has 24 feet of strand (24 strand pattern); for the 2205 stainless steel 24 strands can also be used (Figure 6.1) and substituted directly for plain carbon strand. Therefore, the upfront cost would increase from $80.93 to $132.77 per foot.

$$Cost\ of\ plain\ carbon\ strand\ per\ foot\ of\ pile = .79 * 24 = \$18.96$$
$$Cost\ of\ stainless\ strand\ per\ foot\ of\ pile = 2.95 * 24 = \$70.80$$
$$Strand\ for\ strand\ replacement = \$80.93 - \$18.96 + \$70.80 = \$132.77$$

However, additional strands are required for lower Grade stainless steel. A conservative estimate, using the lowest strength grade 316 stainless steel with strength of 180ksi requires an increase in the amount of stainless from 24 to 36 strands which corresponds to a cost of $168.17.

$$\$80.93 - \$18.96 + 70.80(1.50) = \$168.17$$

This is a 108% increase when considering the pile unit as a whole but far less in comparison to the cost of the entire structure.

The structural engineer often only includes a footnote about maintenance to achieve its design life. Historically, not only maintenance but preventative and effective repairs such as cathodic protection within an FRP pile jacket are required. Bridge structures are expected to reach service lives ranging from 55 to 80 years with this treatment (Sumiden, 2012). This satisfies the 75 year design life required by AASHTO that most states adopt.

The National Bridge Inventory has a rating system to identify "structurally deficient" (SD) bridges. A rating of 4 or less signifies a SD bridge at which point it has reached the end of service life unless repair, rehabilitation or replacement occurs (NBI, 2007). Florida ranks second in the nation for the least percentage of SD bridges in the state at just 2.4% (Nevada leads the nation with the best bridges at only 2.2% SD).

The Georgia Department of Transportation reports its SD age at 32 years (Moser, 2011). According to a report by the FDOT corrosion research laboratory "older structures in marine environments typically exhibited corrosion deterioration between fifteen and twenty years after construction" (Powers, 2001). Since the late 1980's high performance concrete has been used which is expected to increase the service life of newer bridges, as such the conventional wisdom of a 50 year service life will be used as the age of first repair for bridges constructed today.

A cathodic protection (CP) integral pile jacket, non-structural, 16"-30" costs $1571.10 per foot (FDOT, 2013). The life of the galvanic CP pile jackets typically protect piles between 15-25 years (Powers, 2001).

Assume at 50 years the plain carbon steel pile needs a CP repair. The minimum pile jacket length is 5ft but typically much more is used. 6ft length is used for this example.

$$Today's\ value\ for\ the\ 6ft\ section\text{: } \$1{,}571.10/\text{ft} * 6\text{ft} = \$9{,}426.60$$

Assuming a 2.8% annual increase in cost, the 50 year future value of a repair will be:

$$\$9{,}420.60(1.028)^{50} = \$37{,}498.23 \text{ per pile}$$

The present value of this cost assuming a 4% discount rate is:

$$\frac{\$37{,}498.23}{1.04^{50}} = \$5{,}276.47$$

These two calculations can be combined and repeated at 50 years and again at 75 years and added to the original cost of the pile to attain the cost of materials and repair for a 100 year service life.

$$\frac{\$80.39}{ft} * \frac{75\ ft}{pile} + \$9{,}426.6 * \left[\frac{1.028}{1.04}\right]^{50} + \$9{,}426.6 * \left[\frac{1.028}{1.04}\right]^{75} = \$15{,}293.87$$

The present day cost of a 75 and 100yr repair (terms two and three above) is $9,224.12 or 61% of the cost of the pile.

Multiple grades of stainless steel pc strand have been shown to exceed a 75 year period (by extrapolation) before signs of corrosion appear (Fernandez, 2013). This data is conservative in nature but will be used for the life cycle cost comparison. Substituting the initial material costs for stainless and using just one repair at 75 years the cost for a 100 year service life is computed below for Grade 316 (more strands) and the duplex 2205 (no additional strands required):

$$\frac{\$168.17}{ft} * \frac{75\ ft}{pile} + \$9{,}426.6 * \left[\frac{1.028}{1.04}\right]^{75} = \$16{,}560.70 \text{ for Grade 316}$$

$$\frac{\$132.77}{ft} * \frac{75\ ft}{pile} + \$9{,}426.6 * \left[\frac{1.028}{1.04}\right]^{75} = \$13905.70 \text{ for Duplex 2205}$$

Consider two factors that may bring down the cost: the 75 years to first sign of corrosion (not necessarily repair level) is derived from laboratory tests with no protection from chloride deposits.

Table C.1 Present day value of 75ft piles for various grades of steel and life spans.

Grade 270 low-lax Carbon	**Grade 316 Stainless**	**Duplex 2205 Stainless**
$15,293.87 100 year life	$16,560.70 100 year life	$13,905.70 100 year life
$11345.92 75 year life	$12,612.75 75 year life	$9,957.75 75 year life
Repair at 50 and 75 years. Neither estimate includes any secondary losses such as MOT, loss time or resources which are estimated to be more than the repair costs themselves.	Repair at 75 years. Does not consider the longer service life expected when embedded in concrete and assumes the weakest stainless, Grade 316 with 180ksi tensile strength is assumed.	Repair at 75 years. Does not consider longer life when embedded in concrete. Fewer strands needed with higher strength 2205 strands.